PROCESSING PARAMETER EFFECTS ON THE MOLECULAR ORDERING AND CHARGE TRANSPORT OF POLY(3-HEXYLTHIOPHENE) THIN FILMS

A Thesis
Presented to
The Academic Faculty

by

Mincheol Chang

In Partial Fulfillment
of the Requirements for the Degree
Doctor of Philosophy in the
School of Chemical and Biomolecular Engineering

Georgia Institute of Technology
December 2014

PROCESSING PARAMETER EFFECTS ON THE MOLECULAR ORDERING AND CHARGE TRANSPORT OF POLY(3-HEXYLTHIOPHENE) THIN FILMS

Approved by:

Dr. Elsa Reichmanis, Advisor
School of Chemical and Biomolecular Engineering
Georgia Institute of Technology

Dr. Michael A. Filler
School of Chemical and Biomolecular Engineering
Georgia Institute of Technology

Dr. Dennis W. Hess
School of Chemical and Biomolecular Engineering
Georgia Institute of Technology

Dr. Robert M. Dickson
School of Chemistry and Biochemistry
Georgia Institute of Technology

Dr. J. Carson Meredith
School of Chemical and Biomolecular Engineering
Georgia Institute of Technology

Date Approved: September 26th, 2014

This dissertation is dedicated to my grandmother, mother, and wife, whose love and support provided me the strength and perseverance that I needed to achieve my goals; and to my lovely son, Yoon, whose innocence and happiness taught me the beauty of life and gave encouragement to live with patience.

ACKNOWLEDGEMENTS

First and foremost, I would like to thank my advisor, Prof. Elsa Reichmanis for her support, understanding, and patience over the past five years. Without her guidance as a great mentor, this work would not be possible, and I certainly would not be here. I was very fortunate to meet her because I could learn how I resolve the problems that I face in my life as well as in my research, through her invaluable advice and guidance.

I would also like to thank to my committee, Profs. Dennis Hess, Carson Meredith, Michael Filler and Robert Dickson for their helpful comments during my proposal and pre-doctoral review. I am proud to be associated with such luminaries in their respective fields.

My special gratitude goes to the Reichmanis group members, Prof. Byoungnam Park (now at Hongik University in South Korea), Zhaokang Hu (now at SABIC Innovative Plastics in USA), Avishek Aiyar (now at IBM in USA), Boyi Fu, Ji-Hwan Kang, Dalsu Choi, Nabil Kleinhenz, Jeff Hernandez, Ashwin Ravi-Sankar, Ping-Hsun Chu, Jiho Lee (now at Seoul National University in South Korea), Nils Person, Rui Chang and Zhibo Yuan for all the friendship, discussion in the group meetings and assistance in the lab.

I would like to express special thanks to my friends in the ChBE Korean Student Association for their warm friendship and support to living in this community.

Finally and most importantly, I cannot forget to say thanks to my family. I could achieve successful completion of my Ph.D with the continuous support and love of my family. I would like to thank and love forever my family, grandmother, mother, sisters, brothers-in-law, nephews and nieces, and my lovely wife and son.

TABLE OF CONTENTS

LIST OF TABLES

Page

LIST OF FIGURES

Page

SUMMARY

Conjugated polymers have attracted much interest as promising alternatives to inorganic semiconductors, due to their low-temperature, solution-based processability, which may provide for low-cost, large-area electronic device fabrication. However, commercialization of polymer-based electronic devices has been restricted owing to low device performance of solidified thin-films. In order to enhance charge transport of polymer semiconductor thin-films, the self-organization of organic polymer semiconductors into ordered supramolecular assemblies has been achieved by tuning a range of process parameters including film deposition method (spin vs. drop cast), solvent boiling point (low vs. high boiling point), polymer-dielectric interface treatment, and post-deposition processing (solvent vapor or thermal annealing). However, these strategies give rise to limitations for large-scale high-throughput processing due to associated pre- and/or post semiconductor deposition steps.

Therefore, this thesis outlines 1) our findings of alternative processing parameters which can contribute to enhancement in charge transport of a model polymer semiconductor, poly(3-hexylthiophene) (P3HT), eliminating the additional pre- and/or post-steps mentioned above, and 2) understanding of how the processing parameters effect intra- and intermolecular interactions of the polymer chains, micro- through macroscopic morphologies, and charge transport characteristics of the resultant films.

An alternative processing parameter (i.e., dipole-dipole interactions between a good and a poor solvent for P3HT) was found to profoundly impact molecular ordering of the polymer chains and micro- through macroscopic morphologies of the resultant thin-films,

which concomitantly impact film charge transport characteristics. Addition of small amounts of a more volatile poor solvent, which can interact with the majority solvent, facilitated supramolecular assembly and subsequent enhancement of charge transport characteristics of P3HT. We believe that the improvement is associated with the dipole-dipole interactions between acetone and chloroform which decrease the evaporation rate of the mixed solvent. P3HT is less soluble in the binary solvent than in the more readily vaporized chloroform component, and this characteristic enables the supramolecular assembly of P3HT chains at the nanoscale. Hansen solubility parameters were used to systematically understand how the solvent mixture enhances the alignment and assembly of polymer chains and influences subsequent thin film properties. The solvent mixture gradually changed from one which is a good solvent to one that is a poor solvent. Consequently, molecular ordering of the polymer chains improves due to a gradual transition from favorable to unfavorable solvent-solute interactions.

The low UV treatment of the P3HT solutions provided for enhanced intramolecular ordering of solubilized polymer chains, and thereby effects formation of anisotropic supramolecular polymer assemblies via favorable π-π stacking (intermolecular interaction). The nanofibrillar aggregates formed in solution survived the film deposition process and in turn, evidently improved the supramolecular ordering and charge transport characteristics of resultant polymer films. As the UV irradiation time increased, intra- and intermolecular interactions were enhanced, and thereby the crystalline-like nanofibrillar aggregates became longer than 1 μm, indicating a reduction in the number of grain boundaries in the resultant films. Consequently, the charge carrier mobility of resultant films was increased with UV irradiation time.

Finally, the charge carrier mobility of P3HT thin films was maximized by sequentially using two different solution treatment methods (i.e., ultrasonication and UV irradiation) along with optimization of the processing conditions. A sequential ultrasonication and UV irradiation of the precursor solution led to enhanced intra- and intermolecular interactions with a concomitant reduction in grain boundaries within the films. As a result, sequentially combined, the two methods very significantly further improved charge transport characteristics of the resultant films, compared to treatment via either method alone.

CHAPTER 1

INTRODUCTION

1.1 Organic semiconductors

1.1.1 Introduction

Over approximately the past fifty years, organic semiconductors (OSCs) have been synthesized and studied, because they represent a new class of materials for applications such as organic light-emitting diodes (OLEDs),[1-3] optical and amperometric sensors,[4-7] organic solar cells[8-10] and organic field-effect transistors (OFETs),[11-14] due to their unique optical and electrical properties. In the 1950s, drift mobility measurements and the photoconductivity response of small molecules such as anthracene were investigated.[15] Although these materials exhibited semiconducting properties with conductivities in the range of 10^{-9}–10^{-6} S/cm, their opto-/electrical performance and stability were poor.[16] However, the prospects of commercially using OSCs in a range of applications such as OLEDs, OFETs, and organic solar cells is now greater than ever, because of drastic improvements in synthesis and processing of new classes of materials such as conjugated polythiophenes.[17] In 2002, the *Sensotec Philishave*[18] was introduced by Philips as the first product in the market featuring a display panel based on OLED technology, and then Kodak introduced the *Kodak EasyShare LS633* digital zoom camera[18] equipped with an OLED display. In recent years, the applicability of OSCs has expanded tremendously with improvement in charge carrier mobility and processability. OSCs have been successfully applied to a flashlight based on organic photovoltaics,[19] radio frequency identification (RFID) tags,[20] and commercial TV based on OLED displays[21] as shown in Figure 1.1.

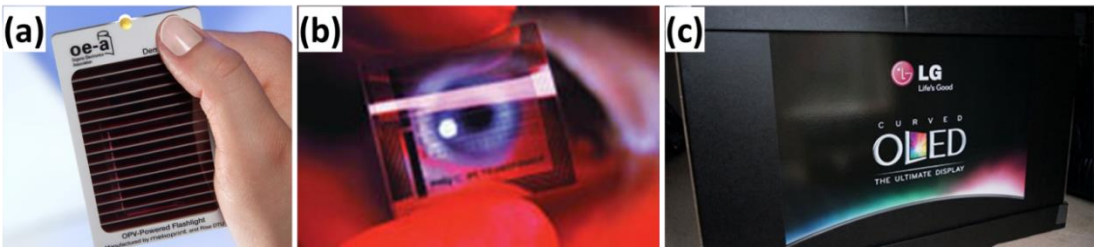

Figure 1.1: Examples of devices based on organic semiconductors: (a) a flashlight based on organic photovoltaics[19], (b) RFID tags[20], and (c) the first commercial OLED based display from LG Electronics[21].

The primary advantage of OSCs is ease of processability; OSCs can be readily deposited on any substrate such as plastic, metal, or glass, and are compatible with low-cost fabrication methods including direct printing, ink-jet and other solution-based processes,[18, 22] which may provide for low cost, large-area, and flexible electronic device fabrication.

1.1.2 Chemical Structure

OSCs can be categorized into two main groups[23-25]: (i) molecular semiconductors such as anthracene, pentacene, and rubrene. Also, oligomeric materials such as those belonging to the thiophene and acene family are classified into molecular semiconductors and (ii) polymeric semiconductors or conjugated polymers which will be the primary materials focused on in this thesis. Representative molecular and polymeric semiconductors are shown in Figure 1.2. Molecular semiconductors are composed of a few units consisting of alternating single and double bonds, while polymeric semiconductors are composed of many identical units bonded together in a long chain.

1.1.3 Electronic Structure

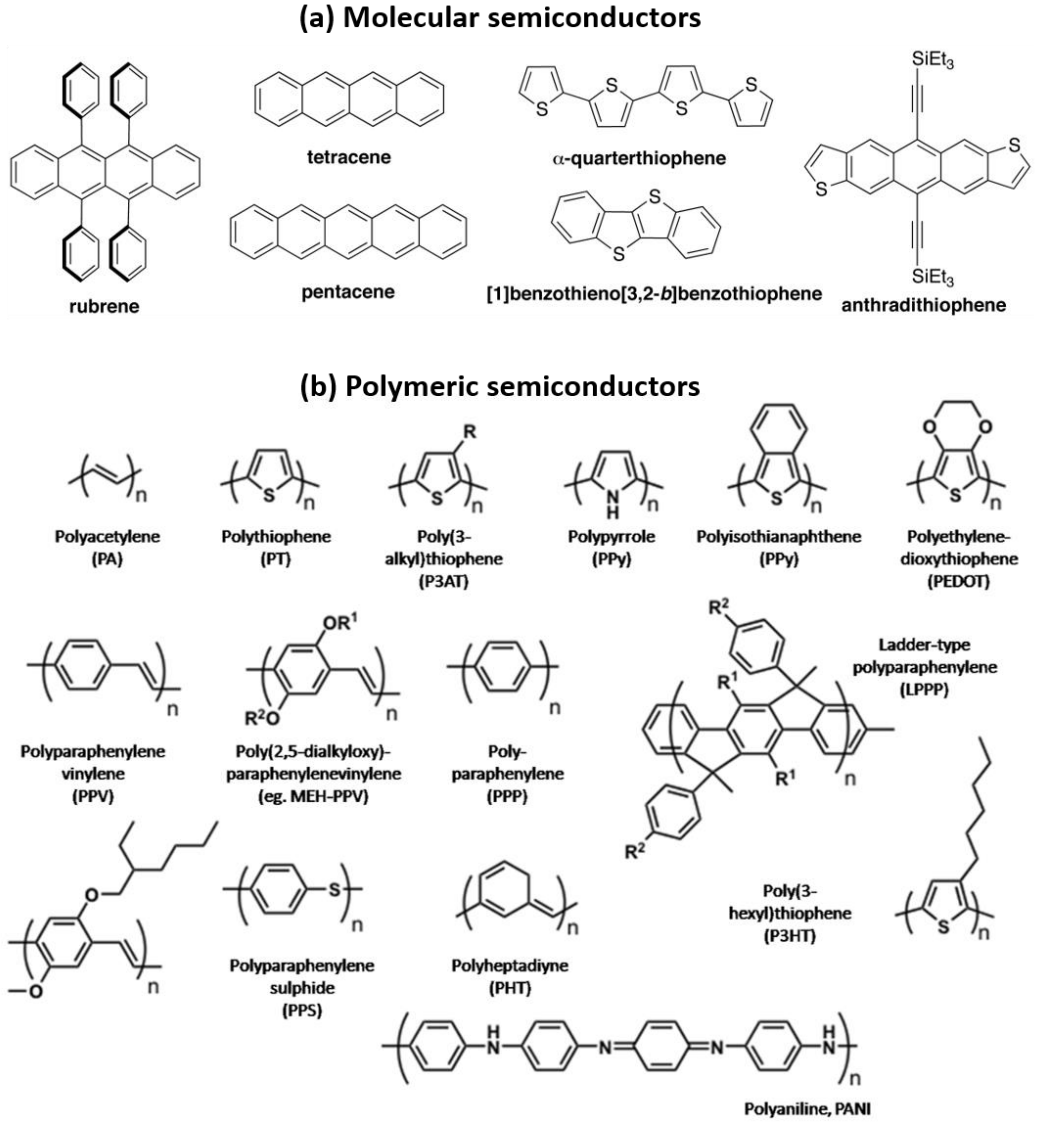

Figure 1.2: Representative examples of (a) molecular[23] and (b) polymeric semiconductors[24].

Organic materials are mainly composed of carbon. The electronic structure of conventional saturated polymers such as polyethylene (PE) is fundamentally different from that of conjugated organic semiconductors; all four valence electrons from each sp^3-hybridized carbon atom in PE are utilized in covalent sigma (σ) bonds while organic

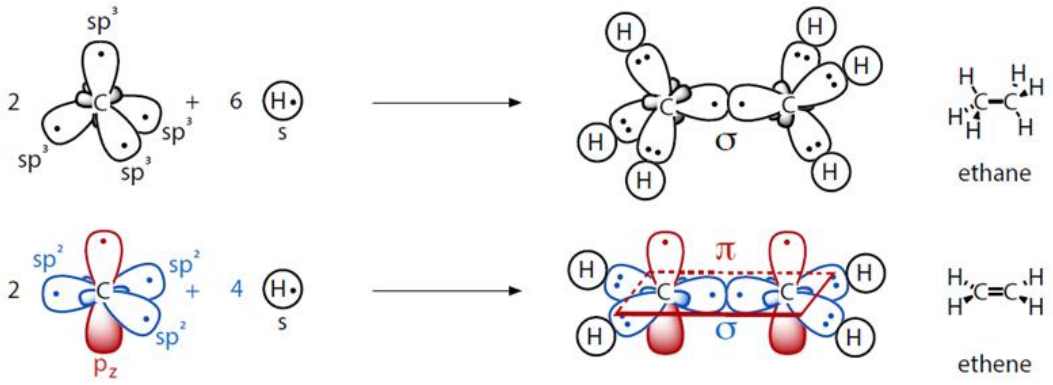

Figure 1.3: Comparison of non-conjugated and conjugated π-system.[26]

semiconductors consist of a system of carbon atoms with alternating single and double bonds, exhibiting an $sp^2 + p_z$ character (π-conjugated system) (Figure 1.3).

The electron in the p_z orbital is free to delocalize along the backbone when the orbital effectively overlaps between successive carbon atoms that leads to extended π-conjugation states. In other words, the extended π-conjugation states provide the "highway" for charge carriers to move along the backbone of the polymer chain leading to a conducting system. In addition, the extended π-conjugation states result in a reduction of the band-gap, i.e., $E_g(\pi) < E_g(\sigma)$, where E_g is the electronic band-gap (the energy difference between the highest occupied molecular orbital (HOMO) and the lowest unoccupied molecular orbital (LUMO)), and the use of π and σ represents conjugated and non-conjugated systems, respectively.

As in traditional inorganic semiconductors, the band-gap in OSCs is relatively small, typically between 1 and 4 eV, which can explain why many OSCs absorb light in the visible region of the spectrum.[27] However, unlike inorganic semiconductors like silicon, conjugated systems are quasi one-dimensional in nature since the covalent bonding is restricted within a chain, while interchain interactions are of Van der Waals type, and

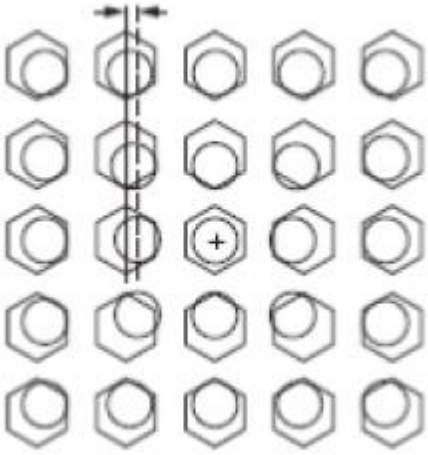

Figure 1.4: The polarization effects induced by the presence of an extra charge on the central benzene atom. The cloud always travels with the charge. Figure taken from[29].

therefore significantly weaker compared to crystalline silicon (c-Si) which has a three dimensional covalently bonded lattice. As a result, charge carriers observed in OSCs are actually self-localized quasi-particles, or polarons or bipolarons in condensed matter physics terminology, which indicates that they are not conventional free electrons or holes, such as those observed in c-Si.[28] Polarons and bipolarons are the manifestation of electron-phonon coupling which is invariably present in OSCs and is critical in explaining the properties of conjugated systems. As shown in Figure 1.4, the presence of polarons and bipolarons leads to local change in the geometry of the lattice.[29] As an example, Figure 1.5 shows the strong electron-phonon coupling (i.e., coupling between the electronic structure and the lattice structure) in butadiene,[30] which can represent a universal feature in all π-conjugated systems. The change of bond lengths between carbon and carbon is led by addition of π electrons to the existing σ framework which provides structural integrity to the molecule; the bond lengths are dictated by the π electron densities which in turn are

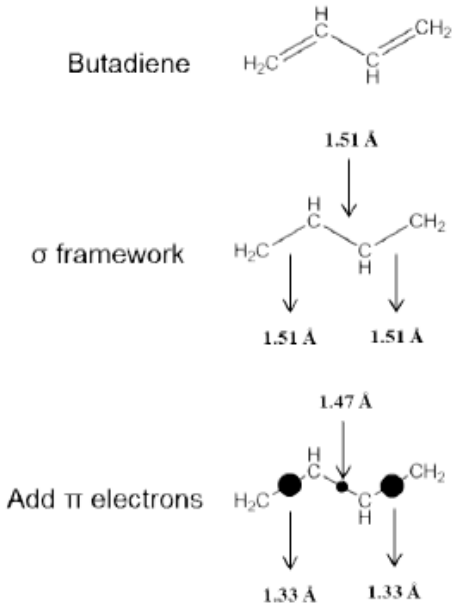

Figure 1.5: The geometrical (lattice) structure strongly coupled with the electronic structure in butadiene. The black circles indicate the π electron densities of the HOMO. Figure obtained from[30].

reshuffled due to electron-electron interactions. The π electrons in conjugated systems are highly polarizable and readily delocalized.[30]

As seen from Figure 1.5, a polaron consists of a radical cation or anion and a free radical while a bipolaron consists of two electrons or two holes; these species can be generated in OSCs through a multitude of processes including optical absorption, chemical charge transfer doping, or charge injection in neutral systems.[31] Such new localized energy states, which appear within the forbidden gap, are responsible for the hopping transport regime in disordered semiconductors, and thereby profoundly impact charge transport. This phenomenon will be discussed in more detail in Chapter 1.2.

1. 1. 4 Poly(3-hexylthiophene)

Although drastic strides towards development of single crystal arrays and solution processed small molecules have been achieved,[32, 33] polymeric semiconductors may be more suitable for large-area and flexible printed electronics due to their better mechanical and rheological properties.[34] Therefore, polymeric semiconductors are used as the primary materials in this thesis.

Polythiophenes are one of the earliest conjugated materials that have been used as excellent model polymers to investigate the nature of charge transport of organic polymer semiconductors. In 1986 Tsumura et al. demonstrated the first OFET composed of an electrochemically synthesized polythiophene film, showing a field effect mobility of 10^{-5} $cm^2V^{-1}s^{-1}$.[35] However, polythiophenes are restricted in processability for film formation, owing to their poor solubility and associated infusibility. In order to overcome such problems, alkyl side chains were functionalized along the polymer backbones by Elsenbaumer et al.[36] As a result, polythiophenes laterally substituted with alkyl side chains were found to be soluble and therefore processable, without significant loss in either physical or electronic performance.[36] A typical example of a laterally substituted polythiophene is poly(3-hexylthiophene) (P3HT), which has been extensively used and investigated in organic electronics because of its solution based processability and acceptable mobility.[36, 37] Significant improvement in the performance of P3HT based OFETs has been achieved by improving the molecular design,[38, 39] and identifying the importance of processing conditions[40, 41] on micro- and macrostructure of the resultant films. In this thesis, P3HT is also used as the primary model polymer to study how processing parameters like polarity, solubility and boiling point of solvents, film deposition

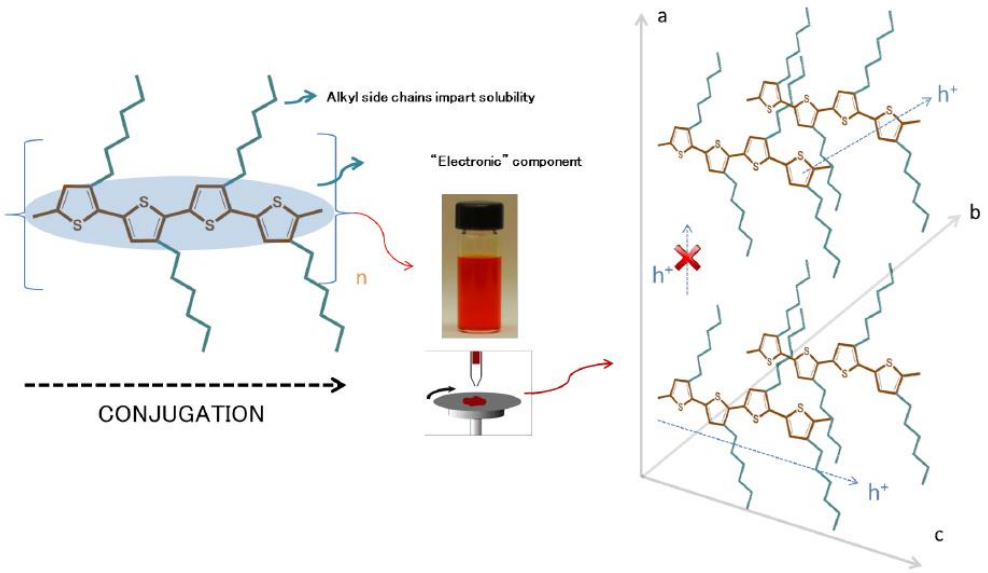

Figure 1.6: The molecular structure of P3HT and the packing of the polymer chains in a thin film. Image taken from [27].

methods, solution treatment methods and so on, effect micro- and macrostructures and thus charge transport of OSC films.

Figure 1.6 shows the molecular structure of P3HT and its packing in the final films.[27] The main backbone consisting of the conjugated aromatic core represents the direction of delocalization of the π electrons, and alkyl side chains imparting solubility to the polymer system. As depicted in Figure 1.6, charge carrier transport can be envisaged in three directions: (1) along the conjugated polymer backbone (the c-axis), (2) between polymer chains through the direction of π-π stacking (the b-axis), and (3) along the direction of the side chains (the a-axis). The c-axis is expected to provide the highest degree of electronic wave-function overlap, which means that charges would prefer to delocalize in that direction. Although not as easily as along the c-axis, the π-stacking direction (the b-axis) also affords a favorable pathway for the carriers to move, provided that π-π stacking occurs between polymer chains. Meanwhile, the direction along the side chains (the a-axis)

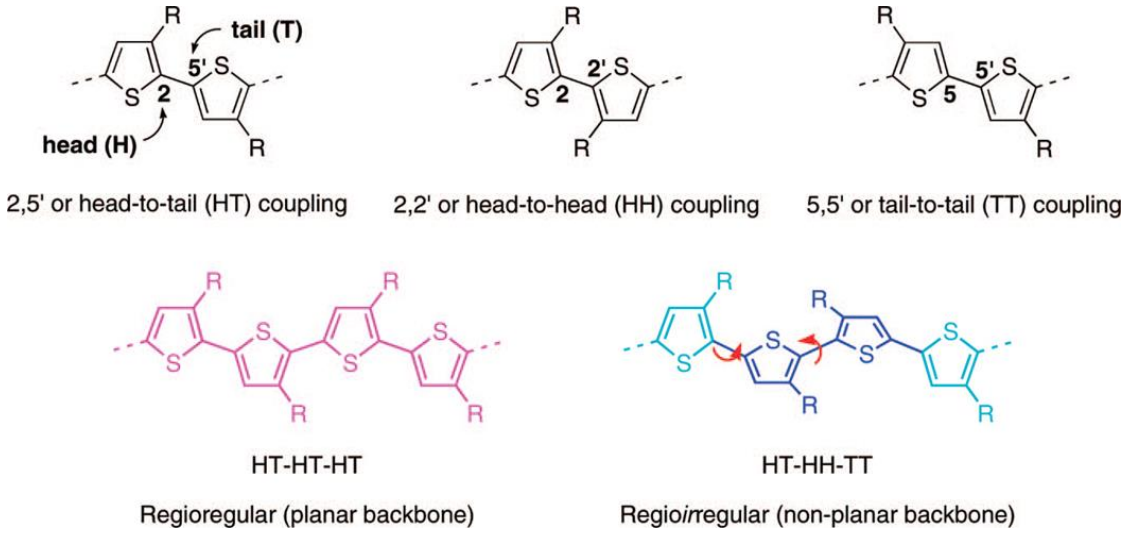

Figure 1.7: Regioisomeric couplings of 3-alkylthiophenes (top) and regioregular and regioirregular P3AT (bottom). Figure taken from[52].

would be expected not to allow favorable charge carrier transport but quantum mechanical tunneling, because the alkyl side chains act as a good insulator.

Molecular parameters such as polymer molecular weight (MW) and regioregularity (RR) significantly effect P3HT thin-film microstructure and resultant electrical properties.[42-45] The degree of RR is defined as the percentage of monomers adopting a head-to-tail configuration rather than head-to-head, which are depicted in Figure 1.7.

Higher MW material has been found to enhance macroscopic charge transport because it can provide favorable intramolecular charge transport through longer conjugated segments over interchain hopping, and the longer chains can act as conduits connecting crystalline domains that are separated by low conductivity amorphous regions.[43, 44] Further, it has been suggested that higher RR P3HT can afford better charge transport because of an increase in the charge hopping rate due to reduced reorganization energies and a reduction in the number of grain boundaries as a result of wider nanofibrils.[42]

In addition to modification of molecular parameters, processing parameter modifications have also been explored to achieve thin-film morphologies commensurate with efficient charge transport.[40, 46-51] Parameters such as solvent boiling point,[40] post-deposition processing (thermal or solvent vapor annealing),[46, 49] solution preparation method (sonication)[48, 50] and conjugated polymer solubility[47, 51] are known to impact the supramolecular self-assembly of the π-conjugated materials. For example, first, it was theorized that the higher boiling point limits solvent evaporation from the polymer matrix and thus increases the time available for crystallization during the spin-coating process.[52] Second, post-deposition thermal annealing of the P3HT films was reported to enhance polymer crystallinity and improve contact between the semiconductor and device electrodes, resulting in an increase of charge transport.[46] Third, molecular ordering of P3HT chains was enhanced upon exposure of the polymer film to *o*-dichlorobenzene vapor, resulting in enhanced mobility of resultant films.[49] Finally, ultrasonic irradiation of P3HT solution was found to promote π-stacking induced molecular aggregation, which leads to an increase in mobility.[48]

1.2 Charge transport in Polymeric Semiconductors

1.2.1 Characterization of Charge Mobility

The performance of any device such as OLEDs, OFETs, and solar cells, depends critically on the charge carrier mobility of OSCs which are employed as active layers. In this section, an introduction to the fundamental theory of charge transport in OSCs will be described, which will be useful for understanding some of the results presented in this thesis.

Over the years, OSCs have been designed that preferentially transport holes or electrons.[53] In most cases, such distinction reflects the ease of charge injection from electrodes used in devices rather than the actual ability of the materials to transport charges. In that context, a material is referred to as hole [electron] transporter, when its ionization energy (HOMO level) [electron affinity (LUMO level)] closely matches the Fermi level of the electrode material.[53] In addition, some materials, which can transport both holes and electrons, are referred to as ambipolar transporters.[53]

The charge carrier mobility is the key characteristic that quantifies charge transport in a material. In the absence of any externally applied potential difference, charge carriers are diffusive via a random walk process and can be described by Equation1.1:

$$< x^2 > = nDt \tag{1.1}$$

where $< x^2 >$ denotes the mean square displacement of the charges, D is the diffusion coefficient, t is the time and n represents 2, 4, or 6 for one-, two-, and three-dimensional systems, respectively. The charge mobility μ can be correlated with the diffusion coefficient by the Einstein-Smoluchowski equation (Equation 1.2):

$$\mu = eD/k_BT \tag{1.2}$$

where k_B is the Boltzmann constant, e is the electron charge, and T is the temperature.

An external electric field is typically applied across the organic semiconductors in practical devices, and thus causes the charge carriers to drift in response. The mobility is now defined as the ratio between the velocity, v, of the charges and the amplitude of the applied electric field, F, as depicted in Equation 1.3:

$$\mu = v/F \tag{1.3}$$

Since the carrier mobility corresponds to velocity over electric filed, it is expressed in cm^2/Vs.

1.2.2 Charge Motion in Organic Semiconductors

In inorganic semiconductors, band theory can be applied to model the transport of charges; three dimensionally bonded constituent atoms lead to the delocalization of the electronic states and the formation of well-established valence and conduction bands, through which charge carriers ballistically move with occasional scattering of the carriers at defects, contamination sites, and phonons.[17, 54] Therefore in inorganic semiconductors, room temperature mobilities typically reach high values ranging from 10^2–10^4 $cm^2V^{-1}s^{-1}$.[17] Meanwhile, charge transport in organic semiconductors is limited by hopping between conjugated segments since intermolecular interactions between adjacent semiconductor molecules are of much weaker van der Waals and London forces, which leads to highly disordered semiconductors, and thereby electron localization in polymer chains even in the presence of weak disorder.[17, 54] As a result, the mobilities in OSCs are found to be orders

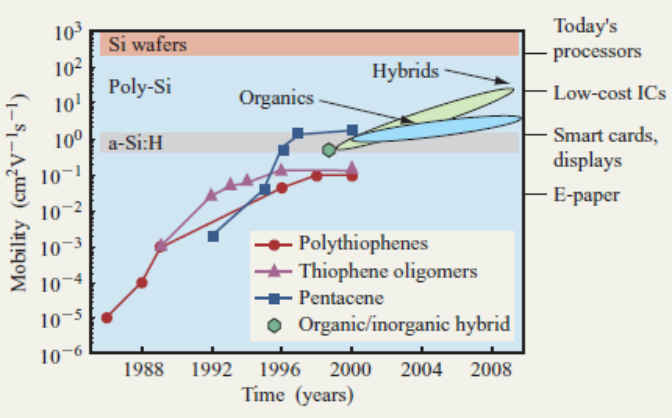

Figure 1.8: Mobility of typical organic semiconductors. Figure obtained from[17].

of magnitude lower (≤ 10 $cm^2V^{-1}s^{-1}$) than those in inorganic counterparts.[17] Figure 1.8 shows the mobility of representative set of organic semiconductors relative to that of c-Si.

1.2.3 Main Charge Transport Models

As aforementioned, the motion of carriers in OSCs is typically governed by hopping transport. Although many hopping models have been suggested to explain charge transport in OSCs, those models are mainly based on two popular models, the Miller-Abrahams and Marcus models.[25, 54-56]

The Miller-Abrahams model represents two different processes, phonon-assisted hopping or direct tunneling, which can occur between two localized states.[55] Tunneling can take place, provided that the electronic wavefunctions of the two sites effectively overlap, while charge carriers hop to the next available site (i.e., from *i* to *j* site) when carriers trapped in localized states absorb a phonon through a thermally activated process.[55] The transition rate (V_{ij}) associated with the processes is depicted by Equation 1.4:[55]

$$V_{ij} = \nu_0 \exp\left(-2\gamma R_{ij}\right) \times \begin{cases} \exp\left[-\left(\frac{\varepsilon_j - \varepsilon_i}{k_B T}\right)\right] & \varepsilon_j > \varepsilon_i \\ 1 & \varepsilon_j < \varepsilon_i \end{cases} \quad (1.4)$$

where ν_0 is the phonon vibration frequency (sometimes called attempt-to-escape frequency), γ is the inverse localization radius, R_{ij} is the distance between two localized states, and $\mathcal{E}_i$ and $\mathcal{E}_j$ are the energy levels of the respective sites. The first exponential term denotes the tunneling contribution, which decreases in electronic coupling with distance. The last term is a Boltzmann factor for a jump upward in energy ($\Delta\mathcal{E}_{ij} > 0$) and is equal to 1" for a jump downward in energy ($\Delta\mathcal{E}_{ij} < 0$), which represents the contribution of absorbing

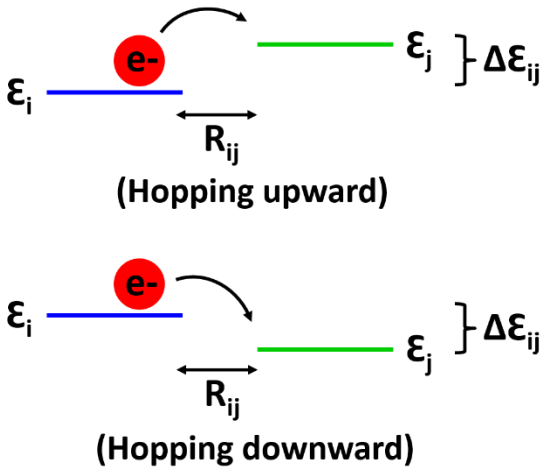

Figure 1.9: Charge transfer between two localized states: hopping upward and hopping downward.

a phonon for carriers to hop to the next available site. For better understanding, both hopping modes are depicted in Figure 1.9. This model does not account for relaxation of the local site configurations.[25, 54]

In contrast, the Marcus expression for semi-classical electron transfer rates accounts for the relaxation of the local site configuration, which is the theory of electron transfer reactions in chemical systems.[56] Figure 1.10 depicts the process of charge hopping suggested in the Marcus theory. In this model, the hopping process is the transfer of a charge carrier from an ionized molecule M^- to a neutral molecule M. The ionized and neutral states exhibit different geometries, and thus intra- or intermolecular relaxation takes place as the geometries switch between the two states of the molecule in the redox reaction. The hopping rate from site *i* to *j* across the distance R_{ij} is described by Equation 1.5:[56]

$$V_{ij} = \frac{J^2}{\hbar}\left[\frac{\pi}{\lambda_{reorg} k_B T}\right]^{1/2} exp\left[-\frac{(\lambda_{reorg}+\varepsilon_j-\varepsilon_i)^2}{4\lambda_{reorg} k_B T}\right] \quad (1.5)$$

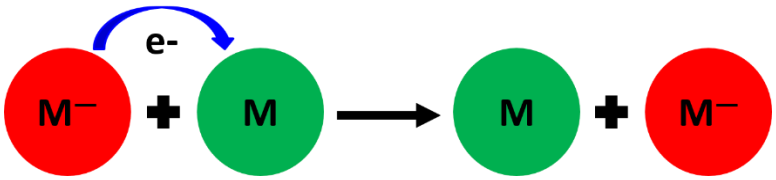

Figure 1.10: The process of charge hopping proposed in the Marcus theory.

where J is the transfer integral (i.e., the wavefunction overlap between sites i and j), which is proportional to the tunneling contribution ($J = J_0 \exp(-\gamma R_{ij})$), ħ is the Plank's constant, λ_{reorg} is the reorganization energy related the polaron relaxation, which is sometimes called self-trapping because the molecule is distorted by the charge, resulting in a lattice polarization and thus decrease in site energy, and $\Delta\mathcal{E}_{ij}$ ($= \mathcal{E}_i - \mathcal{E}_j$) is the energy difference of the two chosen sites. The transfer integral is a measure of the degree of electronic coupling between the molecules involved in the self-exchange reaction, and the reorganization energy is the energy required to bring about these geometry switches. Only the transfer integral is approximated instead of the attempt-to-escape frequency, unlike the Miller-Abrahams model. In addition, reorganization energy is considered as well as energetic site differences derived from a (often Gaussian) density of states distribution.[56]

Although both models yield similar results under many conditions, they are used in different contexts and are not exactly equivalent. The Miller-Abrahams expression is valid for weak electron-phonon (vibration) couplings and low temperatures, while Marcus theory is valid for strong electron-phonon couplings and high temperatures.[25, 54-56]

For macroscopic polycrystalline OSC layers, charge transport is often cast in the framework of a multiple trapping and release model.[25, 57] In this model, the OSC films are composed of small crystallites separated by amorphous grain boundaries. The carriers are delocalized in the crystallites, while the carriers are trapped and localized in the grain

boundaries. The trapped carriers in localized states hop to the next available sites through a thermally activated process, which is very similar to hopping transport described in both Miller-Abrahams and Marcus theory.

1.2.4 Experimental Measurements of Charge Carrier Mobility

The mobility of charge carriers can be an index of performance of OSC based devices, as mentioned in section1.2.1. Furthermore, it can also be used to understand correlations between morphology (micro- and macrostructure) and charge transport of OSC films. Various techniques have been developed that are useful to characterize the mobility of charge carriers in a range from the nano- to the macroscale distances. The basic principles of some of the most widely referenced methods are briefly discussed below.

1.2.4.1 Time of Flight (TOF)

An organic layer with a few micron thickness is sandwiched between two electrodes. The material is then irradiated by a laser pulse in close proximity to one of electrodes to generate photo-carriers. A potential difference applied across the two electrodes and the corresponding electric field (in the 10^4–10^6 V/cm range) cause the photo-generated holes and electrons to migrate across the material toward the second electrode. The photo-current at the collecting electrode is recorded as a function of time, indicative of the mobility of carriers. A sharp signal of photo-current vs. time profile is obtained in the case of highly ordered materials while the signal is broaden due to a dispersive distribution of arrival times of the photo-generated carriers. The mobility of the holes or electrons is calculated via Equation 1.6:

$$\mu = v/F = d/Ft = d^2/Vt \tag{1.6}$$

where μ is the TOF mobility, v is the drift velocity of the photo-generated carriers under the applied electric field, F, t is the averaged transient time, d is the sample thickness, and V is the applied voltage.

1.2.4.2 Diode Configuration

Like the geometry of a typical TOF measurement setup, diode configurations have a sandwich structure with an OSC film sandwiched between two electrodes, which can also be used to obtain the mobility of charge carriers, provided that charge transport is bulk limited and not contact limited. Electrodes are generally selected in such a way that either electrons or holes but not both are favorably injected at low voltage. This technique provides for an independent estimation of both the electron and hole mobilities. A space charge region is formed by the injected charge carriers in close proximity to the injecting electrode for an ohmic contact between the semiconductor and the metal. Characteristics of a space-charge limited current (SCLC) appears in the absence of traps and at low electric fields; the current density (*J*) through the semiconductor scales quadratically as a function of the applied bias (*V*), which is obtained by Equation 1.7:

$$J = \frac{9}{8}\varepsilon_0\varepsilon_r\mu\frac{V^2}{L^3} \tag{1.7}$$

where ε_0 and ε_r represents the permittivity of free space and the semiconductor respectively, and L is the film thickness. The field-dependent mobility can be then extracted from the *J–V* characteristics of the SCLC diode.

1.2.4.3 Pulse-Radiolysis Time-Resolved Microwave Conductivity (PR-TRMC)

Charge carrier mobilities of bulk films as well as single polymer chains in solution can be estimated by PR-TRMC, which unlike SCLC is a contact-free technique, and

therefore is not affected by space-charge effects. The sample is excited with a pulse of highly energetic electrons, which creates a low density of free charge carriers. The change in electrical conductivity is led by the advent of free charge carriers in the sample, which is estimated by measuring the change in the microwave power reflected by the sample and is therefore frequency dependent. The change in conductivity, $\Delta\sigma$, can be defined by Equation 1.8:

$$\Delta\sigma = e \sum \mu N_{e-h} \tag{1.8}$$

Where $\sum\mu$ is the sum of hole and electron mobilities and $N_{e\text{-}h}$ is the density of generated electron-hole pairs, which is estimated by dividing the total energy dose transferred to the material by the energy required to create an electron-hole pair. The PR-TRMC technique can be particularly useful to investigate intra- and interchain transport in conjugated polymers because the spatial extent, over which the mobility is averaged, can be readily tuned by changing the frequency of the microwave radiation, indicating that mobility of OSCs can be estimated in a range spanning multiple length scales.

1.2.4.4 Field-Effect Transistor Configuration

The carrier mobilities can also be estimated by an FET geometry which is more popularly known as the metal oxide semiconductor field-effect transistor (MOSFET). OFETs are the organic equivalents of the MOSFET and thus represent a 3-terminal (i.e., source, drain, and gate) device configuration. Moreover, as well as being a measurement technique, OFETs are directly used in the active matrix circuitry of liquid crystal displays, in which they are employed as thin film transistors or TFTs.[58] In this thesis, the OFET is used as the primary device that is fabricated and tested in order to investigate charge

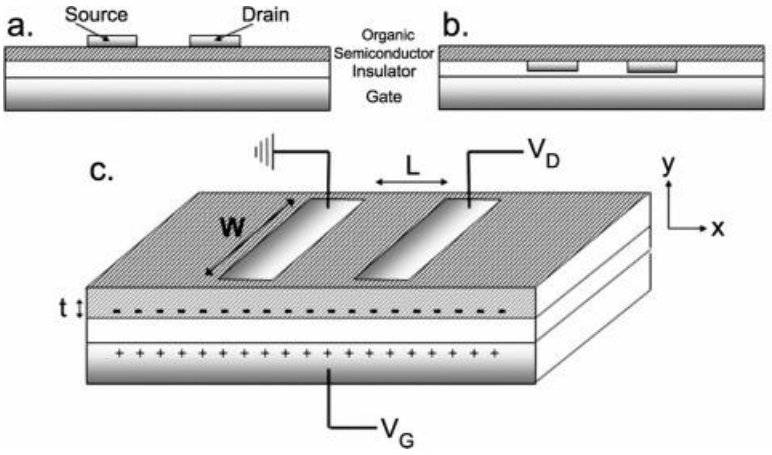

Figure 1.11: Schematic illustration of (a) top and (b) bottom contact OFETs. (c) Relevant voltages and geometry for an OFET. Figure taken from[53].

transport properties in the OSC thin films and hence the operation of OFETs will be discussed in more detail.

OFETs have been commonly fabricated with bottom-gate/top-contact and bottom-gate/bottom-contact transistor geometries as depicted in Figure 1.11a and b.[53] An organic semiconductor film is deposited on a gate/insulator substrate and is contacted with metallic source and drain electrodes. Typically, the channel length (L) between the source and drain electrodes is in the range of 10–100 μm, and the channel width (W) is between 100 μm and 1 mm (Figure 1.11c).[53] In this thesis, a bottom-gate/bottom-contact geometry is employed because of the ease of device fabrication. The processes of OFET device fabrication will be described in more detail in Chapter 2.

The operation of OFETs takes place in the accumulation mode, unlike that of MOSFETs, which occurs in the inversion mode. The gate electrode is separated from the organic semiconductor by the gate dielectric, forming a metal-insulator-semiconductor (MIS) capacitor.[53] As depicted in Figure 1.11c, the application of a gate voltage (V_G) induces accumulation of charge carriers at the semiconductor-dielectric interface, and then

the charge carriers subsequently flow upon the application of a potential difference between the source and drain electrodes ($V_D - V_S$). The source is typically grounded. For example, in p-channel operation of the OFET, application of a negative gate voltage causes the accumulation of holes in the channel region of the transistor, which flow under the influence of a negative drain voltage. The total capacitance of the dielectric (i.e., dielectric thickness and constant) determines the density of accumulated charges in the channel region of the transistor. In general, the charges accumulate in a 1–2 nm thick region of the semiconductor at the interface with the gate dielectric, which forms a conducting channel for hole transport.[59] Therefore, the charge carrier mobility in OFETs would be profoundly affected by the micro- and macrostructures of the first few monolayers of the organic film in contact with the gate dielectric.

The gradual channel or Shockley approximation is considered to calculate current-voltage characteristics of the OFET, which assumes that the lateral electric field between the source and drain is negligible compared to the vertical field across the thickness of the film. This condition is fairly well satisfied since typically channel lengths of the transistor, L, are orders of magnitude higher than the thickness (a few tens of nanometers).[27, 53] OFETs can operate in two regions (i.e., the linear and the saturation region), depending on the magnitude of the drain voltage relative to the gate voltage.[29, 53] Figure 1.12a shows that the charge density is uniform under a gate voltage (V_G) when drain voltage (V_D) is equal to "0". As shown in Figure 1.12b, a linear gradient of the charge concentration within the channel region begins to appear as V_D increases up to some point less than the difference between V_G and V_T (i.e., $V_D < V_G - V_T$). V_T is the threshold voltage defined as the voltage

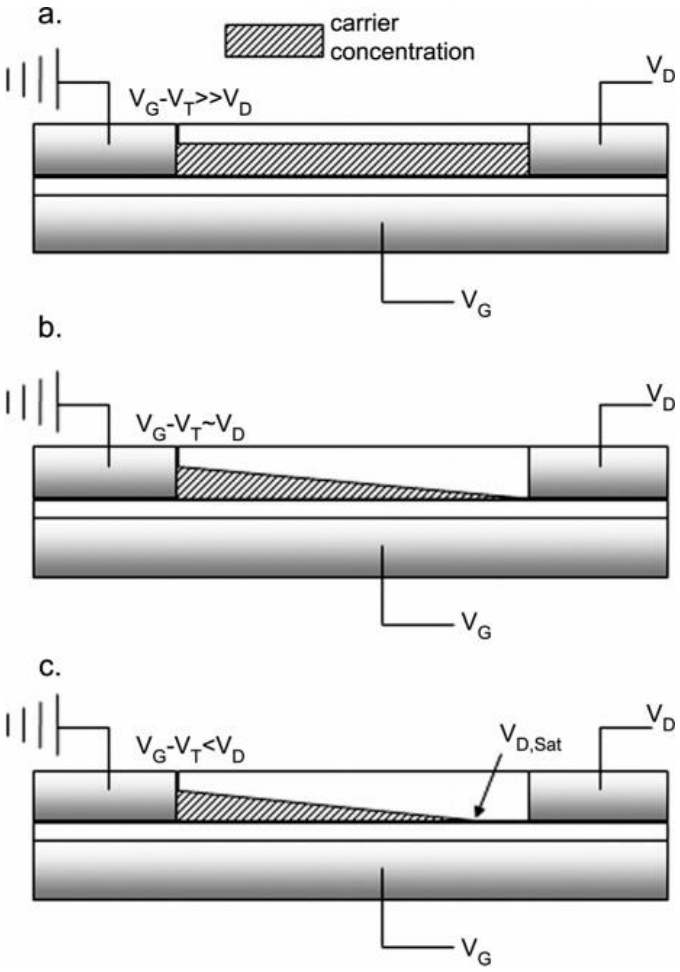

Figure 1.12: (a) Carrier concentration profile of OFET in the linear region. (b) Pinch-off occurs when $V_D \approx V_G - V_T$. (c) Carrier concentration profile of OFET in the saturation region. Figure taken from[53].

required to induce mobile charge carriers in the channel. Equation 1.9 depicts current-voltage characteristic of the OFET in the linear region:

$$I_{D,linear} = \frac{W}{L}\mu C_{ox}(V_G - V_T)V_D \tag{1.9}$$

where I_D is drain current, μ depicts charge carrier mobility, and C_{ox} is the capacitance of the gate dielectric. As V_D is further increased up to some point, where V_D is equal to $V_G - V_T$, charge carriers become depleted near the drain contact, so called "pinch point" (Figure 1.12b). This pinch point is slightly moved backward toward the source electrode with

further increases in V_D (i.e., $V_D > V_G - V_T$) (Figure 1.12c). With further increases in V_D, carriers are swept away across the narrow space charge region from the pinch point to the drain by the high electric field in the depletion region, while the integrated resistance of the channel from the source to the pinch point remains the same provided that the device length, L, is much longer than the width of this depletion region.[53] The current-voltage characteristics of the OFET in the saturation region is defined by Equation 1.10:

$$I_{D,sat} = \frac{W}{2L}\mu C_{ox}(V_G - V_T)^2 \quad (1.10)$$

In this thesis, the mobility of OFETs is calculated in the saturation region because the mobility in the linear region is often affected by source and drain contact resistance or high electric fields.[53, 54]

1.3 Motivation and Outline of Thesis

Commercialization of polymer-based electronic devices has been restricted largely due to low device performance, even though such devices can provide for generally lighter, more flexible, and cheaper to fabricate structures than inorganic-based electronic devices (Figure 1.13). In order to enhance the charge carrier mobility of OSC thin films, various processing parameters such as film deposition method (spin vs. drop cast),[60] solvent boiling point (low vs. high boiling point),[40] polymer-dielectric interface treatment,[61] and post-deposition processing (solvent vapor or thermal annealing)[46, 49] have been modified, as well as molecular parameters (e.g., polymer molecular weight (MW) and regioregularity (RR)).[42-45] In this thesis, the modification of processing parameters will be the primary strategy to enhance charge carrier mobility of the semiconducting polymer thin films.

Typically, process modifications have been explored for enhancing the crystallinity, namely intra- and intermolecular ordering of organic materials in the solid state.[40, 42-49, 60] Given the importance of crystallinity on the intra- and intermolecular charge transport properties of conjugated polymer films, the enhancement of crystallinity of such materials should lead to improved charge carrier mobility within the resultant films.

However, the methods mentioned above are not appropriate for large-scale fabrication and high-throughput processing of polymer-based devices. The use of high boiling point solvents[40] and thermal annealing[46] involves high temperature processes after thin-film deposition, which should be conducted under extremely low oxygen and moisture concentrations to avoid polymer degradation, and could give rise to deformation of a flexible, low glass transition temperature substrate. Polymer-dielectric interface treatments[61] using self-assembled monolayers have been used as another technique for mobility enhancement. However, it is often difficult to achieve monolayer coverage through the deposition steps, and also moisture free environments are required. Unfortunately, the approaches using different deposition techniques (dip-coating and drop-casting)[60] have not achieved significant improvement in mobility.

Therefore, in this thesis, we identify alternative processing parameters, which can contribute to enhancement of molecular ordering and charge transport characteristics of OSCs, eliminating the additional pre- and/or post-steps mentioned above. Further, we developed an understanding of the relationship between the processing parameters, intra- and intermolecular ordering of the polymer chains, micro- through macroscopic morphologies, and thus charge transport characteristics of the thin-films. In this thesis, P3HT is used as a primary model polymer, and the OFET is used as the primary device

that is fabricated and tested to characterize charge transport properties in the polymer films. The processes involved with fabrication of the OFET devices are detailed in Chapter 2. The results and analysis of the data follow in the next three chapters. Each chapter is divided into several sections (i.e., Introduction, Experimental methods, Results and Discussion, and Conclusion).

In Chapter 3, we demonstrate that supramolecular assembly and subsequent enhancement of charge transport characteristics of P3HT can be facilitated simply by adding small amounts of a more volatile poor solvent, which can interact with the majority solvent through dipole-dipole interactions. The relationship between processing conditions, micro- to macroscopic morphologies, and field-effect mobilities of resultant films is investigated. Hansen solubility parameters are used to systematically understand how the solvent mixture enhances the alignment and assembly of polymer chains and influences subsequent thin film properties. A mechanistic illustration of the molecular ordering process during film formation is postulated.

Chapter 4 highlights that UV irradiation can enhance intramolecular ordering of solubilized polymer chains, and thereby promote formation of anisotropic supramolecular polymer assemblies via favorable π-π stacking (intermolecular interaction), resulting in dramatic enhancement in charge transport characteristics of corresponding films. The study on how UV irradiation times effect micro- through macrostructures, and thus charge carrier mobilities of resultant films is conducted.

In Chapter 5, we investigate how a sequentially combined two different solution treatment methods (i.e., ultrasonication and UV irradiation) impact on inter- and intramolecular interactions of P3HT chains, micro- to macroscale morphologies, and

charge transport characteristics of the resultant films. It is demonstrated that the sequentially combined ultrasonication and UV irradiation of P3HT solutions can maximize the charge carrier mobility of the corresponding films via a synergetic effect of the solution treatment methods.

Chapter 6 summarizes the main findings in each chapter and discusses recommendations for future research.

1.4 References

[1] Burroughes, J. H.; Bradley, D. D. C.; Brown, A. R.; Marks, R. N.; Mackay, K.; Friend, R. H.; Burns, P. L.; Holmes, A. B. Light-Emitting Diodes Based on Conjugated Polymers. *Nature* **1990**, *347*, 539-541.

[2] Friend, R. H.; Gymer, R. W.; Holmes, A. B.; Burroughes, J. H.; Marks, R. N.; Taliani, C.; Bradley, D. D. C.; Dos Santos, D. A.; Bredas, J. L.; Logdlund, M.; Salaneck, W. R. Electroluminescence in Conjugated Polymers. *Nature* **1999**, *397*, 121-128.

[3] Han, T. H.; Lee, Y.; Choi, M. R.; Woo, S. H.; Bae, S. H.; Hong, B. H.; Ahn, J. H.; Lee, T. W. Extremely Efficient Flexible Organic Light-Emitting Diodes with Modified Graphene Anode. *Nat. Photon.* **2012**, *6*, 105-110.

[4] Thomas, S. W.; Joly, G. D.; Swager, T. M. Chemical Sensors Based on Amplifying Fluorescent Conjugated Polymers. *Chem. Rev.* **2007**, *107*, 1339-1386.

[5] Huang, H. M.; Wang, K.; Tan, W. H.; An, D.; Yang, X. H.; Huang, S. S.; Zhai, Q.; Zhou, L.; Jin, Y. Design of a Modular-Based Fluorescent Conjugated Polymer for Selective Sensing. *Angew. Chem. Int. Ed.* **2004**, *43*, 5635-5638.

[6] Janata, J.; Josowicz, M. Conducting Polymers in Electronic Chemical Sensors. *Nat. Mater.* **2003**, *2*, 19-24.

[7] You, C. C.; Miranda, O. R.; Gider, B.; Ghosh, P. S.; Kim, I. B.; Erdogan, B.; Krovi, S. A.; Bunz, U. H. F.; Rotello, V. M. Detection and Identification of Proteins Using Nanoparticle–Fluorescent Polymer 'Chemical Nose' Sensors. *Nat. Nanotechnol.* **2007**, *2*, 318-323.

[8] Park, S. H.; Roy, A.; Beaupre, S.; Cho, S.; Coates, N.; Moon, J. S.; Moses, D.; Leclerc, M.; Lee, K.; Heeger, A. J. Bulk Heterojunction Solar Cells with Internal Quantum Efficiency Approaching 100%. *Nat. Photonics* **2009**, *3*, 297-302.

[9] Li, G.; Zhu, R.; Yang, Y. Polymer Solar Cells. *Nat. Photonics* **2012**, *6*, 153-161.

[10] Lipomi, D. J.; Tee, B. C. K.; Vosgueritchian, M.; Bao, Z. N. Stretchable Organic Solar Cells. *Adv. Mater.* **2011**, *23*, 1771-1775.

[11] Kim, B. G.; Jeong, E. J.; Chung, J. W.; Seo, S.; Koo, B.; Kim, J. S. A Molecular Design Principle of Lyotropic Liquid-Crystalline Conjugated Polymers with Directed Alignment Capability for Plastic Electronics. *Nat. Mater.* **2013**, *12*, 659-664.

[12] Qiu, L. Z.; Lee, W. H.; Wang, X. H.; Kim, J. S.; Lim, J. A.; Kwak, D.; Lee, S.; Cho, K. Organic Thin-film Transistors Based on Polythiophene Nanowires Embedded in Insulating Polymer. *Adv. Mater.* **2009**, *21*, 1349-1353.

[13] Sirringhaus, H. Device Physics of Solution-Processed Organic Field-Effect Transistors. *Adv. Mater.* **2005**, *17*, 2411-2425.

[14] Ikawa, M.; Yamada, T.; Matsui, H.; Minemawari, H.; Tsutsumi, J.; Horii, Y.; Chikamatsu, M.; Azumi, R.; Kumai, R.; Hasegawa, T. Simple Push Coating of Polymer Thin-Film Transistors. *Nat. Commun.* **2012**, *3*,1176.

[15] Gutmann, F.; Lyons, L. E. "*Organic Semiconductors"*, John Wiley & Sons, Inc., **1967**.

[16] Garnier, F. Scope and Limits of Organic–Based Thin–Film Transistors. *Phil. Trans*. **1997**, 355, 815-827.

[17] Shaw, J. M.; Seidler, P. F. Organic Electronics: Introduction. *IBM J. Res. Dev.* **2001**, 45, 3-9.

[18] Deboer, C., "Organic LED Display", www.audioholics.com (Accessed September 1, 2014).

[19] Kaminski, I., "Risø DTU and Mekoprint Mass Produce Polymer Solar Cells", www.renewableenergyfocus.com/view/19406/ris-dtu-and-mekoprint-mass-produce-polymer-solar-cells/ (Accessed August 4, 2014).

[20] Jackson, T.N. Organic Semiconductors: Beyond Moore's Law. *Nat. Mater*. **2005**, 4, 581-582.

[21] Teoh, V., "LG 55EA980W Curved OLED TV Review", www.hdtvtest.co.uk/news/55ea980w-201312083487.htm (Accessed August 4, 2014).

[22] Dimitrakopoulos, C. D.; Mascaro, D. J. Organic Thin-Film Transistors: A Review of Recent Advances. *IBM J. Res. Dev.* **2001**, 45, 11-27.

[23] Patel, D. G.; Benedict, J. B. (2012). Crystals in Materials Science, "Recent Advances in Crystallography", Dr. Jason B. Benedict (Ed.), ISBN: 978-953-51-0754-5, InTech, DOI: 10.5772/50791.

[24] http://photonicswiki.org/images/1/1b/Conjugated_polymer_common.png (Accessed August 4, 2014).

[25] Coropceanu, V.; Cornil, J.; Filho, D. A. da Silva; Olivier, Y.; Silbey, R.; Bredas, J. L. Charge Transport in Organic Semiconductors. *Chem. Rev*. **2007**, 107, 926-952.

[26] http://lmom.epfl.ch/courses/class_organic_electronic_materials_22.pdf (Accessed August 4, 2014).

[27] Aiyar, A., "Understanding the Impact of Polymer Self-organization on the Microstructure and Charge Transport in Poly(3-hexylthiophene)", Doctoral dissertation, https://smartech.gatech.edu/handle/1853/43574 (Accessed August 4, 2014).

[28] Salaneck, W. R.; Friend, R. H.; Bredas, J. L. Electronic structure of conjugated polymers: Consequences of electron–lattice coupling. *Phys. Rep.* **1999**, 319, 231-251.

[29] Bao, Z.; Locklin, J. J., "Organic Field-Effect Transistors", volume 128, CRC, **2007**.

[30] Bredas, J. L.; Cornil, J.; Heeger, A. J. The Exciton Binding Energy in Luminescent Conjugated Polymers. *Adv. Mater*. **1996**, 8, 447-452.

[31] Bredas, J. L.; Street, G. B. Polarons, Bipolarons, and Solitons in Conducting Polymers. *Acc. Chem. Res*. **1985**, 18, 309-315.

[32] Briseno, A. L.; Mannsfeld, S. C. B.; Ling, M. M.; Liu, S.; Tseng, R. J.; Reese, C.; Robert, M. E.; Yang, Y.; Wudle, F.; Bao, Z. Patterning Organic Single-Crystal Transistor Arrays. *Nature* **2006**, 444, 913-917.

[33] Appleton, A. L.; Brombosz, S. M.; Barlow, S.; Sears, J. S.; Bredas, J. L.; Marder, S. R.; Bunz, U. H. F. Effects of Electronegative Substitution on the Optical and Electronic Properties of Acenes and Diazaacenes. *Nat. Commun*. **2011**, 1, 91.

[34] McCulloch, I. Thin Films: Rolling Out Organic Electronics. *Nat. Mater*. 2005, 4, 583-584.

[35] Tsumura, A.; Koezuka, H.; Ando, T. Macromolecular electronic device: Field-Effect Transistor with a Polythiophene Thin Film. *Appl. Phys. Lett*. 1986, 49, 1210-1212.

[36] Elsenbaumer, R. L.; Jen, K. Y.; Miller, G. G.; Shacklette, L. W. Processible, Environmentally Stable, Highly Conductive Forms of Polythiophene. *Synth. Met*. **1987**, 18, 277-282.

[37] Bao, Z. N.; Lovinger, A. J. Soluble Regioregular Polythiophene Derivatives as Semiconducting Materials for Field-Effect Transistors. *Chem. Mater*. **1999**, 11, 2607-2612.

[38] McCullough, R. D.; Lowe, R. D.; Jayaraman, M.; Anderson, D. L. Design, Synthesis, and Control of Conducting Polymer Architectures: Structurally Homogeneous Poly(3-alkylthiophenes). *J. Org. Chem.* **1993**, 58, 904-912.

[39] McCulloch, I.; Heeney, M.; Bailwy, C.; Genevicius, K.; MacDonald, I.; Shkunov, M.; Sparrowe, D.; Tierney, S.; Wagner, R.; Zhang, W. Liquid-Crystalline Semiconducting Polymers with High Charge-Carrier Mobility. *Nat. Mater*. **2006**, 5, 328-333.

[40] Chang, J. F.; Sun, B.; Breiby, D. W.; Nielsen, M. M.; Solling, T. I.; Giles, M.; McCulloch, I.; Sirringhaus, H. Enhanced Mobility of poly(3-hexylthiophene) Transistors by Spin-Coating from High-Boiling-Point Solvents. *Chem. Mater*. **2004**, 16, 4772-4776.

[41] Surin, M.; Leclere, P.; Lazzaroni, R.; Yuen, J. D.; Wang, G.; Moses, D.; Heeger, A. J.; Cho, S.; Lee, K. Relationship between the Microscopic Morphology and the Charge Transport Properties in Poly(3-hexylthiophene) Field-Effect Transistors. *J. Appl. Phys*. **2006**, 100, 033712.

[42] Aiyar, A. R.; Hong, J. I.; Reichmanis, E. Regioregularity and Intrachain Ordering: Impact on the Nanostructure and Charge Transport in Two-Dimensional Assemblies of Poly(3-hexylthiophene). *Chem. Mater*. **2012**, 24, 2845-2853.

[43] Kline, R. J.; McGehee, M. D.; Kadnikova, E. N.; Liu, J. S.; Frechet, J. M. J. Controlling the Field-Effect Mobility of Regioregular Polythiophene by Changing the Molecular Weight. *Adv. Mater*. **2003**, 15, 1519-1522.

[44] Kline, R. J.; McGehee, M. D.; Kadnikova, E. N.; Liu, J. S.; Frechet, J. M. J.; Toney, M. F. Dependence of Regioregular Poly(3-hexylthiophene) Film Morphology and Field-Effect Mobility on Molecular Weight. *Macromolecules* **2005**, 38, 3312-3319.

[45] Zhang, R.; Li, B.; Iovu, M. C.; Jeffries-EL, M.; Sauve, G.; Cooper, J.; Jia, S. J.; Tristram-Nagle, S.; Smilgies, D. M.; Lambeth, D. N.; et al. Nanostructure Dependence of Field-Effect Mobility in Regioregular Poly(3-hexylthiophene) Thin Film Field Effect Transistors. *J. Am. Chem. Soc*. **2006**, 128, 3480-3481.

[46] Cho, S.; Lee, K.; Yuen, J.; Wang, G. M.; Moses, D.; Heeger, A. J.; Surin, M.; Lazzaroni, R. Thermal Annealing-Induced Enhancement of the Field-Effect Mobility of Regioregular Poly(3-hexylthiophene) Films. *J. Appl. Phys*. **2006**, 100, 114503.

[47] Park, Y. D.; Lee, H. S.; Choi, Y. J.; Kwak, D.; Cho, J. H.; Lee, S.; Cho, K. Solubility-Induced Ordered Polythiophene Precursors for High-Performance Organic Thin-Film Transistors. *Adv. Funct. Mater*. **2009**, 19, 1200-1206.

[48] Aiyar, A. R.; Hong, J. I.; Nambiar, R.; Collard, D. M.; Reichmanis, E. Tunable Crystallinity in Regioregular Poly (3-Hexylthiophene) Thin Films and Its Impact on Field Effect Mobility. *Adv. Funct. Mater.* **2011**, 21, 2652-2659.

[49] Fu, Y.; Lin, C.; Tsai, F. Y. High Field-Effect Mobility from Poly(3-hexylthiophene) Thin-Film Transistors by Solvent–Vapor-Induced Reflow. *Org. Electron.* **2009**, 10, 883-888.

[50] Kim, B. G.; Kim, M. S.; Kim, J. Ultrasonic-Assisted Nanodimensional Self-Assembly of Poly(3-hexylthiophene) for Organic Photovoltaic Cells. *ACS Nano* **2010**, 4, 2160-2166.

[51] Park, J. H.; Kim, J. S.; Lee, J. H.; Lee, W. H.; Cho, K. Effect of Annealing Solvent Solubility on the Performance of Poly(3-hexylthiophene)/Methanofullerene Solar Cells. *J. Phys. Chem. C* **2009**, 113, 17579-17584.

[52] Osaka, I.; McCullough, R. D. Advances in Molecular Design and Synthesis of Regioregular Polythiophenes. *Acc. Chem. Res.* **2008**, 41, 1202-1214.

[53] Newman, C. R.; Frisbie, C . D; Filho, D. A. da Silva; Bredas, J. L.; Ewbank, P. C.; Mann, K. R. Introduction to Organic Thin Film Transistors and Design of n-Channel Organic Semiconductors. *Chem. Mater*. **2004**, 16, 4436-4451.

[54] Tessler, N.; Preezant, Y.; Rappaport, N.; Roichman, Y. Charge Transport in Disordered Organic Materials and Its Relevance to Thin-Film Devices: A Tutorial Review. *Adv. Mater*. **2009**, 21, 2741-2761.

[55] Miller, A.; Abrahams, E. Impurity Conduction at Low Concentrations. *Phys. Rev*. **1960**, 120, 745-755.

[56] Marcus, R. A. Electron Transfer Reactions in Chemistry. Theory and Experiment. *Rev. Mod. Phys*. **1993**, 65, 599-610.

[57] Noolandi, J. Multiple-Trapping Model of Anomalous Transit-Time Dispersion in a-Se. *Phys. Rev. B* **1977**, 16, 4466-4473.

[58] Street, R. A. Thin-Film Transistors. *Adv. Mater.* **2009**, 21, 2007-2022.

[59] Horowitz, G.; Hajlaoui, R.; Bourguiga, R.; Hajlaoui, M. Theory of the Organic Field-Effect Transistor. *Synth. Met.* **1999**, 101, 401-404.

[60] Aiyar, A. R.; Hong, J. I.; Izumi, J.; Choi, D.; Kleinhenz, N.; Reichmanis, E. Ultrasound-Induced Ordering in Poly(3-hexylthiophene): Role of Molecular and Process Parameters on Morphology and Charge Transport. *ACS Appl. Mater. Interfaces* **2013**, *5*, 2368-2377.

[61] Kim, D. H.; Jang, Y.; Park, Y. D.; Cho, K. Surface-Induced Conformational Changes in Poly(3-hexylthiophene) Monolayer Films. *Langmuir* **2005**, *21*, 3203-3206.

CHAPTER 2

EXPERIMENTAL TECHNIQUES

As aforementioned, in this thesis, a bottom-gate/bottom-contact OFET device is fabricated and tested to investigate charge transport properties in P3HT thin films. Therefore, in this chapter, the processes involved with fabrication of the OFET device are described.

2.1 Substrate

SiO_2/Si substrates were purchased from Rogue Valley Microdevices, Inc. The first layer is highly doped silicon (~ 5 mm) that acts a common gate electrode. The second layer is a thermally grown silicon oxide (SiO_2) with a thickness of around ~ 300 nm, which serves as a dielectric that insulates the gate from the rest of the transistor. Such a SiO_2-layer has a capacity of $C_{OX} = 1.15 \times 10^{-8}$ F/cm^2.

2.2 Electrode Fabrication

Figure 2.1 depicts the sequence of steps required for the fabrication of the source and drain electrodes on the SiO_2/Si substrate described above. The source and drain contact is fabricated using a standard photolithography based lift-off process. A silicon oxide thermally grown on top of silicon is used as the substrate (Figure 2.1a). Photoresist (S1813, Shipley) is spin-coated on top of the SiO_2 layer at 3000 rpm for 30 sec, and then baked at 115 °C for 4 min in contact with a hot plate to remove residual solvents (Figure 2.1b). Subsequently, the resist is exposed using 405 nm UV light (Karl Suss MA6 mask aligner) with a total dose of 220 mW/cm^2 (Figure 2.1c), and in turn developed in MF-319 developer (Rohm and Haas, subsidiary of Dow Chemical Co.) for ca. 90 sec in order to define the

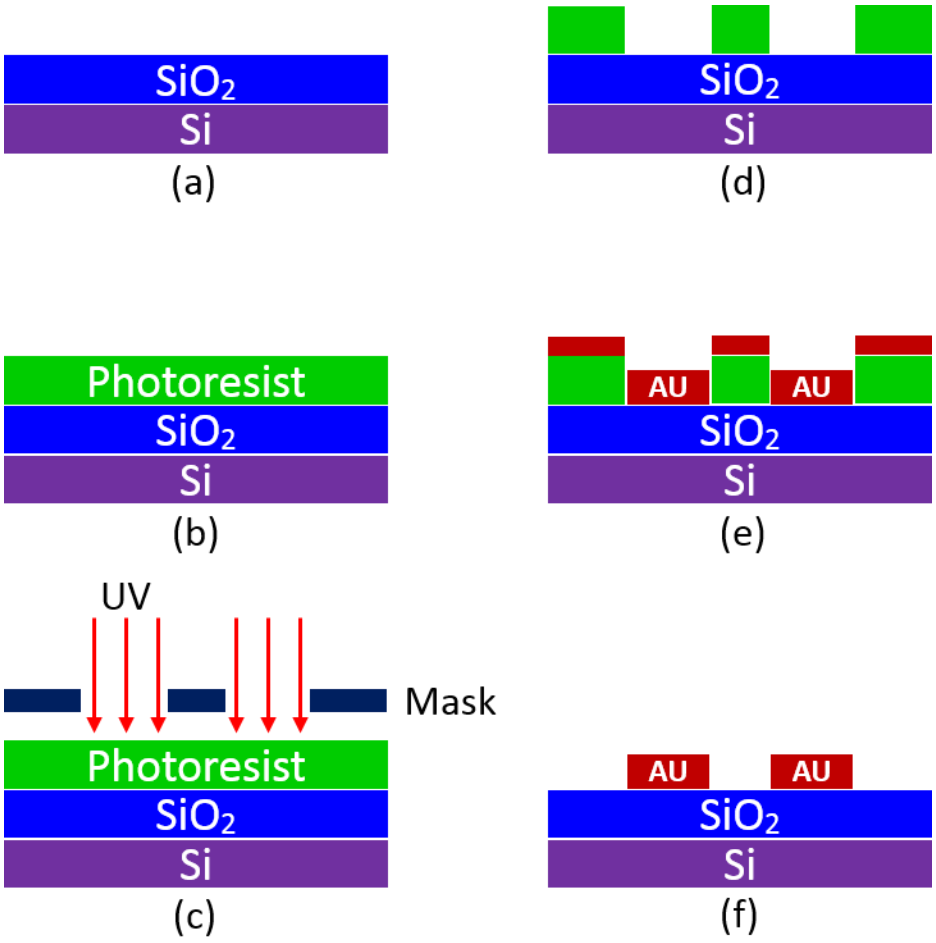

Figure 2.1: Fabrication steps of a bottom-gate/bottom-contact-OFET device: (a) SiO_2/Si substrate, (b) photoresist deposition, (c) UV exposure to the photoresist for patterning, (d) photoresist development, (e) metal electrode deposition, and (f) removal of the photoresist (lift-off) to define electrode.

electrode patterns in the resist (Figure 2.1d). Chromium as an adhesion layer is deposited with a thickness of 3 nm, followed by deposition of gold (50 nm) on the patterned substrate using Electron-Beam Evaporation (Denton Explorer) (Figure 2.1e). As the final step, any metal outside of the electrode pattern is removed along with the underlying photoresist through a resist lift-off process (Figure 2.1f). This process is performed by soaking the substrate in acetone over-night, and then the substrate is cleaned using ultrasonication of the substrate in acetone, methanol and isopropanol alcohol, sequentially. Figure 2.2 shows

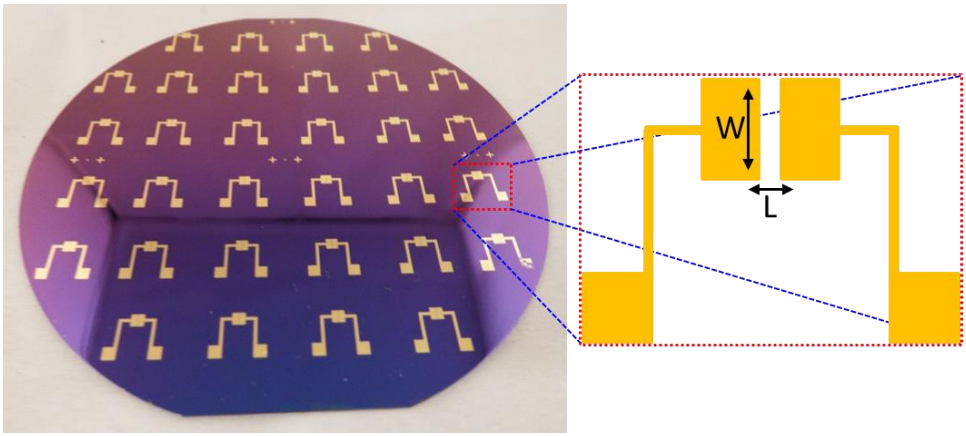

Figure 2.2: Schematic structure and photoimage of OFET devices fabricated on the SiO_2/Si substrate.

the OFET device substrate fabricated from the processes above. The wafer substrate consists of 32 devices, which is cut into individual device pieces before spin-coating polymer semiconductor solutions. In an individual device, the transistor channel width (*W*) is ca. 2000 μm and the length (*L*) is ca. 50 μm.

2.3 Organic Semiconductor Deposition

Prior to deposition of polymer semiconductors on the as-prepared OFET device substrates above, all device substrates are cleaned for 15 min in a UV-ozone cleaner (Novascan PSD-UV) to ensure complete removal of any residual photoresist and other organic contaminants. In a typical preparation of the polymer solutions, polymer semiconductors are dissolved in organic solvents with a concentration of 5 mg/mL in air. Subsequently, the solutions are stirred in a sealed vial for at least 30 min at ca. 55 °C, and then cooled down to room temperature. Deposition of polymer semiconductors is conducted by spin coating (WS-650MZ-23NPP, Laurell) as-prepared solutions onto pre-cleaned device substrates at a spin speed of 1500 rpm for 60 s in air. The devices are stored in a vacuum oven (1 Torr) overnight at room temperature to remove residual solvent.

CHAPTER 3

SOLVENT-SOLVENT INTERACTIONS: IMPACT OF POLY(3-HEXYLTHIOPHENE) NANOSCALE MORPHOLOGY AND CHARGE TRANSPORT CHARACTERISTICS*

3.1 Introduction

Conjugated polymer semiconductors have attracted great interest due to their low-temperature, solution-based processability, which may provide for low-cost, large-area electronic device fabrication.[1-6] While significant advances have been made, polymeric semiconducting materials are disadvantaged because of relatively low field-effect mobilities owing to the relatively low degree of polymer thin-film crystallinity.[7-9] Solution processed conjugated polymer films are typically semi-crystalline, comprised of many small crystalline regions embedded within a largely disordered matrix. This thin-film architecture impedes efficient charge hopping between transport sites.[7-9]

Poly(3-hexylthiophene) (P3HT) is a representative conjugated polymer that has been investigated for device applications due to its hole transporting properties, solubility in a range of organic solvents, and good film-forming properties.[10-17] Molecular parameters such as polymer molecular weight (MW) and regioregularity (RR) have been studied as means to control thin-film microstructure and resultant electrical properties.[16, 18-20] It was proposed that for higher MW material, the longer chain length enhances macroscopic charge transport because i) intramolecular charge transport through longer conjugated segments becomes favorable over interchain hopping, and ii) the longer chains connect crystalline domains that are separated by low conductivity amorphous regions.[18,

* *ACS Nano* **2013**, 7, 5402.

[19] Further, it was suggested that mobility increases as the RR increases because of an increase in the charge hopping rate due to reduced reorganization energies and a reduction in the number of grain boundaries as a result of wider nanofibrils.[16]

In addition to modification of molecular parameters, process modifications have also been explored for achieving thin-film morphologies commensurate with efficient charge transport.[13, 15, 21-27] Parameters such as solvent boiling point,[27] post-deposition processing (thermal or solvent vapor annealing),[13, 23] solution preparation method (sonication)[21, 24] and conjugated polymer solubility[15, 25] have been shown to impact the supramolecular self-assembly of the π-conjugated materials. For example, Sirringhaus et al. reported that use of high boiling point solvents helps promote formation of highly self-ordered microcrystalline structures in P3HT, thus significantly improving P3HT field effect mobility relative to that obtained from lower boiling point alternatives (ca. 10^{-1} cm^2 V^{-1} s^{-1} vs. 10^{-2} cm^2 V^{-1} s^{-1}).[27] It was theorized that the higher boiling point limits solvent evaporation from the polymer matrix and thus increases the time available for crystallization during the spin-coating process. Lee et al. demonstrated that annealing P3HT at high temperature (~ 150° C) increases polymer crystallinity and improves contact between the semiconductor and device electrodes, affording an increase in P3HT field-effect mobility,[13] while Tsai et al. showed that molecular ordering of P3HT chains was enhanced upon exposure of the polymer film to *o*-dichlorobenzene vapor.[23] Order of magnitude improvements in P3HT mobility can also be achieved by the solution preparation method. Aiyar et al. reported that ultrasonic irradiation of P3HT solutions promotes π-stacking induced molecular aggregation, which effects an increase in mobility.[21]

However, the approaches described above have limitations that may be undesirable for large-scale fabrication and high-throughput processing. The use of high boiling point solvents requires additional high temperature treatment to remove residual solvent after thin-film deposition. Thermal annealing could give rise to deformation of a flexible, low glass transition temperature substrate, or risk degradation of the semiconducting polymer itself; and solvent vapor annealing might present safety concerns.[28-31] The ultrasonic irradiation process requires immersion of the solution into a bath, presenting its own set of scale-up challenges.

Approaches that do not require a post-treatment to improve molecular ordering and charge transport in polymer semiconductors which use poor solvents have recently been reported.[15, 32-34] A poor solvent having a boiling point higher than that of the main solvent induced formation of ordered aggregates of polymer semiconductors during solvent evaporation. The less volatile poor solvent resides within the evolving film for a longer period of time and thus promotes aggregation. For example, Cho et al. reported that addition of the higher boiling non-solvent acetonitrile (bp 81° C) to a precursor solution of P3HT in chloroform (bp 61° C) led to enhanced two-dimensional ordering of P3HT chains and concomitant charge transport characteristics.[15] No post-treatment steps were required; the non-solvent is believed to promote formation of ordered P3HT aggregates during deposition via spin coating.[15] The same report emphasized that use of a lower boiling point poor solvent has no impact on the structure and morphology of resultant P3HT thin-films.[15] Thus, higher volatility poor solvents with respect to the majority component have not been investigated for inducing well-ordered π-conjugated polymer aggregates even though they present many favorable attributes with regard to processing thin films.[35-40]

In this chapter, we demonstrate that a higher volatility solvent that additionally undergoes molecular interactions with the majority solvent leads to enhanced supramolecular assembly of P3HT, a representative π-conjugated polymer semiconductor. Two-dimensional molecular ordering of the conjugated polymer film is controlled by varying the "poor" to "good" solvent ratio. A correlation between the molecular ordering of P3HT chains and resultant charge transport characteristics as measured by the field-effect mobility is demonstrated. The role of interactions between the main solvent and minority poor solvent is investigated by analysis of the evaporation rates. Hansen solubility parameters, including the dispersive solubility parameter (δ_D), the polar solubility parameter (δ_P) and the H-bonding solubility parameter (δ_H) of the polymer and solvent mixtures are used to understand how the binary solvent can enhance polymer supramolecular assembly and subsequently, the macroscopic charge transport characteristics of resultant thin-films. A mechanistic illustration of the polymer chain molecular ordering process is presented.

The approach described here utilizes fundamental principles and presents quantitative insights that could facilitate identification of solvent systems applicable to polymer semiconductor processing for electronic devices. Extension to organic-organic blends or organic-inorganic nanocomposites can be envisioned. The mechanistic approach using Hansen solubility parameters enhances understanding of the evolution of the nano- through macroscale morphology of solution processed polymer π-conjugated polymer materials and further, the complex relationship between materials morphology and charge transport characteristics.

3.2 Experimental Methods

3.2.1 Materials

P3HT (catalog no. 445703), chloroform (HPLC grade), acetone (HPLC grade), chlorobenzene (HPLC grade) and 2,3-dimethylbutane (analytical standard grade) were purchased from Sigma Aldrich and used without further purification. The P3HT used in this study had a M_n of 40.3 kD and M_w of 91.4 kD with respect to polystyrene standards as determined by Gel Permeation Chromatography (Waters 1515 Isocratic HPLC equipped with a Waters 2489 UV/Vis detector and Styragel HR 5E column) using tetrahydrofuran as the eluent. All data were processed using Breeze 2 software. The head to tail regioregularity (RR) was estimated to be approx. 92 % (Bruker DSX 300 1H NMR in deuterated chloroform solution at 293 K).

3.2.2 OFET Fabrication and Characterization

Two contact FET devices were prepared via spin coating the relevant P3HT solution onto a 300 nm thick SiO_2 gate dielectric. The highly doped silicon wafer served as the gate electrode, while Au/Cr was used for the source and drain contacts. The source and drain contacts were fabricated using a standard photolithography based lift-off process, followed by E-beam evaporation (Denton Explorer) of 50 nm Au contacts with 3 nm of Cr as the adhesion layer. Before spin coating P3HT solutions, all devices were cleaned for 15 min in a UV-ozone cleaner (Novascan PSD-UV) to ensure complete removal of any residual photoresist and other organic contaminants. In a typical preparation of the polymer solutions, 15 mg of P3HT was introduced into 3 mL of relevant solvent mixtures containing small amount of poor solvent (0, 0.5, 1, 2, 3 and 5 vol %) in air. Subsequently, the solutions were stirred in a sealed vial for at least 30 min at ca. 60 °C. OFETs were prepared by spin coating (WS-650MZ-23NPP, Laurell) the solutions onto pre-cleaned substrates at a spin

speed of 1500 rpm for 60 s in air, and tested in a nitrogen ambient using an Agilent 4155C semiconductor parameter analyzer.

3.2.3 UV-vis Spectroscopy

The solution and solid state UV-vis spectra were recorded using an Agilent 8510 UV-vis spectrophotometer. Films for solid state studies were prepared by spin coating the requisite solution onto pre-cleaned glass slides following the same procedures used to prepare OFET devices.

3.2.4 Grazing Incidence X-ray Diffraction (GIXD)

Out-of-plane grazing incidence X-ray diffraction data were obtained using a Panalytical X'Pert Pro system equipped with a Cu X-ray source operating at 45 kV and 40 mA. The grazing incidence angle was fixed at 0.2° and the detector was scanned from 3° to 30°. Peak positions were obtained from the measured profiles by fitting the peaks using the analysis software (MDI JADE). For the preparation of samples for GIXD measurements, P3HT solutions were spin coated onto hydrophilic silicon substrates with native oxide that were cleaned using the procedure employed for fabrication of bottom contact FET devices. The spin coating procedures and solutions were identical to those used for fabrication of OFET devices.

3.2.5 Atomic Force Microscopy (AFM)

The AFM measurements were performed on films spin coated onto bottom contact OFET substrates using a Veeco Digital Instruments Dimension 3100 scanning probe microscope operating in tapping mode with a silicon tip (NSC14, Mikro Masch).

Table 3.1: Solubility of P3HT in selected organic solvents.

Solvents	**P3HT (mg/mL at 25 °C)**
Chloroform	> 5
Hexane	< 1
Dimethyl Sulfoxide (DMSO)	< 1
Dimethyl Formamide (DMF)	< 1
N-Methyl-2-Pyrrolidone (NMP)	< 1
Acetonitrile	< 1
Acetone	< 1
Cyclohexanone	< 1
Benzyl Alcohol	< 1
Tetrahydrofuran (THF)	1 – 3
o-Dichlorobenzene	> 5
p-Xylene	1 – 3
Methanol	< 1
Trichloroethylene	> 5
1,2,4-Trichlorobenzene	> 5
Chlorobenzene	> 5
Toluene	2 – 4
Carbon Disulfide	> 5
Diethyl Ether	< 1
Thiophene	> 5
Pyridine	< 1

3.2.6 Hansen Solubility Parameter Determination

P3HT (1, 5 and/or 10 mg/mL) was mixed with 3 mL of solvent as per the defined procedure for solubility parameter determination (a list of solvents examined in this study are presented in Table 3.1) and heated at 60 °C for at least 3 h. Subsequently, the solutions

Table 3.2: Hansen solubility parameters of selected organic solvents and their relative energy difference (RED) to P3HT. δ_D, δ_P, and δ_H represent the dispersive, polar, and H-bonding solubility parameter, respectively.

Solvents	δ_D **(MPa$^{1/2}$)**	δ_P **(MPa$^{1/2}$)**	δ_H **(MPa$^{1/2}$)**	**RED**
Chloroform	17.80	3.10	5.70	0.89
Hexane	14.90	0.00	0.00	2.57
Dimethyl Sulfoxide (DMSO)	18.40	16.40	10.20	3.33
Dimethyl Formamide (DMF)	17.40	13.70	11.30	3.03
N-Methyl-2-Pyrrolidone	18.00	12.30	7.20	2.22
Acetonitrile	15.30	18.00	6.10	3.91
Acetone	15.50	10.40	7.00	2.52
Cyclohexanone	17.80	8.40	5.10	1.33
Benzyl Alcohol	18.40	6.30	13.70	2.39
Tetrahydrofuran (THF)	16.80	5.70	8.00	1.61
o-Dichlorobenzene	19.20	6.30	3.30	0.61
p-Xylene	17.80	1.00	3.10	1.09
Methanol	14.70	12.30	22.30	5.26
Trichloroethylene	18.00	3.10	5.30	0.77
1,2,4-Trichlorobenzene	20.20	4.20	3.20	0.43
Chlorobenzene	19.00	4.30	2.00	0.57
Toluene	18.00	1.40	2.00	1.06
Carbon Disulfide	19.90	5.80	0.60	0.98
Diethyl Ether	14.50	2.90	4.60	2.37
Thiophene	18.90	2.40	7.80	0.97
Pyridine	19.00	8.80	5.90	1.24

were cooled to ambient temperature where they remained for 6 h. The solubility parameters were determined from these solutions via visual examination. Solvents were categorized

as poor if they were unable to dissolve more than 5 mg of P3HT/mL of solvent and good if they were able to dissolve more than 5mg of polymer/mL of solvent. For the purposes of Hansen solubility parameter (HSP) analysis using requisite software (Hansen Solubility Parameters in Practice 3rd edition), a poor solvent was assigned a value of "0" and good solvent was assigned a value of "1". The HSP software package creates a sphere in Hansen space based on the coordinates of the good solvents, while excluding those of the poor solvents. The center of the sphere represents the HSPs for P3HT. The fitting accuracy appeared with a value of "1", indicating the best fit. The value is determined by the program which evaluates the input data using a quality of fit function.[41] Table 3.1 summarizes the solubility results of P3HT in the organic solvents evaluated here, and Table 3.2 presents the HSPs for the solvents along with values of their relative energy difference (RED) to P3HT.

3.3 Results and Discussion

3.3.1 Selection of Solvent Mixtures

The effect of solvent-solvent and solvent-solute interactions on the optical properties, nano- through macro-structure, and charge transport characteristics of solidified P3HT thin-films were evaluated using alternative deposition solvents comprised of a "good"/"poor" solvent blend. Chloroform (bp 61° C) and chlorobenzene (bp 131° C) were used as representative good solvents for the polythiophene (solubility > 10 mg/mL), and are among the most commonly used solvents for π-conjugated polymer semiconductor processing.[25, 26, 42] Two poor solvents, both of which are relatively volatile, were selected. P3HT exhibits poor solubility (solubility less than 0.1 mg/mL) in acetone and 2,3-dimethylbutane which have similar boiling points (56° C vs. 58° C, respectively),[25, 26, 42]

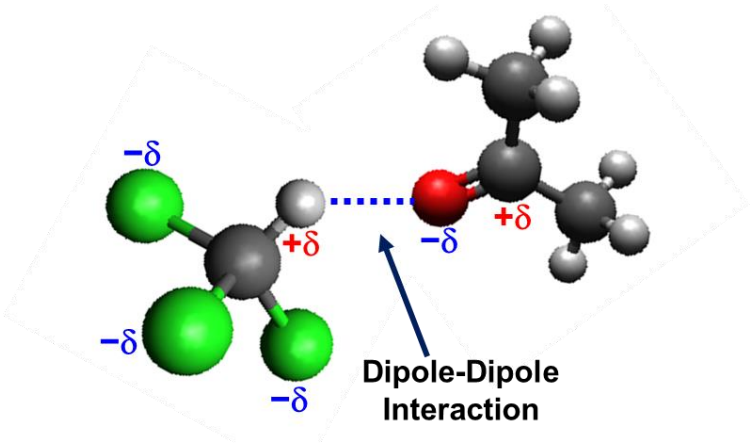

Figure 3.1: A schematic representation of dipole-dipole interactions between acetone and chloroform molecules.

and should have no impact on P3HT final thin-film morphology or charge transport characteristics.[15] The "poor" solvents were selected because they are volatile, with similar evaporation rates, and yet they have widely different polarities. While the substituted butane is a nonpolar hydrocarbon, acetone is a polar solvent that readily interacts with other moieties through dipole-dipole interactions.

The chloroform/acetone system in particular is one of the most studied complexes that are formed via C–H···O dipole-dipole interactions.[43-47] As shown in Figure 3.1, both chlorine and oxygen are highly electronegative, facilitating interactions. Alternatively, 2, 3-dimethylbutane is a nonpolar hydrocarbon. While dipole-dipole interactions can occur with the chloroform/acetone system, they are not likely to form within either the chloroform/2,3-dimethylbutane or chlorobenzene/acetone solvents.[45, 47]

Dipole–dipole attraction generally occurs between a proton donor (X−H) and proton acceptor (Y), where X and Y are highly electronegative atoms (N, O, F, Cl and S).[45-47] In mixed solvent systems, dipole-dipole interactions can lead to complexes that may impact the boiling point (evaporation rate) of the system. It is anticipated that a

molecular complex containing a dipole-dipole interaction will be less volatile than the individual constituent molecules.[43] Further, use of a multi-component solvent for the preparation of polymer films requires not only understanding of the solubility characteristics of the polymer in the individual constituents, but also the impact of the mixed system over a wide range of ratios.

For π-conjugated polymers, a solvent system comprised of molecular complexes may markedly effect the evolution of polymer thin-film morphology and thus macroscopic charge carrier transport. Hypothetically, a blended solvent that can form a molecular complex could promote molecular ordering between polymer chains during the film formation if the solubility characteristics relative to the polymer are unfavorable.[15, 32] This concept was investigated using P3HT as a representative π-conjugated polymer.

3.3.2 Field-Effect Mobility Measurements

Solutions of P3HT were prepared in either chloroform or chlorobenzene, and to avoid macroscopic aggregation of P3HT, the concentration of poor solvent was limited to less than 5 vol %. At higher proportions of poor solvent, the polymer precipitates, forming large aggregates which carry through to the solidified thin-films and lead to poor macroscopic charge transport.[15] Bottom contact field-effect transistors (FETs) were fabricated by spin coating as-prepared P3HT solutions onto pre-fabricated device substrates. Figure 3.2a shows the impact of an increase in poor solvent concentration on the mobility of resultant semiconducting polymer films. The average mobility was calculated in the saturation regime of transistor operation (V_{DS} = −80 V) by plotting the drain current (I_{DS}) versus gate voltage (V_{GS}) and fitting the data to the following equation (Equation 3.1):[48]

$$I_{DS} = \frac{WC_{OX}}{2L}\mu(V_{GS} - V_T)^2 \quad (3.1)$$

where W (2000 μm) and L (50 μm) are the transistor channel width and length, respectively, V_T is the threshold voltage and C_{OX} is the capacitance per unit area of the silicon dioxide gate dielectric (1.15×10^{-8} F/cm^2).

P3HT mobility gradually increases from 4.3×10^{-3} to 1.7×10^{-2} cm^2 V^{-1} s^{-1} for thin-films prepared from solutions of chloroform with increases in acetone concentration up to 2 vol % (Figure 3.2a). The mobility observed here is similar to that reported for P3HT where 3.3 vol % of a high boiling poor solvent was used to enhance the crystallinity and electrical performance of P3HT films (1.5×10^{-2} cm^2 V^{-1} s^{-1}),[15] and is about a factor of four greater than that of P3HT prepared via spin coating from chloroform solution (4.3×10^{-3} cm^2 V^{-1} s^{-1}). Rapid evaporation of chloroform during the spin coating process leads to relatively poor molecular ordering of the polymer chains with commensurately lower macroscopic mobility.[15, 16, 49] Addition of acetone as a co-solvent is believed to enhance P3HT molecular ordering resulting in improved charge carrier transport characteristics. Increasing the concentration of acetone from 2 to 5 vol % effects a decrease in mobility (Figure 3.2a) which is attributed to inhomogeneity of the resultant P3HT films;[15] while the increased concentration of poor solvent may enhance the degree of molecular ordering and crystallinity of the polymer thin-films,[15] it may lead to an increase in the number of interfaces between crystalline domains thus preventing efficient charge transport.

In contrast to the results obtained with the chloroform/acetone solvent system, neither the chloroform/2,3-dimethylbutane nor chlorobenzene/acetone blends noticeably impact P3HT charge transport properties. Rather, they provide results that are similar to

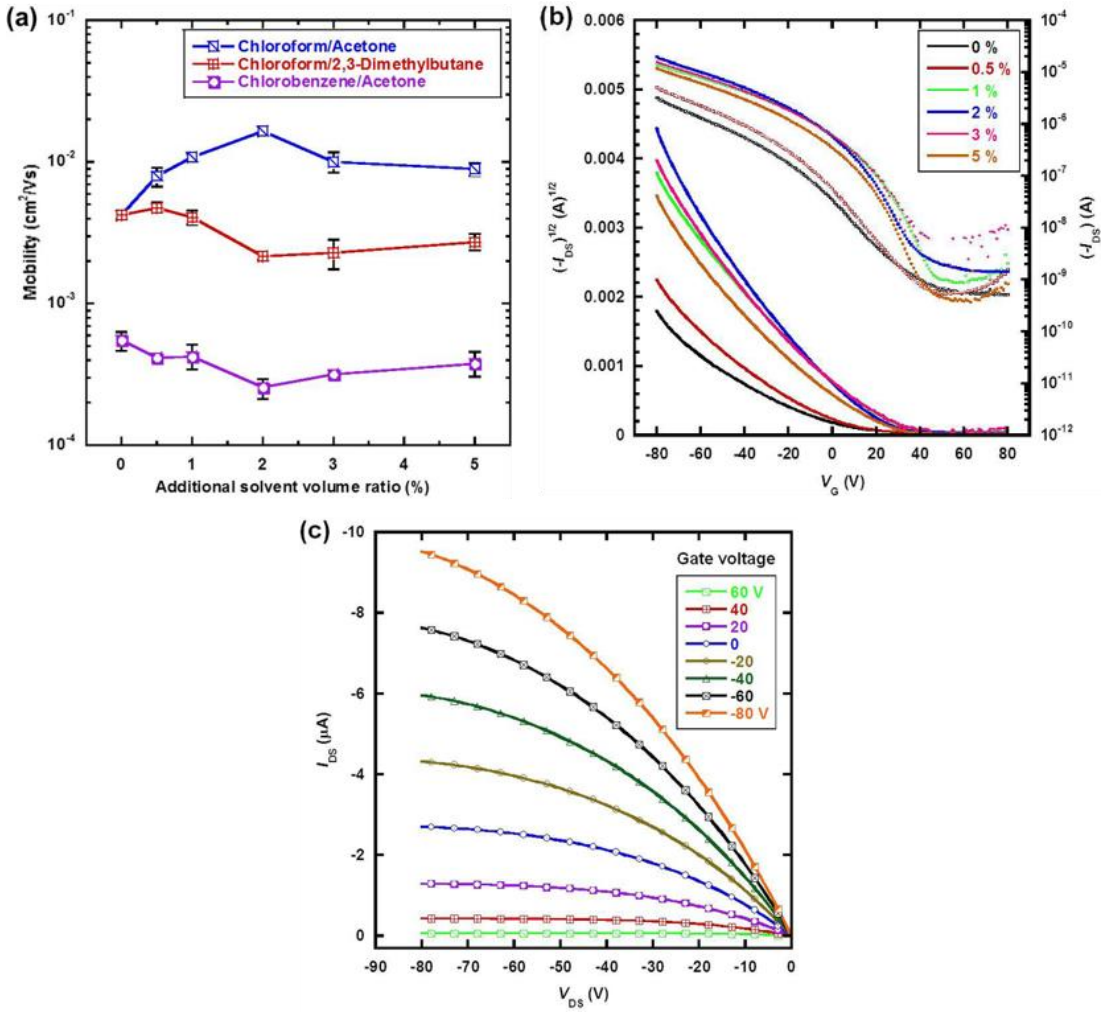

Figure 3.2: a) Average field-effect mobilities obtained from P3HT films obtained via spin coating from chloroform/acetone, chloroform/2,3-dimethylbutane and chlorobenzene/acetone solvent blends having a range of poor solvent volume ratios. Mobilities were calculated in the saturation regime of operation with V_D = – 80 V; b) Transfer characteristics of P3HT OFETs fabricated using chloroform/acetone blends; c) Typical output characteristics obtained from a P3HT OFET prepared via spin coating from chloroform/acetone where the acetone content is 2 vol %. All measurements were performed in a nitrogen glovebox.

those of P3HT films prepared from the respective single component solvents, chloroform and chlorobenzene. Figures 3.2b and c exhibit transfer and output characteristic curves which are typical of p-channel OFET operation in the accumulation mode. The high turn-

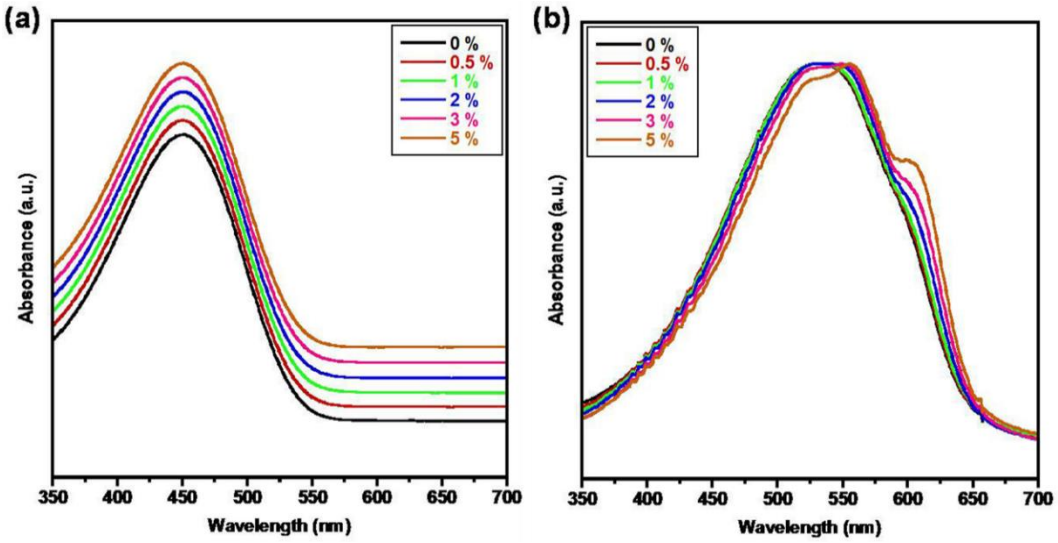

Figure 3.3: Normalized UV-visible absorption spectra of a) P3HT/chloroform-acetone solutions with differing volume ratios of acetone to chloroform, and b) the corresponding P3HT thin-films obtained by spin coating. The spectra obtained from the solutions were shifted for better comparison.

on voltages (V_{ON}) apparent in Figure 3.2b are attributed to the effects of residual doping and/or acceptor-like traps at the P3HT–oxide interface.[50]

3.3.3 Electronic Absorption Spectroscopy

Figure 3.3 depicts the electronic absorption spectra obtained from P3HT/chloroform-acetone solution and the corresponding semiconductor thin-films. The absorption maximum, λ_{max}, associated with the π–π^* intraband transition, appears at ca. 450 nm for all solutions, while absorption bands associated with a vibronic structure having a 0–0 transition at ca. 610 nm and a vibronic side band at ca. 570 nm are noticeably absent (Figure 3.3a).[51, 52] Thus, addition of the poor solvent, acetone, with volume ratios below 5 % relative to chloroform, does not appear to effect aggregation of the P3HT chains in solution.

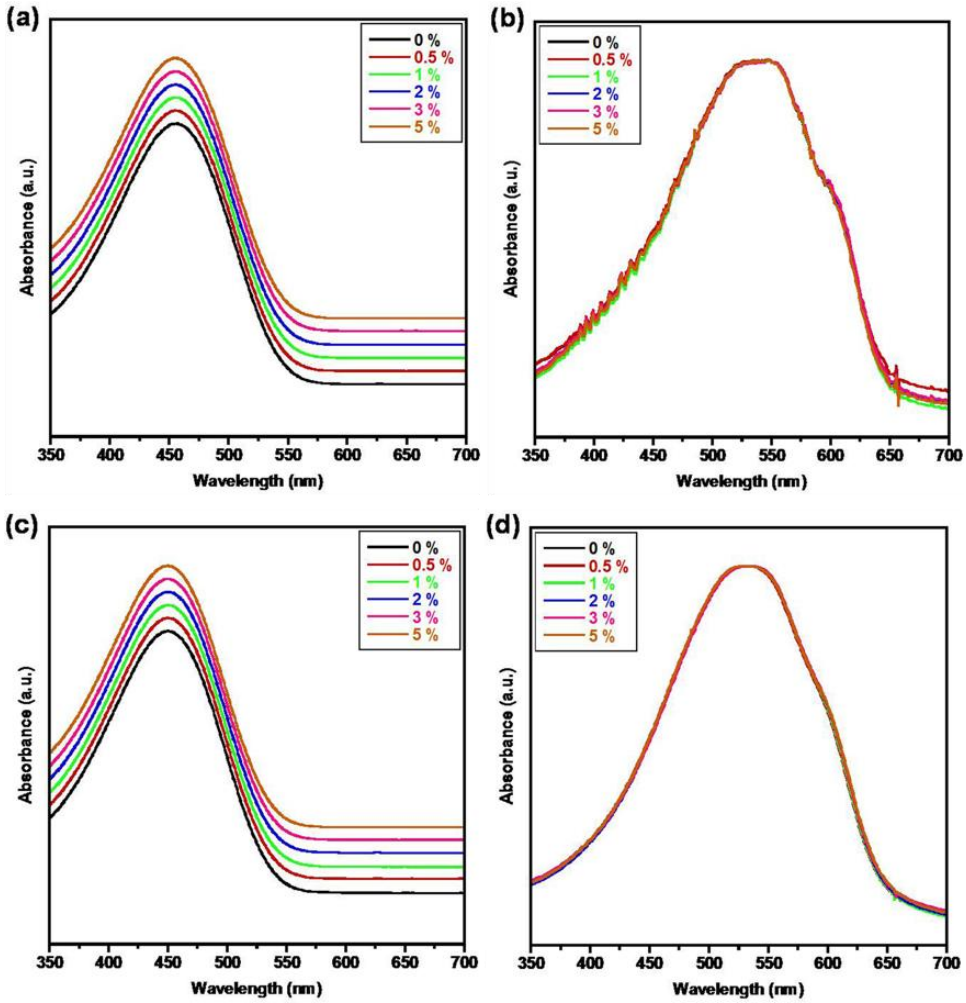

Figure 3.4: Normalized UV-visible absorption spectra of a) P3HT in chlorobenzene/acetone solution, b) corresponding P3HT films obtained by spin coating, c) P3HT in chloroform/2,3-dimethylbutane solutions, and d) corresponding P3HT films obtained by spin coating.

In contrast to the solution results, P3HT thin-films obtained from chloroform/acetone blends display clearly different spectral features in comparison to the pristine film, as shown in Figure 3.3b. The band appearing at ca. 533 nm sequentially red-shifts as the concentration of acetone increases. Additionally, weak absorption bands begin to develop at lower energies (λ ca. 555 and 605 nm), indicative of vibronic structure originating from improved co-facial π-stacking of P3HT.[53] These features are attributed

to enhanced planarization and thus, effective conjugation length of the polymer main chain. Addition of acetone to solutions of P3HT in chloroform appears to promote that planarization resulting in improved molecular ordering of P3HT chains through π–π stacking.

However, spectroscopic studies of P3HT prepared using chloroform/2,3-dimethylbutane or chlorobenzene/acetone solvent systems presented no substantive differences in comparison to results obtained from the single component solvents. Figure 3.4 shows the electronic absorption spectra obtained from P3HT/chlorobenzene-acetone and P3HT/chloroform-2,3-dimethylbutane solutions and the corresponding semiconductor thin-films. As shown in Figures 3.4a and c, the absorption bands associated with a vibronic structure having a 0–0 transition at ca. 610 nm and a vibronic side band at ca. 570 nm are noticeably absent.[51, 52] Thus, aggregation of the P3HT chains does not appear in either of these solvent systems containing less than 5 vol % poor solvent. In contrast to the thin films obtained from the chloroform-acetone solvent system, thin films obtained from chlorobenzene/acetone and chloroform/2,3-dimethylbutane solvents reveal no apparent change in the respective absorption spectra and concomitantly, no enhancement of the degree of molecular ordering (Figures 3.4b and d).

3.3.4 Crystallinity and Microstructure of Thin Films

Enhanced intermolecular interactions between P3HT chains are expected to give rise to films that are more crystalline.[54] Figure 3.5 shows the X-ray diffractograms obtained from grazing incidence (GIXD) measurements of P3HT films obtained from the chloroform/acetone solutions. As shown in Figure 3.5a, increases in poor solvent concentration effects a gradual increase in intensity of the (100) peak associated with

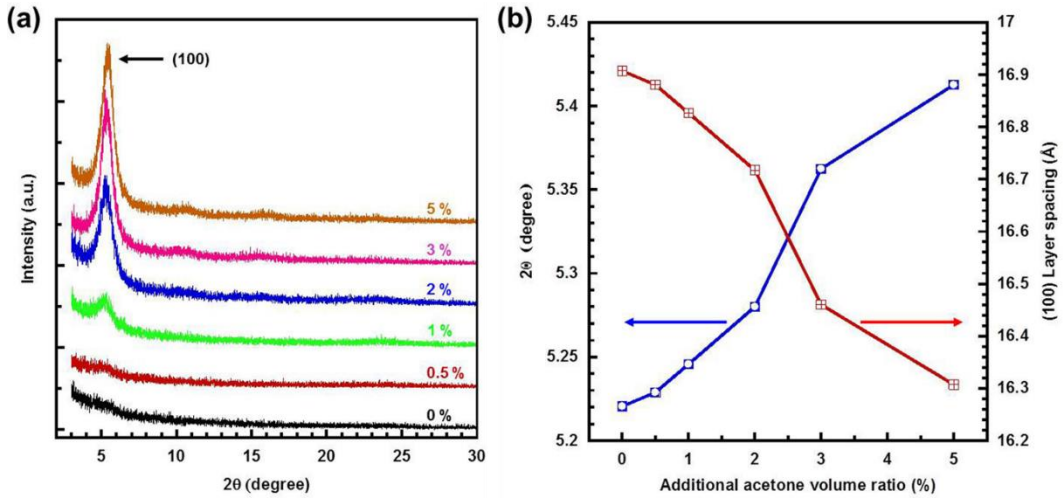

Figure 3.5: a) Grazing incidence X-Ray diffraction profiles of the P3HT films spin-coated from P3HT/chloroform solutions containing a range of added acetone. b) 2θ angle (left axis) of (100) peak and corresponding layer spacing (right axis) as a function of the additional acetone volume ratio.

lamellar packing of the polymer chains along the crystallographic direction perpendicular to the backbone.[55] This increase could be attributed to either an increase in the size of individual crystallites, the number of crystallites, or both.[21] Also, the (100) peak gradually shifts to higher angle, from 5.22 to 5.41°, when the acetone volume ratio is increased from 0 to 5 vol %, indicating that the d-spacing in the (100) plane decreases from 16.91 to 16.31 Å (Figure 3.5b). This decrease may result from increased interdigitation between the P3HT alkyl side chains, or a change in side chain tilt because of unfavorable solvent-solute interactions as poor solvent is incorporated into the system.[34, 56]

In contrast to crystallographic results of P3HT films obtained from P3HT/chloroform-acetone solution, as shown in figure 3.6, addition of the poor solvents leads to no discernible change in intensity of the (100) peak of the polymer chains in P3HT films obtained from P3HT/chlorobenzene-acetone and P3HT/chloroform-2,3-dimethylbutane solutions with 0 and 5 vol % of each poor solvent. Therefore,

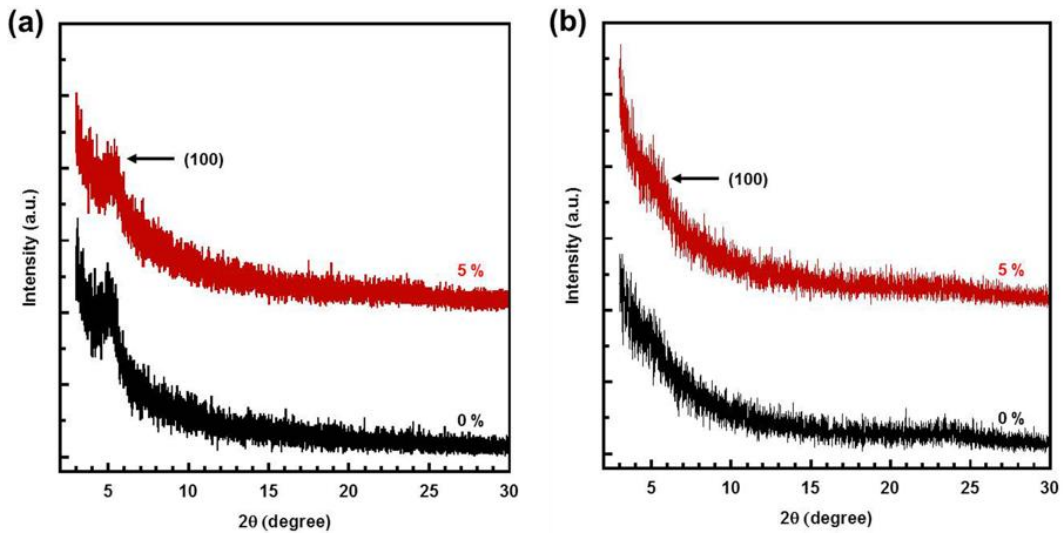

Figure 3.6: Grazing incidence X-Ray diffraction profiles of films spin-coated from a) P3HT/chlorobenzene solutions with 0 and 5 vol % of acetone and b) P3HT/chloroform solutions with 0 and 5 vol % of 2,3-dimethylbutane, respectively.

intermolecular interactions between P3HT chains are not enhanced in these solvent systems.

3.3.5 Morphology of Thin Films

Atomic Force Microscopy (AFM) was used to investigate the surface morphologies of P3HT thin-films prepared from 0, 0.5, 1, 2, 3 and 5 vol % chloroform/acetone solutions. Phase and height images are presented in Figure 3.7, where P3HT thin-film nano- and microstructure distinctively evolves from an initial featureless and amorphous structure as the acetone content increases. Consistent with previous reports, rapid evaporation of chloroform during the coating process hinders formation of well-ordered, supramolecular structures.[21, 27] Using the binary chloroform/acetone solvent system, randomly shaped, nano-sized grains begin to appear, and then increase in size, as the volume ratio of acetone increases. Addition of the poor solvent appears to induce supramolecular assembly of the P3HT chains either in solution and/or during the coating process. Concomitant with

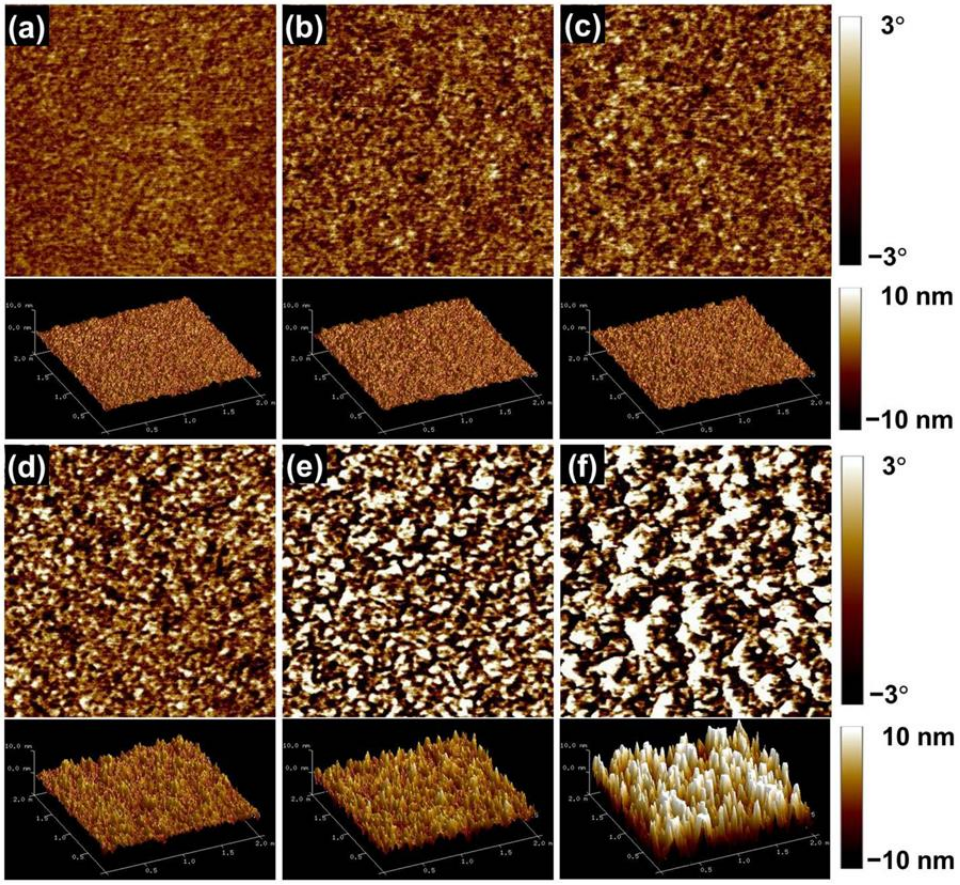

Figure 3.7: Tapping mode AFM phase (upper) and height images (lower) of P3HT films obtained via spin casting from chloroform/acetone solution; the P3HT films were fabricated from solutions containing a) 0, b) 0.5, c) 1, d) 2, e) 3 and f) 5 vol % acetone. The scan area of phase and height images is 1 μm × 1 μm and 2 μm × 2 μm, respectively.

assembly/alignment of P3HT chains is an increase in long range lateral order, expected to benefit efficient charge transport.[14, 40] The observed increase in field-effect mobility upon addition of up to 2 vol % acetone is consistent with this expectation. However, as seen from the height images, when the proportion of acetone is greater than 2 vol %, both grain size and surface roughness increase significantly. Thus, the interfaces between grains become more resistive to charge transport because interconnectivity is lacking, and the corresponding field-effect mobility decreases (Figure 3.2a).

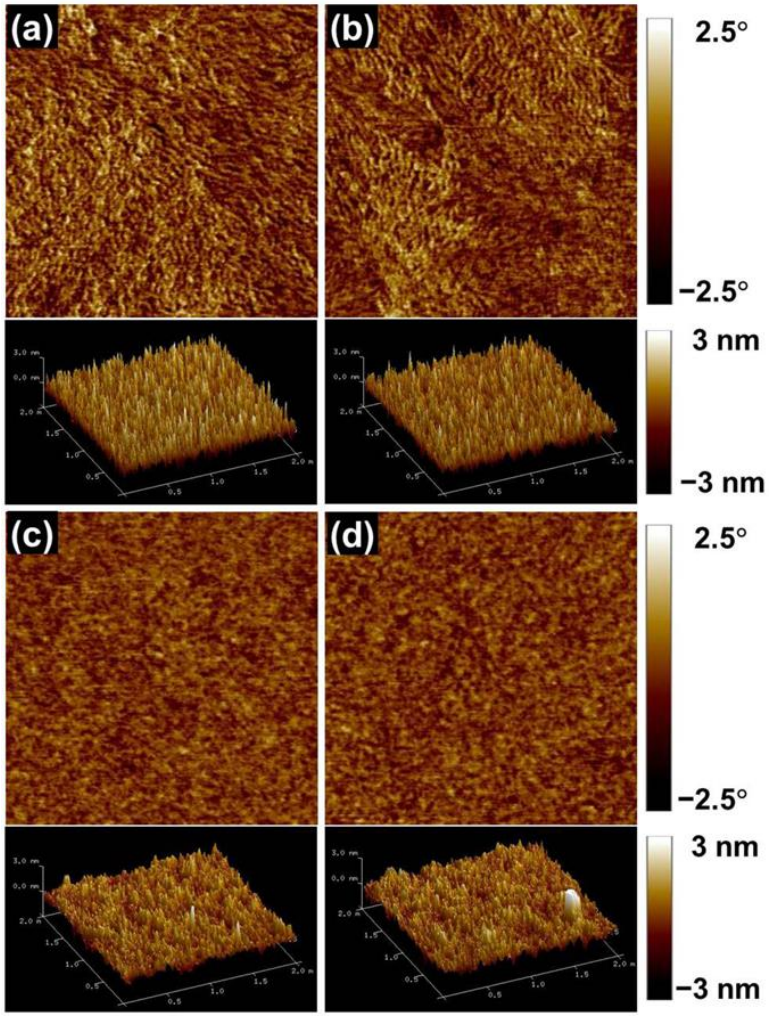

Figure 3.8: Tapping mode AFM phase (upper) and height images (lower) of films obtained by spin coating from P3HT/chlorobenzene solutions with a) 0 and b) 5 vol % of acetone, and P3HT/chloroform solutions with c) 0 and d) 5 vol % of 2,3-dimethylbutane. The scan area of phase and height images is 1 μm × 1 μm and 2 μm × 2 μm, respectively.

Figure 3.8 presents AFM phase and height images of films prepared using 0 and 5 vol % of each poor solvent in chlorobenzene/acetone and chloroform/2,3-dimethylbutane solutions. Unlike the P3HT films obtained from chloroform/acetone solvent system, no discernable change in the morphology was observed from the resultant films, as expected.

3.3.6 Role of Solvent-Solvent Interactions

From the results presented above, blends of a relatively good solvent with a poor solvent can afford markedly different results with respect to charge transport characteristics. We have shown that use of a poor solvent able to interact with the majority solvent, can enhance the supramolecular assembly of π-conjugated polymer chains and thus positively influence the charge transport characteristics of the resultant film. Specifically, blends of chloroform and acetone, which are known to undergo dipole-dipole interactions, lead to molecular alignment and ordering at the nanoscale affording a macroscopic thin-film structure conducive to efficient charge transport. From a mechanistic perspective, it is important to understand how such small percentages of a poor solvent additive can promote molecular ordering and thereby transport. We hypothesize that solvent-solvent (majority "good" solvent-minority "poor" solvent) and subsequently, solvent-solute (solvent mixture-P3HT) interactions promote aggregation and favorable π-stacking between the P3HT chains. In the chloroform-acetone system, these interactions lead to formation of a solvent complex that persists in the evolving thin-film for a longer time than either individual "free" component due to a lower evaporation rate of the complex. Concomitantly, polymer solubility decreases, perhaps gradually, as the concentration of the solvent complex increases, thereby promoting favorable π–π stacking interactions between the polymer chains, thus enhancing solidified film charge transport characteristics.[15, 57]

In addition to oxygen, sulfur is also known to interact with hydrogen atoms linked to highly electronegative atoms like N, O, F, Cl and S.[45-47] Thus, P3HT sulfur may also interact with chloroform through dipole-dipole interactions. However, the interactions

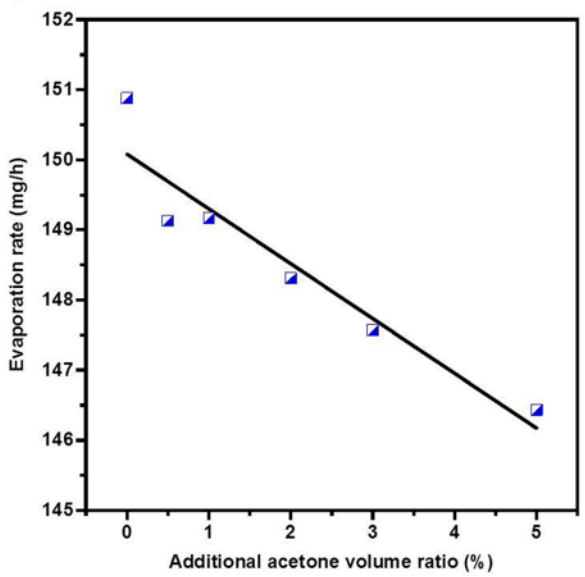

Figure 3.9: Evaporation rate of chloroform/acetone from P3HT solutions as a function acetone volume.

associated with sulfur are weaker than those with oxygen because of the lower electronegativity of sulfur.[58-61] Therefore, dipole-dipole interactions between acetone-chloroform are expected to be stronger than those between P3HT and chloroform; acetone-chloroform complexes would reside for longer time during a film formation process, and thereby more dominantly impact resultant P3HT film structures. Consistently, as shown in Figure 3.9, pure chloroform solvent has a higher evaporation rate than that of acetone-chloroform in the presence of P3HT.

At ambient temperature, we believe that the dipole-dipole interactions effect a decrease in the evaporation rate of a chloroform/acetone blend as the acetone volume ratio increases from 0 to ca. 33 vol %.[43] The change in evaporation rate of the blended solvent in P3HT/solvent solutions was investigated as a function of acetone volume fraction (Figure 3.9). In agreement with expectations, the evaporation rate decreases as the acetone volume ratio is increased to 5vol %.[43]

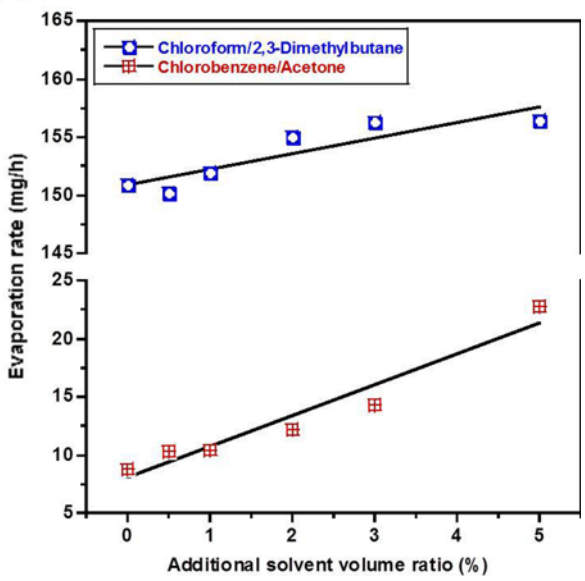

Figure 3.10: Evaporation rate of chlorobenzene/acetone and chloroform/2,3-dimethylbutane as a function of poor solvent volume ratio from P3HT solutions.

Given that the volatility of the chloroform/acetone system is minimized at ca. 33 vol %, it is anticipated that the volume ratio of acetone to chloroform in the P3HT/solvent systems investigated here would converge to ca. 33 vol % during evaporation; the more volatile fractions will exit first, leaving behind a more acetone rich binary solvent regardless of the starting chloroform-acetone ratio.

Figure 3.10 shows the evaporation rates of the P3HT/chlorobenzene/acetone and P3HT/chloroform/2,3-dimethylbutane solutions as a function of poor solvent volume ratio. In contrast to the chloroform/acetone solvent system (Figure 3.9), chlorobenzene/acetone and chloroform/2,3-dimethylbutane fail to show characteristic features associated with dipole-dipole interactions between the constituent solvent molecules, in their evaporation rates.

3.3.7 Solvent-Solvent and Solvent-Polymer Interactions

Solvents are known to affect the growth of organic crystals in a significant manner.[15, 32] Similarly, the organization of polymer based semiconductors into assemblies that are conducive to effective macroscopic charge carrier transport has also been shown to be sensitive to the solvent environment. Use of a poor solvent allows polymer chains to aggregate, thus minimizing unfavorable solute-solvent interactions and facilitating molecular ordering between polymer chains through favorable π-π stacking. A factor that is expected to be useful to aid understanding of polymer/solvent interactions is the total solubility parameter (δ); miscibility is improved when the components of a system have similar cohesive energy densities (E/V),[62] where the cohesive energy density is the energy required to infinitely separate a unit volume of a given species from its neighbors. The total solubility parameter (δ) can be described by three contributions of the Hansen solubility parameters (HSPs), namely the dispersive (δ_D), the polar (δ_P), and H-bonding (δ_H) solubility parameters.[41, 62, 63] The total solubility parameter (δ) is defined by Equation 3.2,[42, 64]

$$\delta^2 = (E/V) = \delta_D^2 + \delta_P^2 + \delta_H^2 \tag{3.2}$$

where E is the cohesion energy or sum of the evaporation enthalpies, and V is the molar volume.

To systematically evaluate the solubility of P3HT in the solvent blends investigated here, the 3-dimensional Hansen space was explored. The three HSPs are used as Cartesian units and each solvent system can be represented by a coordinate. Solvents that effect polymer dissolution define the interaction radius (R_0) which determines the radius of the sphere in Hansen space; solvents falling within R_0 dissolve the polymer, while the solvents outside of R_0 are not effective. The center of the sphere is determined by the polymer

Hansen parameters. The distance between the polymer and solvent Hansen parameters is termed R_a, defined by Equation 3.3,

$$R_a^{\ 2} = 4(\delta_{D1} - \delta_{D2})^2 + (\delta_{P1} - \delta_{P2})^2 + (\delta_{H1} - \delta_{H2})^2 \quad (3.3)$$

where *1* and *2* represent the solute and solvent, respectively. The relative energy difference (RED = R_a/R_0) provides an estimate of whether two materials will be miscible (miscible when RED < 1, partially miscible when RED = 1 and non-miscible when RED > 1).

Abbott and Hansen software was used to determine HSPs for P3HT following methodology reported by Duong et al.,[26] and Brabec and coworkers.[66, 67] Good solvents, defined as solvents which can dissolve more than 5 mg/mL of the polymer, were assigned a value of "1", while poor solvents were assigned a value of "0". The solubility of P3HT in a variety of alternative solvents is summarized in Table 3.2. The Hansen space creates the interaction radius, R_0, for P3HT as shown in Figure 3.11, and also RED values of the solvents are obtained (Table 3.2). Solvents in blue are considered to be good solvents for P3HT, while solvents in red are inferior/poor solvents. P3HT solubility parameters were calculated to be δ_D = 19.45 $MPa^{1/2}$, δ_P = 3.97 $MPa^{1/2}$ and δ_H = 4.19 $MPa^{1/2}$, with an interaction radius R_0 of 4.20 $MPa^{1/2}$.

Solvent solubility parameters were calculated as function of acetone volume fraction using Equation 3.4,

$$\delta_x = \sum (\delta_x)_i \phi_i \quad (3.4)$$

where *x* represents *D*, *P*, or *H*, *i* stands for solvent species and ϕ_i refers to the volume fraction of component *i*. Calculated values of δ_D, δ_p and δ_H for the solvents as a function of acetone content are depicted in Figure 3.12. The range of 0 to 33 vol % acetone was

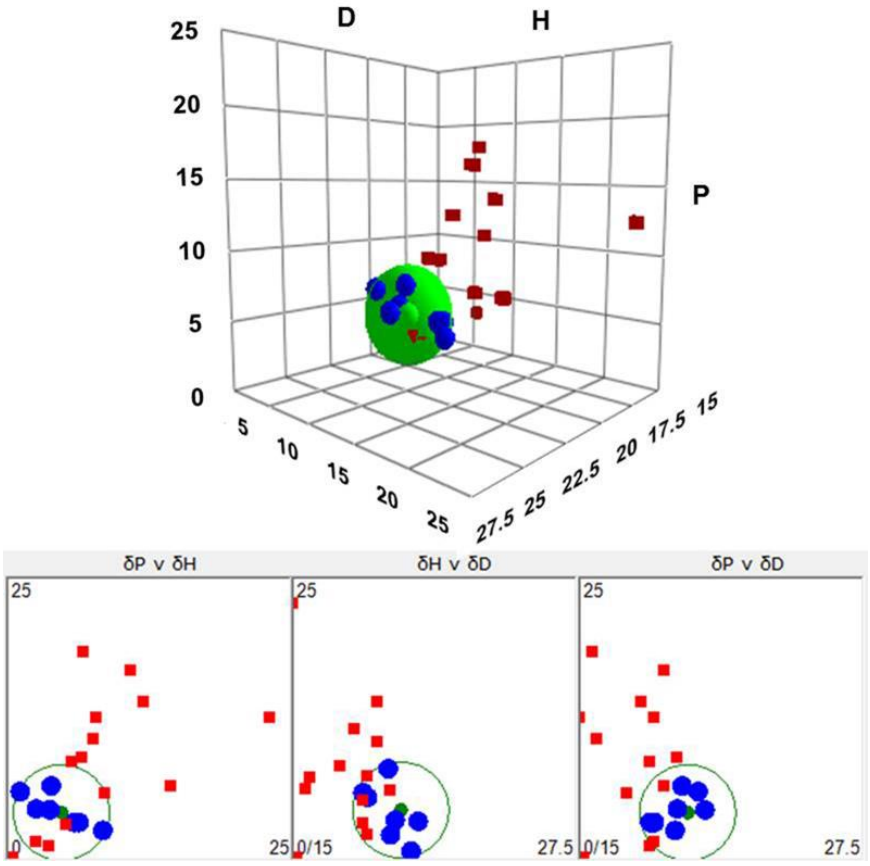

Figure 3.11: Hansen solubility parameter diagrams for P3HT and selected solvents. Solvents in blue are considered to be good solvents for P3HT while solvents in red are poor solvents.

examined because it is anticipated that the composition of the solvent will converge to a 33 vol % acetone solution during thin-film formation. As shown in Figure 3.12a, δ_D for chloroform/acetone decreases with an increase in acetone volume fraction. The difference between the P3HT and solvent values of δ_D increases with acetone incorporation, and thus in terms of δ_D, P3HT solubility in the solvent decreases. Examination of δ_P follows a different trend. The difference in δ_P between the polymer and the solvent increases with increasing acetone content up to a volume fraction of 0.12, but then decreases with increasing volume fraction of poor solvent up to 0.33 (Figure 3.12b). This trend indicates

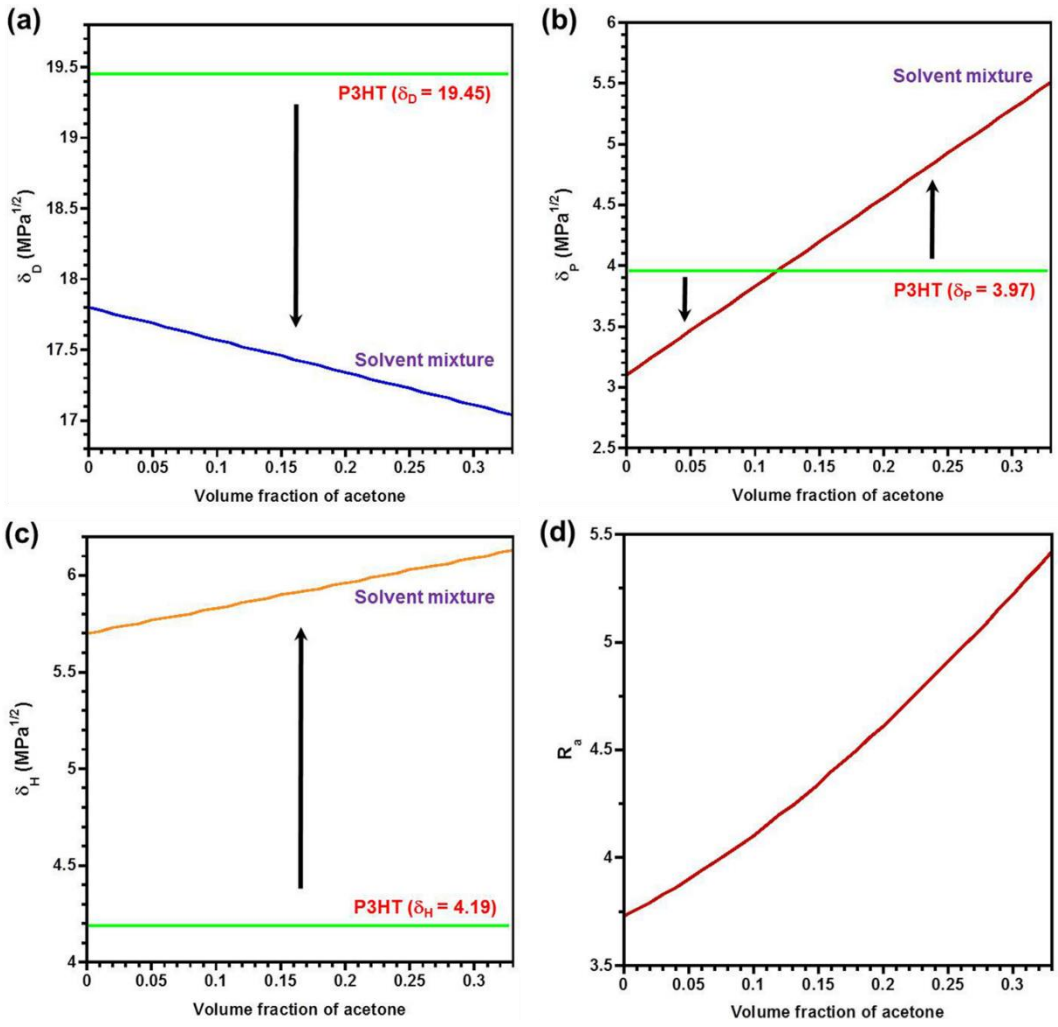

Figure 3.12: Hansen solubility parameters (a) δ_D, b) δ_P and c) δ_H) of chloroform/acetone solvent blends and the distance (d) R_a) between Hansen solubility parameters of the P3HT and chloroform/acetone solvent as a function of acetone volume fraction; δ_D, δ_P and δ_H were numerically calculated by Equation 3.4, and R_a was calculated using Equation 3.3. Solubility parameters of pure solvents and P3HT are as follows; δ_D = 17.80, δ_P = 3.10 and δ_H = 5.70 for chloroform, δ_D = 15.50, δ_P = 10.40 and δ_H = 7.00 for acetone and δ_D = 19.45, δ_P = 3.97 and δ_H = 4.19 for P3HT.

that with respect to δ_P, the polymer solubility initially increases with increasing acetone content, but once the volume fraction of poor solvent reaches 0.12, P3HT solubility decreases. Figure 3.12c shows that in terms of δ_H, the solubility of the polymer relative to the solvent decreases as the acetone content increases. Based upon Eq 3.3, differences in

Table 3.3: Hansen solubility parameters of chloroform/acetone blends containing different proportions of acetone.

Solvents	δ_D (MPa$^{1/2}$)	δ_P (MPa$^{1/2}$)	δ_H (MPa$^{1/2}$)
Chloroform	17.80	3.10	5.70
Acetone	15.50	10.40	7.00
Chloroform/acetone (v/v = 99.5/0.5)	17.79	3.14	5.71
Chloroform/acetone (v/v = 99.0/1.0)	17.78	3.17	5.71
Chloroform/acetone (v/v = 98.0/2.0)	17.75	3.25	5.73
Chloroform/acetone (v/v = 97.0/3.0)	17.73	3.32	5.74
Chloroform/acetone (v/v = 95.0/5.0)	17.69	3.47	5.77
Chloroform/acetone (v/v = 67.0/33.0)	17.04	5.51	6.13

δ_D dominate in the calculation of R_a, which increases with increased levels of the poor solvent, and polymer solubility decreases (Figure 3.12d). The solubility parameters of the solvent mixtures prepared with 0.5, 1, 2, 3, 5 and 33 vol % acetone are tabulated in Table 3.3 along with those of chloroform and acetone.

The RED of the solvents with respect to P3HT were calculated as a function of acetone volume fraction to understand how solubility of the polymer changes upon addition of acetone. As discerned from Figure 3.13a, the RED decreases with increasing acetone content. Thus, P3HT is expected to be soluble (> 5mg/mL) when the volume fraction of acetone is less than 0.12, but become increasingly less soluble for volume fractions of acetone greater than 0.12. These results were experimentally verified: P3HT exhibited good solubility in solvents prepared with up to 10 vol % acetone, appearing bright orange

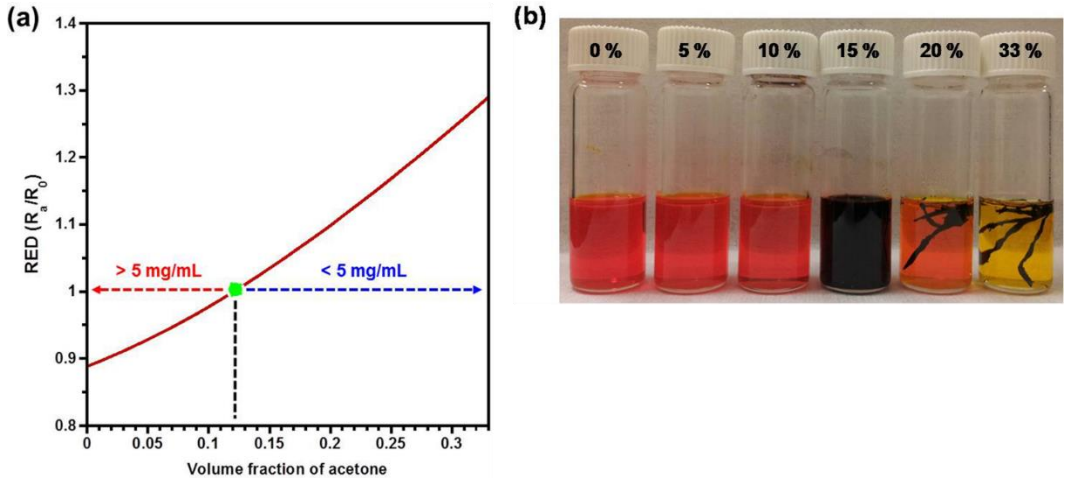

Figure 3.13: a) Relative energy difference (RED) of chloroform/acetone solvent mixtures to P3HT, as a function of volume fraction of acetone and b) photographs of P3HT solutions prepared with 5 mg/mL in various solvents (0, 5, 10, 15, 20 and 33 vol % of acetone relative to chloroform). Solvent mixtures with RED less than 1 dissolve P3HT to more than 5 mg/mL and are considered to be good solvents, while solvent mixtures with RED more than 1 dissolve less than 5 mg/mL of polymer and are considered poor solvents.

with no apparent aggregation. Samples prepared with solvents containing 15 to 33 vol % acetone were poorly soluble and aggregation was readily apparent (Figure 3.13b).

3.3.8 Mechanism for Supramolecular Aggregation

Based upon the solubility parameter analysis, the solubility of P3HT in chloroform/acetone solutions decreases during the thin-film solidification process; excess acetone and chloroform evaporate more quickly than their complexes which are likely to be involved in dipole-dipole interactions, allowing the acetone volume fraction to gradually increase up to approximately 33 vol %, regardless of the initial acetone volume fraction. Thus as P3HT thin-film nanostructure initiates and evolves, the solvent system enhances molecular ordering between P3HT chains, with the degree of the molecular ordering being dependent upon the initial volume fraction of the poor solvent.

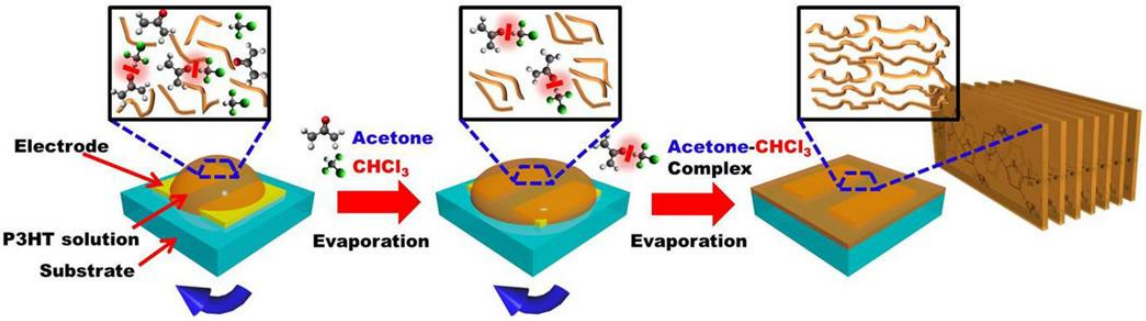

Figure 3.14: A schematic illustration of evolution of molecular ordering of P3HT chains during solvent evaporation.

A mechanism to account for the observed enhanced supramolecular aggregation of P3HT chains during the deposition process is presented in Figure 3.14. At the initial stages, acetone/chloroform solvent complexes formed via solvent-solvent interactions exist alongside "free" acetone and chloroform in the P3HT precursor solutions. Supramolecular aggregation of the polymer is unfavorable because the overall solvent system represents a good solvent. As the film evolves, solvent molecules not associated through dipole-dipole interactions evaporate faster than their counterparts and as a result, the volume ratio of acetone to chloroform gradually increases up to approximately 33 vol %, while P3HT solubility commensurately decreases. Consequently, molecular ordering of the polymer chains improves due to a gradual transition from favorable to unfavorable solvent-solute interactions. The crystallinity of the films increases as well, however, the macroscopic field-effect mobility reaches a maximum at approximately 2 vol % acetone. At this point, even though crystallinity of resultant films continues to increase, other factors such as grain boundaries that negatively impact charge transport begin to predominate.

3.3.9 Kinetic Parameter Effects

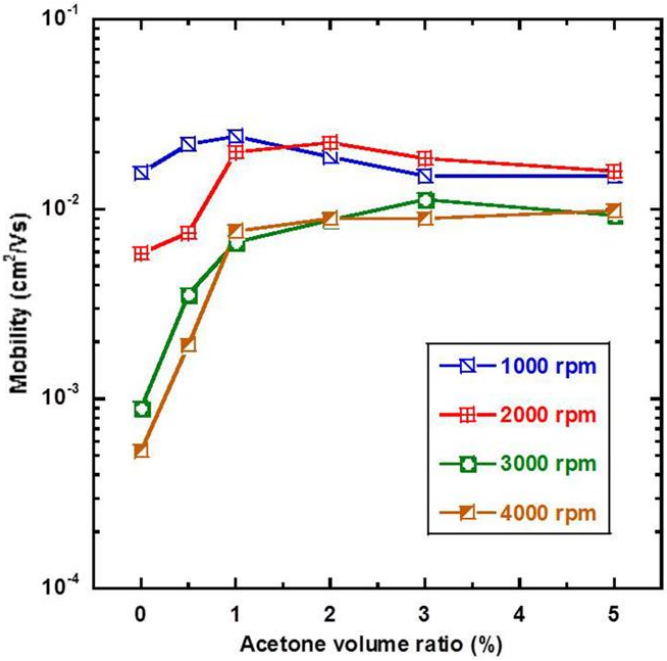

Figure 3.15: Field-effect mobilities obtained from P3HT films obtained via spin coating at different spinning speeds for 60s from chloroform/acetone solvent blends having a range of acetone volume ratios. Mobilities were calculated in the saturation regime of operation with V_D = – 80 V. The measurements were performed in a nitrogen glovebox.

In addition to solvent-solute interactions, kinetic parameters associated with the coating process can impact molecular ordering, thin-film morphology and resultant polymer charge transport characteristics.[21, 68] To gain preliminary insight into the sensitivity of the system to kinetic parameters, the rate of solvent evaporation was varied through control of the spinning speed. Figure 3.15 represents field-effect mobilities of P3HT films prepared via spin coating at different spinning speeds for 60 s from chloroform/acetone solvent mixtures. The spinning speed was varied from 1000 to 4000 rpm for 60 s which is the range that has been typically reported for P3HT thin-film transistor fabrication. Spinning speed was found to impact the critical acetone concentration; the amount of acetone required for maximizing mobility may gradually change from ca. 1 to 5 vol % as the spinning speed increases from 1000 to 4000 rpm.

However, more detailed investigations are required to fully evaluate these results. The time of the process was not investigated because solvent evaporation is complete in significantly less than 60 seconds. Small differences in the optimum critical acetone concentration were observed as seen from Figure 3.15. However investigation into the kinetic processes associated with film formation and their impact on the morphology and charge transport characteristics of polymer based semiconductors will be required to elucidate the complicated relationships.

3.4 Conclusion

In conclusion, the macroscopic charge carrier transport characteristics of solution deposited P3HT thin-films can be enhanced simply by the addition of a small amount of a poor solvent that has a propensity to interact with the majority solvent. Specifically, addition of acetone to solutions of P3HT in chloroform affords improved molecular ordering of P3HT chains, resulting in enhanced macroscopic charge transport characteristics of resultant thin films. The two-dimensional molecular ordering of the polymer film was controlled by varying the amount of poor solvent added to a precursor solution, and a correlation between the field-effect mobility and molecular ordering of the π-conjugated polymer chains was investigated. During film formation, the relative volume fraction of poor to good solvent gradually increased due to interactions between the constituent solvent molecules. Hansen solubility parameters of the polymer and solvent blends were employed to systematically understand how the solvent mixtures can enhance the supramolecular assembly of polymer chains during deposition and subsequently impact the electrical performance of the thin P3HT films. The solubility threshold of P3HT appeared at an acetone volume fraction of 0.12 relative to the majority solvent, chloroform,

and the RED value of the solvent to P3HT varied from less than to greater than 1 during film formation, indicating that the solvent characteristics change from those of a good solvent to those of a poor solvent. This shift in solvent characteristics to a system that presents unfavorable solvent-solute interactions enhances the proportion of well-ordered molecular π-π stacked P3HT chains. These studies provided for a mechanistic illustration of the polymer molecular ordering process during film formation.

This simple solvent assisted process represents a benign alterative for enhancing ordered, aggregated π-conjugated semiconducting polymer architectures. The approach that utilizes both solvent-solvent and solvent-solute interactions, as determined through spectroscopic and solubility parameter analysis, could prove attractive in the pursuit of robust, low-cost, large-area electronic device fabrication methodologies. Further, the spectrum of solvent systems applicable to polymer semiconductor device fabrication may be expanded, enabling facile processing of organic-organic blends or organic-inorganic composites. The mechanistic approach, employing Hansen solubility parameters, used to define a solvent system contributes to understanding the evolution of macroscopic polymer thin-film morphology and charge transport characteristics for a variety of applications including chemical sensors, OFETs, light emitting diodes and organic photovoltaic cells.

3.5 References

[1] Gustafsson, G.; Cao, Y.; Treacy, G. M.; Klavetter, F.; Colaneri, N.; Heeger, A. J. Flexible Light-Emitting-Diodes Made from Soluble Conducting Polymers. *Nature* **1992**, 357, 477-479.

[2] Bao, Z. N.; Lovinger, A. J. Soluble Regioregular Polythiophene Derivatives as Semiconducting Materials for Field-Effect Transistors. *Chem. Mater*. **1999**, 11, 2607-2612.

[3] Lee, K. H.; Schwenn, P. E.; Smith, A. R. G.; Cavaye, H.; Shaw, P. E.; James, M.; Krueger, K. B.; Gentle, I. R.; Meredith, P.; Burn, P. L. Morphology of All-Solution-Processed "Bilayer" Organic Solar Cells. *Adv. Mater*. **2011**, 23, 766-770.

[4] Gaynor, W.; Lee, J. Y.; Peumans, P. Fully Solution-Processed Inverted Polymer Solar Cells with Laminated Nanowire Electrodes. *ACS Nano* **2010**, 4, 30-34.

[5] Zhuang, X. D.; Chen, Y.; Liu, G.; Li, P. P.; Zhu, C. X.; Kang, E. T.; Neoh, K. G.; Zhang, B.; Zhu, J. H.; Li, Y. X. Conjugated-Polymer-Functionalized Graphene Oxide: Synthesis and Nonvolatile Rewritable Memory Effect. *Adv. Mater*. **2010**, 22, 1731-1735.

[6] Lobez, J. M.; Andrew, T. L.; Bulovic, V.; Swager, T. M. Improving the Performance of P3HT-Fullerene Solar Cells with Side-Chain-Functionalized Poly(thiophene) Additives: A New Paradigm for Polymer Design. *ACS Nano* **2012**, 6, 3044-3056.

[7] Coropceanu, V.; Cornil, J.; da Silva, D. A.; Olivier, Y.; Silbey, R.; Bredas, J. L. Charge Transport in Organic Semiconductors. *Chem. Rev*. **2007**, 107, 926-952.

[8] Street, R. A.; Northrup, J. E.; Salleo, A. Transport in Polycrystalline Polymer Thin-Film Transistors. *Phys. Rev. B* **2005**, 71, 165202.

[9] Goffri, S.; Muller, C.; Stingelin-Stutzmann, N.; Breiby, D. W.; Radano, C. P.; Andreasen, J. W.; Thompson, R.; Janssen, R. A. J.; Nielsen, M. M.; Smith, P.; et al. Multicomponent Semiconducting Polymer Systems with Low Crystallization-Induced Percolation Threshold. *Nat. Mater*. **2006**, 5, 950-956.

[10] Chen, D.; Zhao, W.; Russell, T. P. P3HT Nanopillars for Organic Photovoltaic Devices Nanoimprinted by AAO Templates. *ACS Nano* **2012**, 6, 1479-1485.

[11] Sirringhaus, H.; Brown, P. J.; Friend, R. H.; Nielsen, M. M.; Bechgaard, K.; Langeveld-Voss, B. M. W.; Spiering, A. J. H.; Janssen, R. A. J.; Meijer, E. W.; Herwig, P.; et al. Two-Dimensional Charge Transport in Self-Organized, High-Mobility Conjugated Polymers. *Nature* **1999**, 401, 685-688.

[12] Hill, C. M.; Zhu, Y.; Pan, S. Fluorescence and Electroluminescence Quenching Evidence of Interfacial Charge Transfer in Poly(3-hexylthiophene): Graphene Oxide Bulk Heterojunction Photovoltaic Devices. *ACS Nano* **2011**, 5, 942-951.

[13] Cho, S.; Lee, K.; Yuen, J.; Wang, G. M.; Moses, D.; Heeger, A. J.; Surin, M. ThermalAnnealing-Induced Enhancement of the Field-Effect Mobility of Regioregular Poly(3-hexylthiophene) Films. *J. Appl. Phys*. **2006**, 100, 114503.

[14] Yang, H. C.; Shin, T. J.; Yang, L.; Cho, K.; Ryu, C. Y.; Bao, Z. N. Effect of Mesoscale Crystalline Structure on the Field-Effect Mobility of Regioregular Poly(3-hexylthiophene) in Thin-Film Transistors. *Adv. Funct. Mater.* **2005**, 15, 671-676.

[15] Park, Y. D.; Lee, H. S.; Choi, Y. J.; Kwak, D.; Cho, J. H.; Lee, S.; Cho, K. Solubility-Induced Ordered Polythiophene Precursors for High-Performance Organic Thin-Film Transistors. *Adv. Funct. Mater*. **2009**, 19, 1200-1206.

[16] Aiyar, A. R.; Hong, J. I.; Reichmanis, E. Regioregularity and Intrachain Ordering: Impact on the Nanostructure and Charge Transport in Two-Dimensional Assemblies of Poly(3-hexylthiophene). *Chem. Mater*. **2012**, 24, 2845-2853.

[17] Chen, D. A.; Nakahara, A.; Wei, D. G.; Nordlund, D.; Russell, T. P. P3HT/PCBM Bulk Heterojunction Organic Photovoltaics: Correlating Efficiency and Morphology. *Nano Lett*. **2011**, 11, 561-567.

[18] Kline, R. J.; McGehee, M. D.; Kadnikova, E. N.; Liu, J. S.; Frechet, J. M. J. Controlling the Field-Effect Mobility of Regioregular Polythiophene by Changing the Molecular Weight. *Adv. Mater*. **2003**, 15, 1519-1522.

[19] Kline, R. J.; McGehee, M. D.; Kadnikova, E. N.; Liu, J. S.; Frechet, J. M. J.; Toney, M. F. Dependence of Regioregular Poly(3-hexylthiophene) Film Morphology and Field-Effect Mobility on Molecular Weight. *Macromolecules* **2005**, 38, 3312-3319.

[20] Zhang, R.; Li, B.; Iovu, M. C.; Jeffries-EL, M.; Sauve, G.; Cooper, J.; Jia, S. J.; Tristram-Nagle, S.; Smilgies, D. M.; Lambeth, D. N.; et al. Nanostructure Dependence of Field-Effect Mobility in Regioregular Poly(3-hexylthiophene) Thin Film Field Effect Transistors. *J. Am. Chem. Soc.* **2006**, 128, 3480-3481.

[21] Aiyar, A. R.; Hong, J. I.; Nambiar, R.; Collard, D. M.; Reichmanis, E. Tunable Crystallinity in Regioregular Poly(3-Hexylthiophene) Thin Films and Its Impact on Field Effect Mobility. *Adv. Funct. Mater*. **2011**, 21, 2652-2659.

[22] Xiao, X. L.; Hu, Z. J.; Wang, Z. B.; He, T. B. Study on the Single Crystals of Poly(3-octylthiophene) Induced by Solvent-Vapor Annealing. *J. Phys. Chem. B* **2009**, 113, 14604-14610.

[23] Fu, Y.; Lin, C.; Tsai, F. Y. High Field-Effect Mobility from Poly(3-hexylthiophene) Thin-Film Transistors by Solvent-Vapor-Induced Reflow. *Org. Electron*. **2009**, 10, 883-888.

[24] Kim, B. G.; Kim, M. S.; Kim, J. Ultrasonic-Assisted Nanodimensional Self-Assembly of Poly-3-hexylthiophene for Organic Photovoltaic Cells. *ACS Nano* **2010**, 4, 2160-2166.

[25] Park, J. H.; Kim, J. S.; Lee, J. H.; Lee, W. H.; Cho, K. Effect of Annealing Solvent Solubility on the Performance of Poly(3-hexylthiophene)/Methanofullerene Solar Cells. *J. Phys. Chem. C* **2009**, 113, 17579-17584.

[26] Duong, D. T.; Walker, B.; Lin, J.; Kim, C.; Love, J.; Purushothaman, B.; Anthony, J. E.; Nguyen, T. Q. Molecular Solubility and Hansen Solubility Parameters for the Analysis of Phase Separation in Bulk Heterojunctions. *J. Polym. Sci., Part B: Polym. Phys*. **2012**, 50, 1405-1413.

[27] Chang, J. F.; Sun, B. Q.; Breiby, D. W.; Nielsen, M. M.; Solling, T. I.; Giles, M.; McCulloch, I.; Sirringhaus, H. Enhanced Mobility of Poly(3-hexylthiophene) Transistors by Spin-Coating from High-Boiling-Point Solvents. *Chem. Mater*. **2004**, 16, 4772-4776.

[28] Hidber, P. C.; Nealey, P. F.; Helbig, W.; Whitesides, G. M. New Strategy for Controlling the Size and Shape of MetallicFeatures Formed by Electroless Deposition of Copper: Microcontact Printing of Catalysts on Oriented Polymers, Followed by Thermal Shrinkage. *Langmuir* **1996**, 12, 5209-5215.

[29] Hyun, D. C.; Jeong, U. Substrate Thickness: An Effective Control Parameter for Polymer Thin Film Buckling on PDMS Substrates. *J. Appl. Polym. Sci*. **2009**, 112, 2683-2690.

[30] Pandey, S. S.; Gerard, M.; Sharma, A. L.; Malhotra, B. D. Thermal Analysis of Chemically Synthesized Polyemeraldine Base. *J. Appl. Polym. Sci*. **2000**, 75, 149-155.

[31] Henderson, R. K.; Jimenez-Gonzalez, C.; Constable, D. J. C.; Alston, S. R.; Inglis, G. G. A.; Fisher, G.; Sherwood, J.; Binks, S. P.; Curzons, A. D. Expanding GSK's Solvent Selection Guide - Embedding Sustainability into Solvent Selection Starting at Medicinal Chemistry. *Green Chem*. **2011**, 13, 854-862.

[32] Kiriy, N.; Jahne, E.; Adler, H. J.; Schneider, M.; Kiriy, A.; Gorodyska, G.; Minko, S.; Jehnichen, D.; Simon, P.; Fokin, A. A.; Stamm, M. One-Dimensional Aggregation of Regioregular Polyalkylthiophenes. *Nano Lett*. **2003**, 3, 707-712.

[33] Moule, A. J.; Meerholz, K. Controlling Morphology in Polymer-Fullerene Mixtures. *Adv. Mater*. **2008**, 20, 240-245.

[34] Li, L. G.; Lu, G. H.; Yang, X. N. Improving Performance of Polymer Photovoltaic Devices Using an Annealing-Free Approach via Construction of Ordered Aggregates in Solution. *J. Mater. Chem*. **2008**, 18, 1984-1990.

[35] O'Neill, A.; Khan, U.; Nirmalraj, P. N.; Boland, J.; Coleman, J. N. Graphene Dispersion and Exfoliation in Low Boiling Point Solvents. *J. Phys. Chem. C* **2011**, 115, 5422-5428.

[36] Hernandez, Y.; Nicolosi, V.; Lotya, M.; Blighe, F. M.; Sun, Z. Y.; De, S.; McGovern, I. T.; Holland, B.; Byrne, M.; Gun'ko, Y. K.; et al. High-Yield Production of Graphene by Liquid-Phase Exfoliation of Graphite. *Nat. Nanotechnol.* **2008**, 3, 563-568.

[37] Zhang, X. Y.; Coleman, A. C.; Katsonis, N.; Browne, W. R.; van Wees, B. J.; Feringa, B. L. Dispersion of Graphene in Ethanol Using a Simple Solvent Exchange Method. *Chem. Commun*. **2010**, 46, 7539-7541.

[38] He, M.; Ge, J.; Fang, M.; Qiu, F.; Yang, Y. L. Fabricating Polythiophene into Highly Aligned Microwire Film by Fast Evaporation of Its Whisker Solution. *Polymer* **2010**, 51, 2236-2243.

[39] Kim, J. S.; Lee, J. H.; Park, J. H.; Shim, C.; Sim, M.; Cho, K. High-Efficiency Organic Solar Cells Based on Preformed Poly(3-hexylthiophene) Nanowires. *Adv. Funct. Mater.* **2011**, 21, 480-486.

[40] Yang, H. H.; LeFevre, S. W.; Ryu, C. Y.; Bao, Z. N. Solubility-Driven Thin Film Structures of Regioregular Poly(3-hexylthiophene) Using Volatile Solvents. *Appl. Phys. Lett*. **2007**, 90, 172116.

[41] Yao, Y.; Hou, J. H.; Xu, Z.; Li, G.; Yang, Y. Effects of Solvent Mixtures on the Nanoscale Phase Separation in Polymer Solar Cells. *Adv. Funct. Mater*. **2008**, 18, 1783-1789.

[42] Abbott, S. J.; Hansen, C. M., Hansen Solubility Parameters in Practice (software), WWW-solubility.com, (accessed November 2012).

[43] Choi, K.; Tedder, D. W. Molecular Interactions in Chloroform-Diluent Mixtures. *AIChE J*. **1997**, 43, 196-211.

[44] Vargas, R.; Garza, J.; Dixon, D. A.; Hay, B. P. How Strong Is the Cα-H···OC Hydrogen Bond? *J. Am. Chem. Soc*. **2000**, 122, 4750-4755.

[45] Xu, Z.; Li, H. R.; Wang, C. M. Can a Blue Shift of the C-H Stretching Modes of Inactivated C Groups be an Indicator of Weak C-H··· O Hydrogen Bonds? *ChemPhysChem* **2006**, 7, 2460-2463.

[46] Solomonov, B. N.; Varfolomeev, M. A.; Abaidullina, D. I. Cooperative Hydrogen Bonding in Solution: Influence of Molecule Structure. *Vib. Spectrosc.* **2007**, 43, 380-386.

[47] Vaz, P. D.; Nolasco, M. M.; Gil, F. P. S. C.; Ribeiro-Claro, P. J. A.; Tomikinson, J. Hydrogen-Bond Dynamics of C-H...O Interactions: The Chloroform···Acetone Case. *Chem. -Eur. J*. **2010**, 16, 9010-9017.

[48] Horowitz, G. Organic Field-Effect Transistors. *Adv. Mater*. **1998**, 10, 365-377.

[49] Jia, H. P.; Gowrisanker, S.; Pant, G. K.; Wallace, R. M.; Gnade, B. E. Effect of Poly (3-hexylthiophene) Film Thickness on Organic Thin Film Transistor Properties. *J. Vac. Sci. Technol. A* **2006**, 24, 1228-1232.

[50] Chua, L. L.; Zaumseil, J.; Chang, J. F.; Ou, E. C. W.; Ho, P. K. H.; Sirringhaus, H.; Friend, R. H. General Observation of n-Type Field-Effect Behaviour in Organic Semiconductors. *Nature* **2005**, 434, 194-199.

[51] Berson, S.; De Bettignies, R.; Bailly, S.; Guillerez, S. Poly(3-hexylthiophene) Fibers for Photovoltaic Applications. *Adv. Funct. Mater*. **2007**, 17, 1377-1384.

[52] Gurau, M. C.; Delongchamp, D. M.; Vogel, B. M.; Lin, E. K.; Fischer, D. A.; Sambasivan, S.; Richter, L. J. Measuring Molecular Order in Poly(3-alkylthiophene) Thin Films with Polarizing Spectroscopies. *Langmuir* **2007**, 23, 834-842.

[53] Brown, P. J.; Thomas, D. S.; Kohler, A.; Wilson, J. S.; Kim, J. S.; Ramsdale, C. M.; Sirringhaus, H.; Friend, R. H. Effect of Interchain Interactions on the Absorption and Emission of Poly(3-hexylthiophene). *Phys. Rev. B* **2003**, 67, 064203.

[54] Mcculloch, I.; Heeney, M.; Bailey, C.; Genevicius, K.; I, M.; Shkunov, M.; Sparrowe, D.; Tierney, S.; Wagner, R.; Zhang, W. M.; et al. Liquid-Crystalline Semiconducting Polymers with High Charge-Carrier Mobility. *Nat. Mater*. **2006**, 5, 328-333.

[55] Prosa, T. J.; Winokur, M. J.; Moulton, J.; Smith, P.; Heeger, A. J. X-Ray Structural Studies of Poly(3-alkylthiophenes): An Example of an Inverse Comb. *Macromolecules* **1992**, 25, 4364-4372.

[56] Kline, R. J.; Mcgehee, M. D.; Toney, M. F. Highly Oriented Crystals at the Buried Interface in Polythiophene Thin-Film Transistors. *Nat. Mater*. **2006**, 5, 222-228.

[57] Yamamoto, T.; Komarudin, D.; Arai, M.; Lee, B. L.; Suganuma, H.; Asakawa, N.; Inoue, Y.; Kubota, K.; Sasaki, S.; Fukuda, T.; et al. Extensive Studies on pi-Stacking of Poly(3-alkylthiophene-2,5-diyl)s and Poly(4-alkylthiazole-2,5-diyl)s by Optical Spectroscopy, NMR Analysis, Light Scattering Analysis, and X-Ray Crystallography. *J. Am. Chem. Soc*. **1998**, 120, 2047-2058.

[58] Sanderson, R. T. Electronegativity and Bond Energy. *J. Am. Chem. Soc.* **1983**, 105, 2259-2261.

[59] Hammes, G. G; Park, A. C. Kinetic and Thermodynamic Studies of Hydrogen Bonding. *J. Am. Chem. Soc.* **1969**, 91, 956-961.

[60] Abboud, J.-L. M.; Roussel, C.; Gentric, E.; Sraidi, K.; Lauransan, J.; Guiheneuf, G.; Kamlet, M. J.; Taft, R. W. Studies on Amphiprotic Compounds. 3. Hydrogen-Bonding Basicity of Oxygen and Sulfur Compounds. *J. Org. Chem.* **1988**, 53, 1545-1550.

[61] Wierzejewska, M.; Saldyka, M. Are Hydrogen Bonds to Sulfur and Oxygen Different? Theoretical Study of Dimethylsulfide and Dimethylether Complexes with Nitric Acid. *Chem. Phys. Lett.* **2004**, 391, 143-147.

[62] Hildebrand, J. H.; Scott, R. L. The Entropy of Solution of Nonelectrolytes. *J. Chem. Phys*. **1952**, 20, 1520-1521.

[63] Max, J. J.; Chapados, C. Infrared spectroscopy of acetone–water liquid mixtures. I. Factor analysis. *J. Chem. Phys.* **2003,** 119, 5632-5643.

[64] Hansen, C. M.; Smith, A. L. Using Hansen Solubility Parameters to Correlate Solubility of C-60 Fullerene in Organic Solvents and in Polymers. *Carbon* **2004**, 42, 1591-1597.

[65] Hansen, C. M., *"Hansen Solubility Parameters"*: A User's Handbook, 2nd Edition; CRC Press: Boca Raton, **2007**; pp 1-24.

[66] Machui, F.; Langner, S.; Zhu, X. D.; Abbott, S.; Brabec, C. J. Determination of the P3HT:PCBM Solubility Parameters via a Binary Solvent Gradient Method: Impact of Solubility on the Photovoltaic Performance. *Sol. Energy Mater. Sol. Cells* **2012**, 100, 138-146.

[67] Machui, F.; Abbott, S.; Waller, D.; Koppe, M.; Brabec, C. J. Determination of Solubility Parameters for Organic Semiconductor Formulations. *Macromol. Chem. Phys*. **2011**, 212, 2159-2165.

[68] Aiyar, A.; Hong, J.-I.; Izumi, J.; Choi, D.; Kleinhenz, N.; Reichmanis, E. Ultrasound-Induced Ordering in Poly (3-hexylthiophene): Role of Molecular and Process Parameters on Morphology and Charge Transport. *ACS Appl. Mater. Interfaces* **2013**, 5, 2368-2377.

CHAPTER 4

PHOTOINDUCED ANISOTROPIC SUPRAMOLECULAR ASSEMBLY AND ENHANCED CHARGE TRANSPORT OF POLY(3-HEXYLTHIOPHENE) THIN FILMS**

4.1 Introduction

As noted above, conjugated polymer semiconductors have garnered interest for application as opto-electronic device components, because they may provide for low-cost, large-area electronic device fabrication arising from their low-temperature, solution-based processability.[1-4] These polymers exhibit anisotropic optical and electrical properties owing to one-dimensional *p*-orbital overlap along the polymer backbone. Thus, their interesting properties can be realized in opto-electronic devices when the polymer chains are well-ordered via π-π interactions.[5, 6] However, polymer semiconductors often suffer from relatively low charge carrier transport characteristics owing to a low degree of π-stacking between polymer chains in solidified thin-films; semiconducting polymer films prepared via solution-processing are typically composed of many small crystalline regions embedded within a largely disordered matrix which may be unfavorable for efficient charge hopping between transport sites.[7-9]

Regio-regular poly (3-hexylthiophene) (P3HT) is a readily available polymer semiconductor that can serve as a model system to investigate the critical role played by polymer thin-film morphology. P3HT self-organizes into a microcrystalline structure,[10] exhibits acceptable hole transport properties,[11] and exhibits good solubility in various organic solvents.[9] The self-organization of the polymer into ordered supramolecular

** *Adv. Funct. Mater.* **2014**, 24, 4457.

assemblies commensurate with efficient charge transport has been achieved by tuning a range of process parameters (e.g., film deposition method (spin vs. drop cast),[12] solvent boiling point (low vs. high boiling point),[13] polymer-dielectric interface treatment,[14] and post-deposition processing (solvent vapor or thermal annealing))[15, 16] in combination with approaches such as improved molecular design[10] and increased polymer molecular weight (MW).[17, 18] However, these strategies present limitations for large-scale high-throughput processing due to associated pre- and/or post semiconductor deposition steps.

To eliminate the need for ancillary, potentially cumbersome and costly thin-film deposition processes, several approaches including solvent solubility tuning,[19, 20] solution aging,[21, 22] and ultrasonic irradiation[23, 24] have been explored to induce well-ordered nanofibillar aggregates in solution, prior to film deposition. Self-assembled P3HT nanofibers exhibit dramatically improved crystallinity and macroscopic charge transport characteristics compared to a comparatively more amorphous P3HT film, owing to enhanced π-π interactions between conjugated chains.[23] The anisotropic growth of crystalline-like P3HT aggregates is ascribed to strong π-π interactions in direction of the fiber axis, along which charge transport readily occurs.[24, 25] Accordingly, longer P3HT nanofibers may be expected to exhibit more effective charge transport in macroscopic polymer thin-films, owing to long-range ordered crystalline regimes. Among the effective strategies, ultrasonic irradiation leads to the formation of ordered nanofibrillar aggregates of P3HT in solution, where the concentration of aggregates can be controlled by sonication time.[23] Alternative approaches require steps such as the addition of small quantities of poor solvent to the majority solution, and/or aging the solutions to obtain well-ordered nanofibrillar structures.[19, 21, 22] The apparent solution based aggregates appear to persist

through the deposition process, and nanofibrillar features are perceptible in what are believed to be crystalline regimes in the corresponding solid state films.[23] Further, the resultant films exhibit a one to two order of magnitude enhancement in the corresponding field-effect mobilities. Thus, additional pre- or post-treatments to enhance crystallinity and concomitantly, charge transport characteristics, are not essential.[23]

However, P3HT nanofibers formed by ultrasonic irradiation appear to be short. While brief sonication times promote P3HT nanofibrillar aggregate formation, the treatment limits continuous fiber growth (< 400 nm) presumably due to strong agitation, leading to an increase in the number of grain boundaries in resultant thin-films and thus, continued enhancement in charge carrier transport is restricted.[12, 23] Further, the ultrasonic irradiation process requires immersion of the solution into a water bath and is sensitive to a number of experimental parameters, many of which may be difficult to control, thus complicating the experimental results and presenting its own set of scale-up challenges.

In this chapter, we demonstrate for the first time, a facile, scalable strategy to enhance anisotropic supramolecular ordering of P3HT chains in solution using low intensity, limited duration ultraviolet (UV) irradiation. UV treatment of the conjugated polymer solution enhances crystallinity and concomitantly, charge transport characteristics of resultant thin-films. The approach represents a benign alternative for large-scale fabrication and high-throughput processing of polymer-based devices for a range of applications due to the ease with which the polymer solutions could be exposed uniformly to UV light. The apparently crystalline nanofibrillar aggregates formed by UV irradiation are greater than 1μm in length, which is likely the origin of the improvement in charge

carrier mobility for films deposited from the irradiated solutions vs. those prepared via ultrasonication.

4.2 Experimental Methods

4.2.1 Materials

P3HT and P3BT were purchased from Rieke Metals Inc., and used without further purification. The molecular weight of P3HT (M_n of 19.7 kDa and M_w of 43.7 kDa) and P3BT (M_n of 25.8 kDa and M_w of 55.5 kDa) used for the study was obtained through gel permeation chromatography (GPC) using trichlorobenzene as the eluent and polystyrene as standard. The head to tail regioregularity (RR) was estimated to be approximately 96 % for P3HT and 87 % for P3BT from the 1H-NMR spectra obtained from deuterated chloroform solution at 293 K using a Bruker DSX 300. Chloroform used in this study was anhydrous grade, purchased from Sigma Aldrich, and used without further purification.

4.2.2 Anisotropic Growth of P3HT Aggregates in Solution

10 mg of P3HT was introduced into 2 mL of chloroform in a 20 mL borosilicate glass vial fitted with a magnetic stirbar in air. Alternatively, 6 mg of P3HT was introduced into 2 mL of toluene, owing to the relatively lower solubility of P3HT in toluene. Subsequently, the vial was sealed with a cap and the solution was stirred for at least 30 min at ca. 55 °C to ensure complete polymer dissolution. The as-prepared solution was cooled to ambient temperature prior to UV irradiation. The vial containing the solution was placed on a hand-held UV lamp (Entela UVGL-15, 5 mW cm^{-2}, 254 nm) which had been placed on a magnetic stirrer (Corning Inc.). Then, the solution was gently stirred and simultaneously irradiated for times ranging from 0 to 8 min. The irradiation was performed through the bottom wall of the borosilicate glass vial which transmits more than 90 % of

the incident UV 254 nm light. P3HT nanofibrillar aggregates began to appear in the solution and further, increased in both quantity and size with increased irradiation time. The ultrasonic irradiation of P3HT solutions was performed by following the published procedure.[23]

4.2.3 OFET Fabrication and Characterization

The OFET devices used for electrical characterization consisted of two contact devices where P3HT films were deposited via spin-coating the relevant polymer solution onto a 300 nm thick SiO_2 gate dielectric. The highly doped silicon substrate served as the gate electrode while Au/Cr was used for the source and drain contacts. The source and drain contacts were fabricated using a standard photolithography based lift-off process, followed by E-beam evaporation (Denton Explorer) of 50 nm Au contacts with 3 nm of Cr as the adhesion layer. Before spin-coating P3HT solutions, all devices were cleaned for 15 min in a UV-ozone cleaner (Novascan PSD-UV) to completely remove any residual photoresist and other organic contaminants. OFET devices were prepared by spin-coating (WS-650MZ-23NPP, Laurell) the solutions onto precleaned substrates at a spin speed of 1500 rpm for 60 s in air, and tested in nitrogen ambient using an Agilent 4155C semiconductor parameter analyzer. The polymer films spin-coated from the P3HT solutions treated by UV irradiation for times in the range of 0 to 8 min were found to have similar thickness, in the range of 26–30 nm, as determined by spectroscopic ellipsometry (M-2000, JA Woollam). The devices were stored in a vacuum oven (1 Torr) overnight at room temperature to remove residual solvent. The field-effect hole mobility was calculated in the saturation regime of transistor operation (V_{DS} = – 80 V) by plotting the drain current (I_{DS}) versus gate voltage (V_{GS}) and fitting the data to the following equation:[26]

$$I_{DS} = \frac{WC_{OX}}{2L}\mu(V_{GS} - V_T)^2 \quad (4.1)$$

where W (2000 μm) and L (50 μm) are the transistor channel width and length, respectively, V_T is the threshold voltage and C_{OX} is the capacitance per unit area of the silicon dioxide gate dielectric (1.15×10^{-8} F/cm^2).

4.2.4 UV-vis Spectroscopy

The solution and solid state UV-vis spectra were recorded using an Agilent 8510 UV-vis spectrometer. Films for solid state studies were prepared by spin-coating the requisite solution onto precleaned glass slides following the same procedures used to prepare OFET devices.

4.2.5 Grazing Incidence X-ray Diffraction (GIXD)

Out-of-plane grazing incidence X-ray diffraction data were obtained using a Panalytical X'Pert Pro system equipped with a Cu X-ray source operating at 45 kV and 40 mA. The grazing incidence angle was fixed at 0.2° and the detector was scanned from 3° to 30°.

4.2.6 Atomic Force Microscopy (AFM)

The AFM measurements were performed on films spin-coated onto bottom contact OFET devices using an ICON dimension scanning probe microscope (Bruker) operating in tapping mode with a silicon tip (RTESP, Bruker).

4.2.7 Polarized Optical Microscopy (POM)

The POM images were obtained with a Leica DMRX optical microscope equipped with a polarizer and a Nikon D300 digital SLR camera.

4.3 Results and Discussion

4.3.1 Field-Effect Mobility Measurements

Bottom contact organic field-effect transistors (OFETs) (Figure 4.1a) were fabricated by spin-coating the respective P3HT solutions onto device substrates (transistor channel width = 2000 μm and length = 50 μm) using P3HT/chloroform ($CHCl_3$) (5 mg/mL) solutions irradiated by a UV lamp (Entela UVGL-15, 5 mW cm^{-2}, 254 nm) for designated times. Figure 4.1b depicts the observed dramatic increase in the mobility of these P3HT films as a function of UV irradiation time. The observed increase is greater than that obtained with films prepared via ultrasonication (Figure 4.1c); while ultrasonication processing of the P3HT sample used here afforded approximately a 4.6 -fold (from $1.6 \pm 0.42 \times 10^{-2}$ to $7.3 \pm 0.55 \times 10^{-2}$ cm^2 V^{-1} s^{-1}) increase in macroscopic hole mobility, UV irradiation provided for more than a 5.1-fold enhancement (up to $8.2 \pm 0.35 \times 10^{-2}$ cm^2 V^{-1} s^{-1}). The ultrasonication of the polymer solutions was performed following previous reports.[23] Moreover, the mobility of poly(3-butyl thiophene) (P3BT) films was enhanced almost 10.7-fold (from $1.3 \pm 0.11 \times 10^{-3}$ to $13.9 \pm 1.00 \times 10^{-3}$ cm^2 V^{-1} s^{-1}) via UV irradiation, while ultrasonication led to an increase of only approximately 3.5-fold (up to $4.5 \pm 0.41 \times 10^{-3}$ cm^2 V^{-1} s^{-1}) (Figure 4.1d). Saturation of mobility is discerned upon UV irradiation for times in the range of 5 to 8 min. The observation of the saturation is reminiscent of the percolation type transport mechanism proposed for P3HT thin-films prepared from ultrasonicated solutions.[23] Figures 4.1e and f depict transfer and characteristic output curves, respectively, which are typical of p-channel OFET operation in the accumulation mode. The high turn-on voltages (V_{ON}) obtained in Figure 4.1e are attributed to the effects

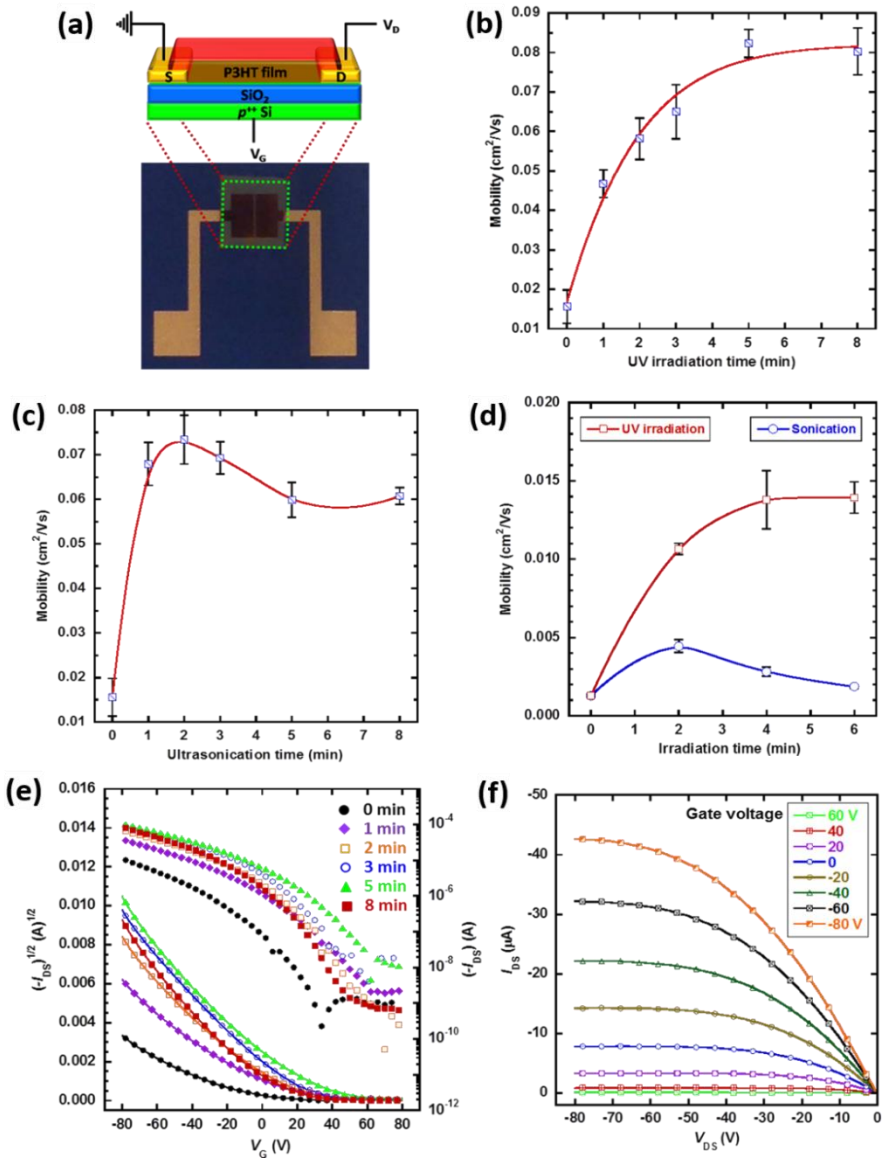

Figure 4.1: a) Schematic structure and photoimage of OFET device. b) Average field-effect mobilities of P3HT films spin coated from P3HT/$CHCl_3$ solutions irradiated by UV for designated times. c) Average field-effect mobilities of P3HT films obtained from P3HT/$CHCl_3$ solutions ultrasonicated for various times. d) Average field-effect mobilities of P3BT films obtained from P3BT/$CHCl_3$ solutions treated with ultrasonication and UV irradiation, respectively for various times. e) Transfer characteristics of P3HT OFETs fabricated from UV irradiated polymer solutions. f) Typical output characteristics obtained from a P3HT OFET prepared via spin-coating from P3HT/$CHCl_3$ solution UV irradiated for 8 min. All measurements were performed in a nitrogen glovebox, and mobilities were calculated in the saturation regime of operation with $V_{DS} = -80$ V.

of residual doping, acceptor like traps at the P3HT-oxide interface, and/or charge trapping

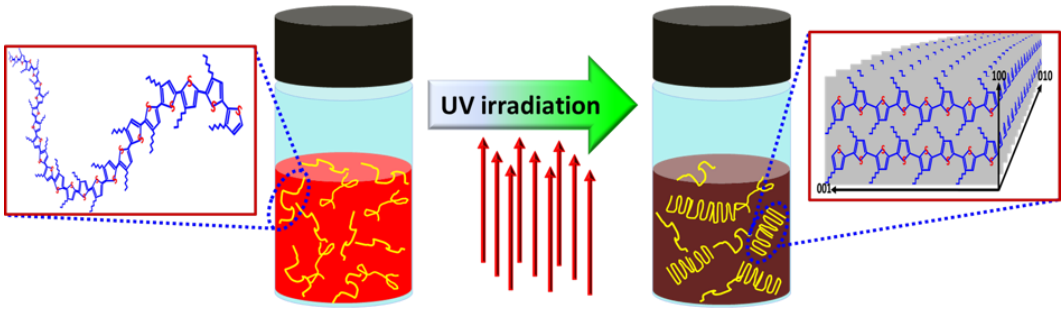

Figure 4.2: Suggested mechanism for the UV irradiation induced anisotropic molecular ordering of P3HT chains.

at grain boundaries/interfaces.[12, 27, 28]

4.3.2 Suggested Mechanism for Anisotropic Supramolecular Assembly

Figure 4.2 presents a schematic illustration of a suggested mechanism for the observed UV induced anisotropic supramolecular ordering of P3HT chains in solution. It appears that the photo-irradiation induces a conformational change of the conjugated polymer chains such that chain segments can more readily interact. [29, 30] In the absence of photo-irradiation, the conjugated polymer chains exhibit largely random coil-like features, while photo-irradiation affords enhanced neighboring π-π interactions.[29-34] In a typical experiment, the P3HT solution is gently stirred in a borosilicate glass vial which is more than 90% transmissive at 254 nm, and it is then irradiated. Upon UV irradiation, the conjugated polymer (in solution) appears to change its conformation[29, 30, 35]. Through the conformational change, P3HT chains favor π-π interchain interactions which over time afford extended supramolecular assemblies of the polymer.[31, 36] It is generally known that UV irradiation, coupled with exposure to oxygen and water, can lead to significant polymer degradation, diminishing polymer properties.[37] No discernable P3HT degradation was observed here. It is believed that the exposure dose (5 mW cm^{-2} for ca. 8 min under air)

Table 4.1: XPS atomic percentages of C, S, and O and the C/S ratio in P3HT films obtained by spin-coating from pristine, 8 min ultrasonicated, and 8 min UV irradiated P3HT solutions.

	XPS atomic percentage			
	C	S	O	C/S
Pristine film	88.12	10.00	1.88	8.81
Ultrasonic irradiated film	89.12	10.11	0.76	8.82
UV irradiated film	88.50	10.27	1.16	8.62

used for even the highest dose is relatively mild compared to that required for polymer degradation (reported as 130 mW cm^{-2} for ca. 1000 min under oxygen atmosphere).[38] The films obtained by spin-coating P3HT solutions exposed to ultrasonic vs. UV treatment, for 8 min showed no discernible oxidation, compared to the pristine P3HT film (Table 4.1). The ratio (C/S) for the films appears similar, ranging from 8.62 to 8.82, and the 0.76–1.88 % observed oxygen concentration is close to the detection limit of the spectrometer (Figure 4.3c), and no discernable difference of elemental composition between the films is detected. Therefore, it is believed that neither ultrasonication nor UV irradiation results in polymer oxidation, rather, any oxidation would be associated with aspects such as synthesis, storage of P3HT precursor polymer, or both. In addition, oxygen uptake (O1s at ca. 532 eV) and important changes in the C1s (284.7 eV) and S2p (163.7 eV) regions by ultrasonication and UV irradiation were not observed (Figure 4.3); decrease in the intensity and change in the peak position of C1s and S2p do not appear. Additionally, increases in intensity or changes in peak position of the O1s band are not apparent upon either ultrasonication or UV irradiation.[39, 40] These results strongly suggest that low intensity UV irradiation for short times leads to no discernable oxidation of the conjugated polymer chains.

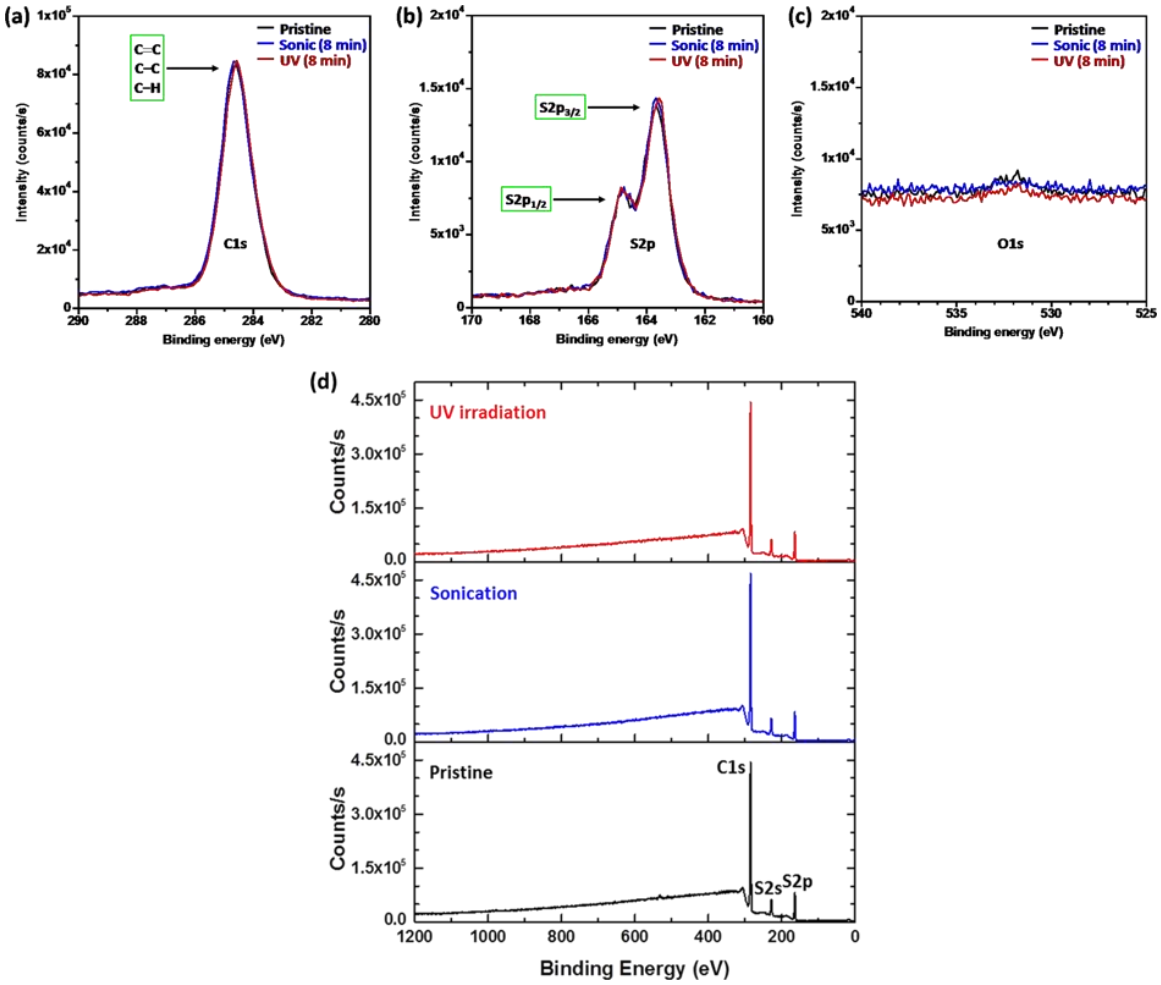

Figure 4.3: XPS spectra of films obtained by spin-coating from pristine, 8 min ultrasonicated, and 8 min UV irradiated P3HT solutions: (a) C1s, (b) S2p, (c) O1s spectra, and (d) broad spectra.

GPC data also depict that short ultrasonication and UV irradiation do not lead to discernable degradation of the polymer chains, showing no remarkable change in molecular weight after treatment for 8 min (Table 4.2). In addition, the 1H-NMR spectra of P3HT was unchanged after either treatment, indicating no chemical changes occurred (Figure 4.4); no difference in P3HT H-T regioregularity was observed after 8 min of ultrasonication or UV irradiation, respectively; the H-T regioregularity was estimated to be 96 % for all samples (pristine, ultrasonicated, and UV irradiated P3HT).[41, 42] In order

Table 4.2: GPC results of P3HT in $CHCl_3$ before and after 8 min ultrasonication and 8 min UV irradiation respectively.

	M_N (kDa)	M_W (kDa)
Pristine	19.7	43.7
Ultrasonication	18.4	43.1
UV irradiation	21.9	46.9

to conduct 1H-NMR characterization, P3HT was dissolved into deuterated chloroform after P3HT was dried from pristine, 8 min ultrasonicated, and 8 min UV irradiated P3HT solutions, respectively. FT-IR data also depict no change of P3HT chemical structure by sonication and UV irradiation (Figure 4.5). The polymer films obtained from 8 min sonicated and 8 min UV irradiated solutions respectively exhibit no discernable spectral changes, compared to the pristine film. The characteristic peaks, thiophene rings (ca. 1510 and 1454 cm^{-1}), aromatic C-H (ca. 3055 cm^{-1}), and alkyl groups (ca. 3000-2850 cm^{-1}) are clearly observed in all films. A carbonyl peak at ca. 1620 cm^{-1} appears in all polymer films, and could be attributed to oxidation associated with polymer synthesis, storage of P3HT precursor polymer, or both, consistent with XPS data (Figure 4.3); new absorption bands do not appear nor propagate in the carbonyl range at 1620-1715 cm^{-1} for the films obtained from sonicated solution and UV irradiated solution, respectively, which indicates that no discernable photooxidation takes place in the P3HT solution by either sonication or UV irradiation.[43]

The effect of UV irradiation was found to be thermally reversible as shown in Figure 4.6; the solution absorption spectra and colors changed through UV irradiation were restored to those of pristine P3HT solutions via mild heating. To investigate the thermal

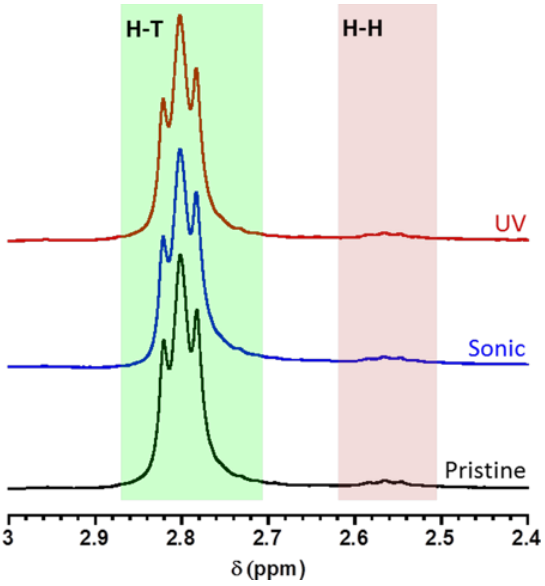

Figure 4.4: 1H-NMR spectra of P3HT solutions in deuterated chloroform at room temperature.

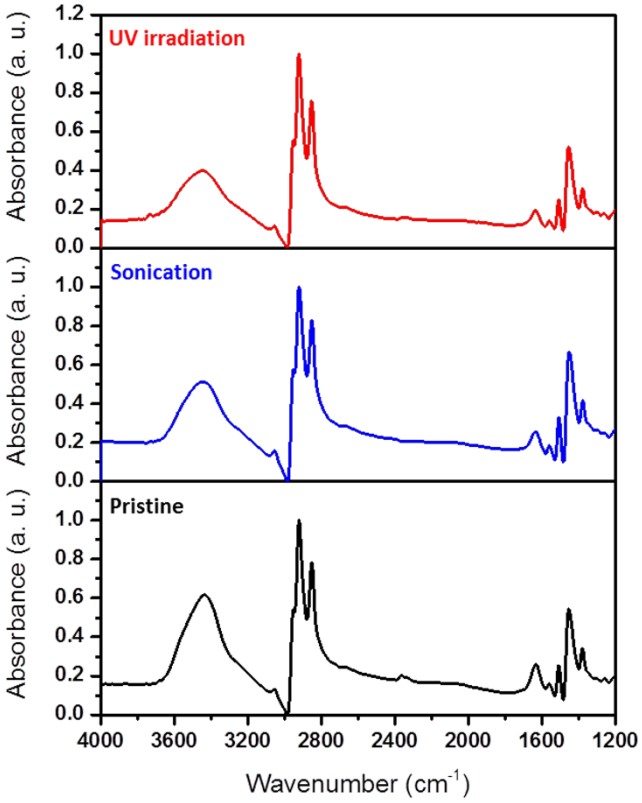

Figure 4.5: FT-IR data of films obtained by spin-coating from pristine, 8 min ultrasonicated, and 8 min UV irradiated P3HT solutions.

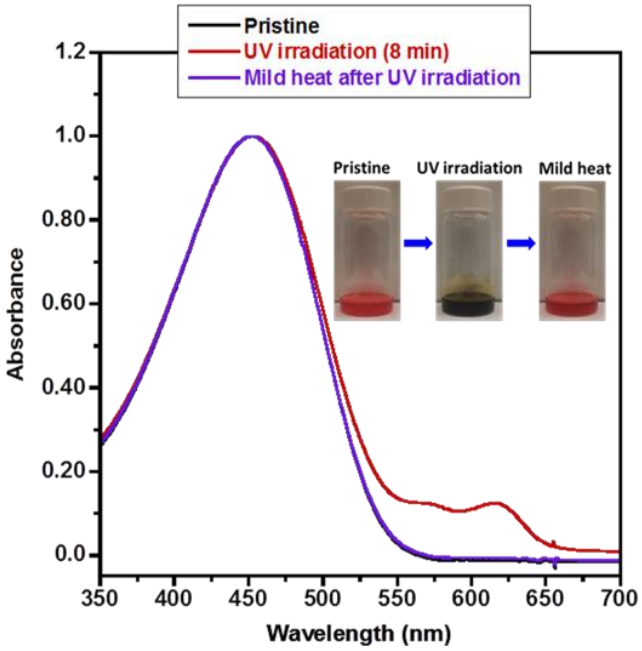

Figure 4.6: Normalized UV-visible absorption spectra of P3HT/$CHCl_3$ solutions after 8 min UV irradiation followed by mild heating of the corresponding solution for a period of 1 hour at 55 °C. The inset images represent the colors of the corresponding solutions.

reversibility of the UV induced spectral changes, the irradiated solutions were mildly heated at approximately 55 °C for ca. 1 hour.

4.3.3 UV-vis Absorption Property of Thin Films

Figures 4.7a and b depict the electronic absorption spectra obtained from P3HT/$CHCl_3$ solutions irradiated by UV for times ranging from 0 to 8 min, and spectra acquired from the corresponding semiconducting thin-films, respectively. The solution changed from bright orange to dark brown with increased UV irradiation time (inset in Figure 4.7a), indicative of an increase in P3HT nanoaggregate concentration.[23] The solution based absorption spectra exhibit low energy features at ca. 570 and 620 nm, suggestive of vibronic bands associated with the (0–1) and (0–0) transitions respectively, which increase with increased UV irradiation time. The emergence of these features is

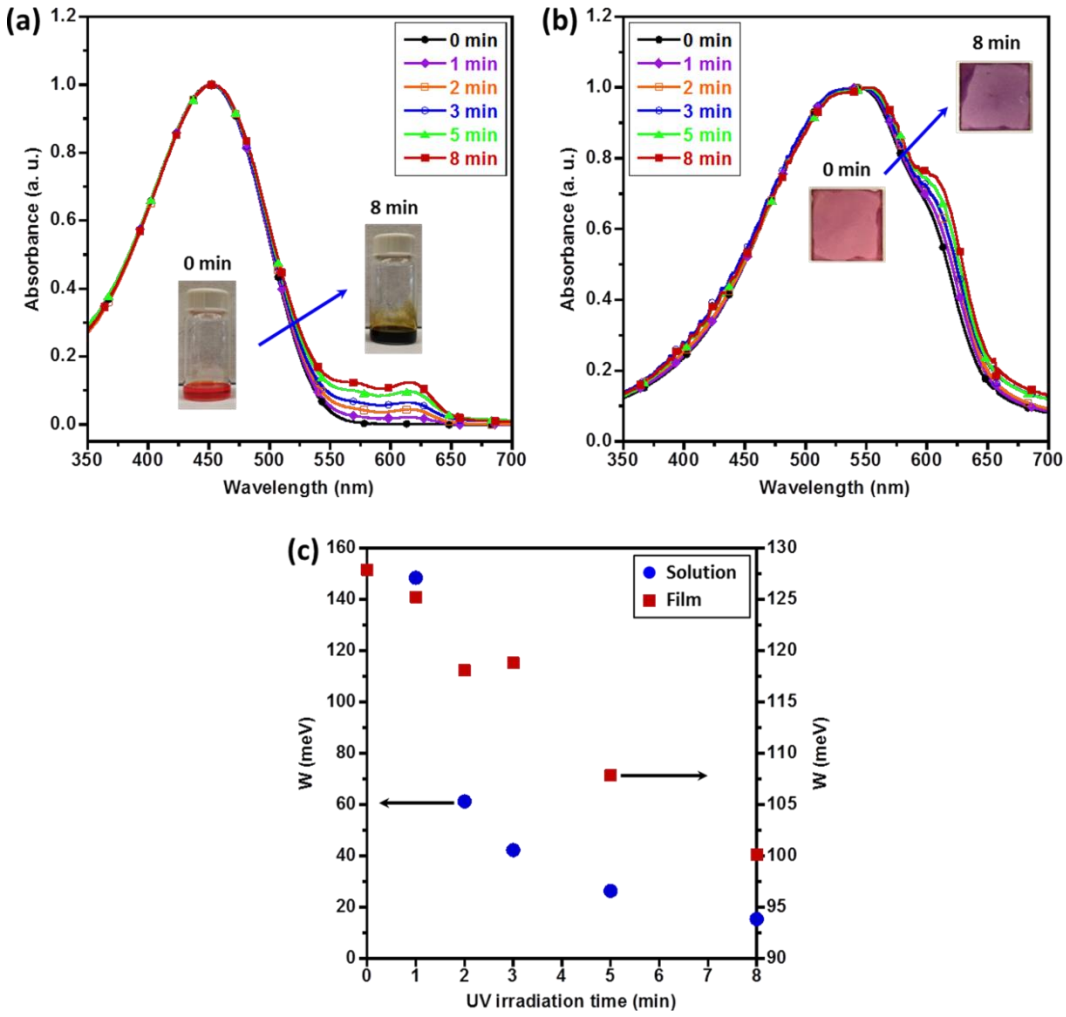

Figure 4.7: Normalized UV-visible absorption spectra of a) P3HT/$CHCl_3$ solutions as a function of UV irradiation time and b) corresponding P3HT films obtained by spin-coating. c) The evolution of exciton bandwidth *W* of ordered aggregates in the solutions and films as a function of UV irradiation time. The inset images in Figure 4.7a show the color change of P3HT/$CHCl_3$ solution from bright orange to dark brown by UV irradiation for 8 min while the inset images in Figure 4.7b represent the corresponding films which exhibit different colors, pale red and dark purple, respectively.

believed to be associated with an increase in ordered aggregates formed via π-π stacking between polymer chains in solution (Figure 4.7a).[23] In the present case, the vibronic features are suggested to result directly from UV induced anisotropic extension of P3HT

chains in solution, i.e., photoinduced polymer chain planarization (intramolecular ordering) followed by ordered aggregate formation (intermolecular ordering).

Consistent with previous reports,[12, 23] the solution based nanoaggregates appear to survive a spin-coating process, and in turn provide for increased molecular order in the solid thin-films as shown in Figure 4.7b; resultant films transform from pale red to dark purple with increased irradiation time (inset in Figure 4.7b). Further, as the irradiation time of the solutions increases, the low energy absorption bands at ca. 555 and 605 nm appear to increase in intensity in resultant polymer films, supporting the presumption that ordered P3HT nanoaggregates in solution survive the thin-film deposition process. While in the solid films, the lower energy bands exhibit an increase in intensity, they are blue-shifted in comparison to their respective solution counterparts. This phenomenon could be attributed to the formation of a larger proportion of disordered aggregates during solvent evaporation.[44]

Detailed analysis of the UV-vis absorption spectra provides further insights relating to polymer chain conjugation length (intramolecular ordering).[10, 45] Examination of the P3HT absorption spectrum reveals bands associated with two phases, a crystalline region due to ordered chains and an amorphous region due to disordered chains.[45] According to Spano's model, the crystalline regions are assumed to be composed of weakly interacting H-aggregates in which interchain coupling leads to vibronic bands in the absorption spectrum.[45] Further, the vibronic bands can be related to the free exciton bandwidth (W) which correlates with the conjugation length (intrachain ordering) of an individual polymer chain.[10, 44, 45] A decrease in W indicates an increase in both average conjugation length and chain order.[10, 45] The W values are calculated using Equation 4.2 and the intensities of

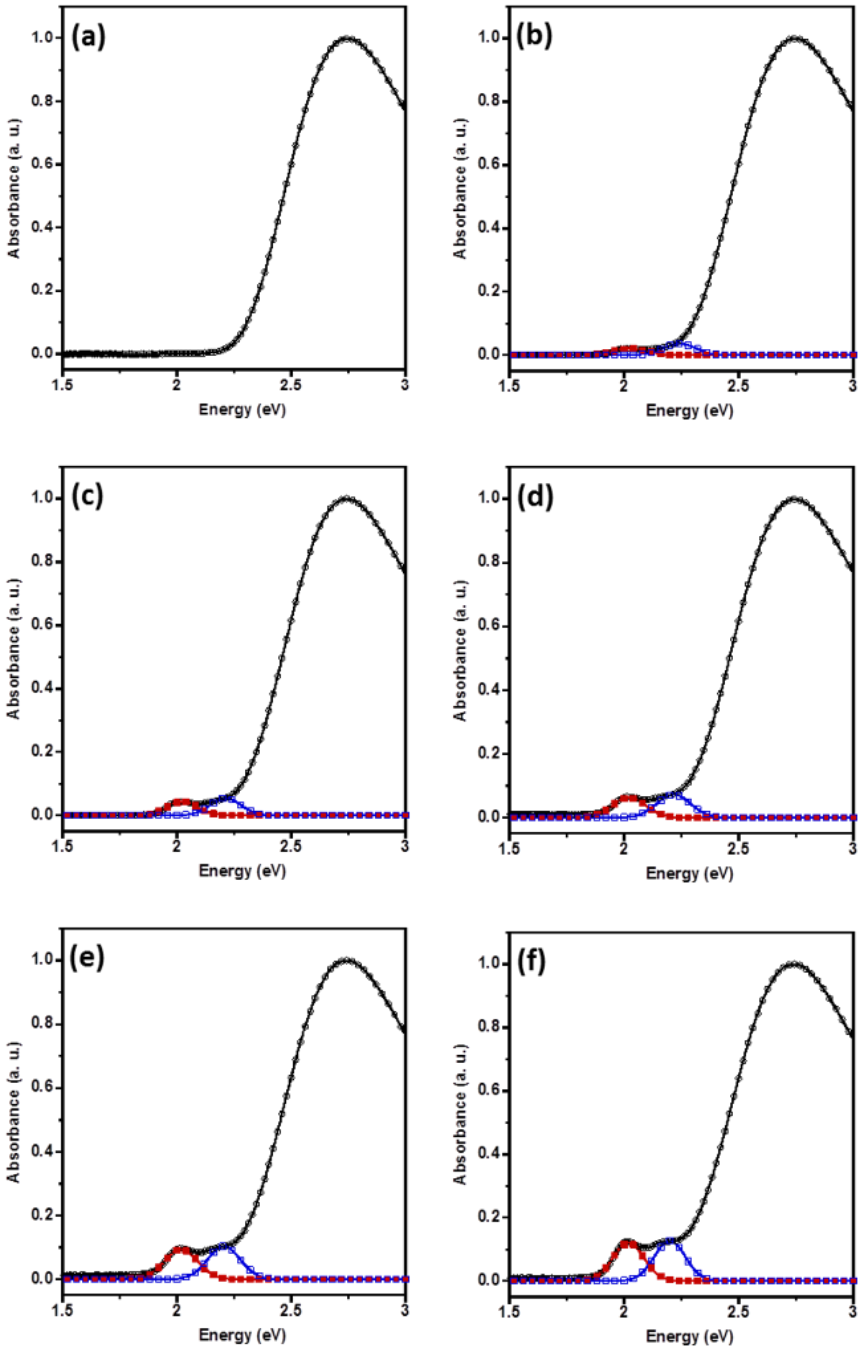

Figure 4.8: Absorption spectra of P3HT/$CHCl_3$ solutions under different UV irradiation times (0, 1, 2, 3, 5, and 8 min). The lines with filled red and open blue squares indicate the Gaussians corresponding to the (0-0) and (0-1) bands respectively. The lines with black open circles depict the experimental absorption spectra.

the (0–0) and (0–1) transitions obtained from fits to the experimental spectra (Figure 4.8

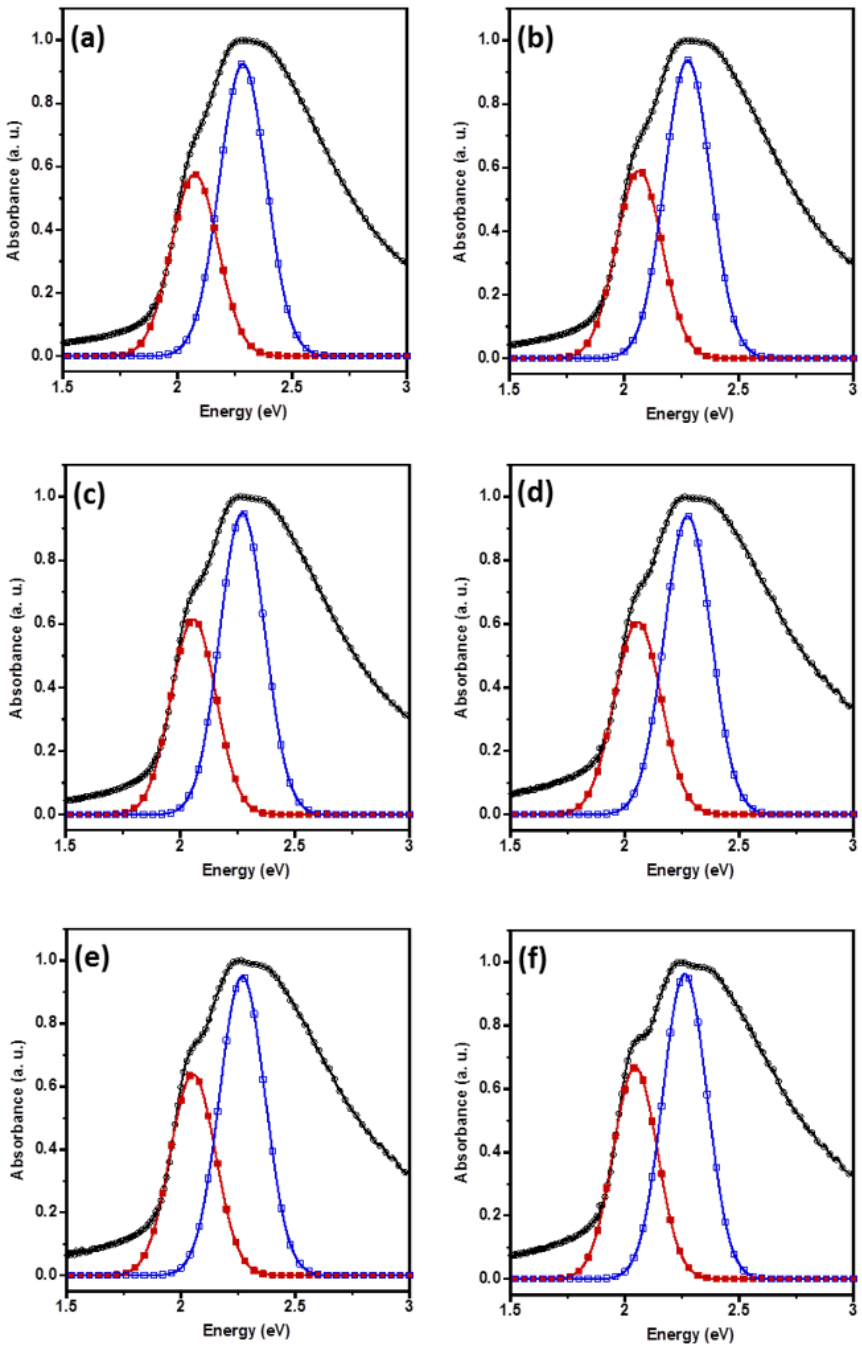

Figure 4.9: Absorption spectra of P3HT films obtained by spin coating from P3HT/$CHCl_3$ solutions under different UV irradiation times (0, 1, 2, 3, 5, and 8 min). The lines with filled red and open blue squares indicate the Gaussians corresponding to the (0-0) and (0-1) bands respectively. The lines with black open circles represent the experimental absorption spectra.

and 4.9).

$$\frac{I_{0-0}}{I_{0-1}} \approx \left(\frac{1 - 0.24W / E_p}{1 + 0.073W / E_p} \right)^2 \quad (4.2)$$

I_{0-0} and I_{0-1} are the intensities of the (0–0) and (0–1) transitions, respectively and E_P is the vibrational energy of the symmetric vinyl stretch (taken as 0.18 eV).[45] Polymer intrachain ordering in solution is found to be enhanced by UV irradiation based on observed decreasing free exciton bandwidth with increased UV irradiation time (from 148.42 to 15.37 meV) as shown in Figure 4.7c. *W* of the pristine polymer solution could not be calculated because no aggregates were detected in the solution. UV irradiation of the polymer solutions evidently impacts intra- and intermolecular ordering of resultant polymer films; as the irradiation time increases, the intensity of the low energy features increases (Figure 4.7b), while *W* decreases from 127.90 to 100.13 meV in the corresponding polymer thin-films (Figure 4.7c). *W* calculated from the solution spectra has lower values than *W* of the corresponding films; the solution based nanoaggregates formed upon UV irradiation are thus suggested to contain a higher degree of well-ordered polymer chains while the aggregates in the corresponding films present more disordered polymer chains formed during solvent evaporation together with well-ordered polymer chains formed by UV irradiation of the precursor solutions.

4.3.4 Crystallinity and Microstructure of Thin Films

The enhanced intra- and intermolecular interactions of P3HT chains are expected to lead to higher thin-film crystallinity.[9, 23] Figure 4.10a shows X-ray diffractograms obtained from grazing incidence (GIXD) measurements of P3HT films spin-coated from P3HT/$CHCl_3$ solutions irradiated by UV for a series of different times. Increase in UV irradiation time of the precursor solutions effects a gradual increase in intensity of the (100)

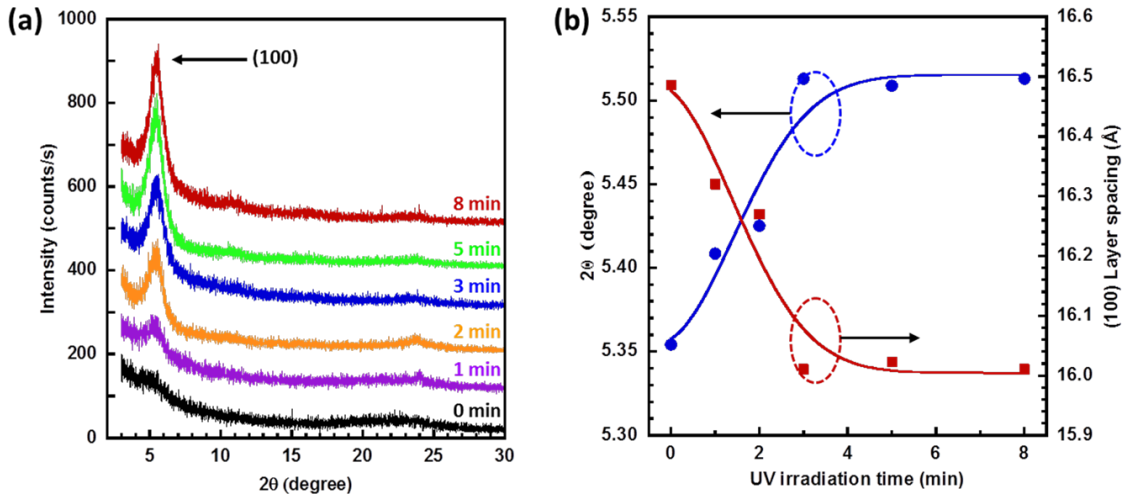

Figure 4.10: a) Grazing incidence X-ray diffraction profiles of P3HT films obtained from the UV irradiated solutions. b) 2θ angle (left axis) of the (100) peak and corresponding layer spacing (right axis) as a function of precursor solution UV irradiation time.

peak associated with polymer chain lamellar packing along the crystallographic direction perpendicular to the backbone. This increase could result from either an increase in the size of individual crystallites, the number of crystallites, or both.[9, 23] The micro-structural change is further characterized by a (100) peak shift to higher angle, from 5.35 to 5.51° after 8 min of UV irradiation, indicative of a decrease in d-spacing in the direction along the side chains from 16.49 to 16.01 Å (Figure 4.10b) and suggestive of either increased interdigitation between P3HT alkyl side chains or a change in side chain tilt.[9, 23]

4.3.5 Morphology of Thin Films

The morphological change of the resultant films is also observed through polarized optical microscopy (POM) as shown in Figure 4.11. With increased UV irradiation time, images of the resultant thin-films as observed through crossed polarizers appear to brighten. While the film cast from a pristine solution appears dark and therefore isotropic (amorphous), the films cast from solutions exposed to UV for longer durations exhibit

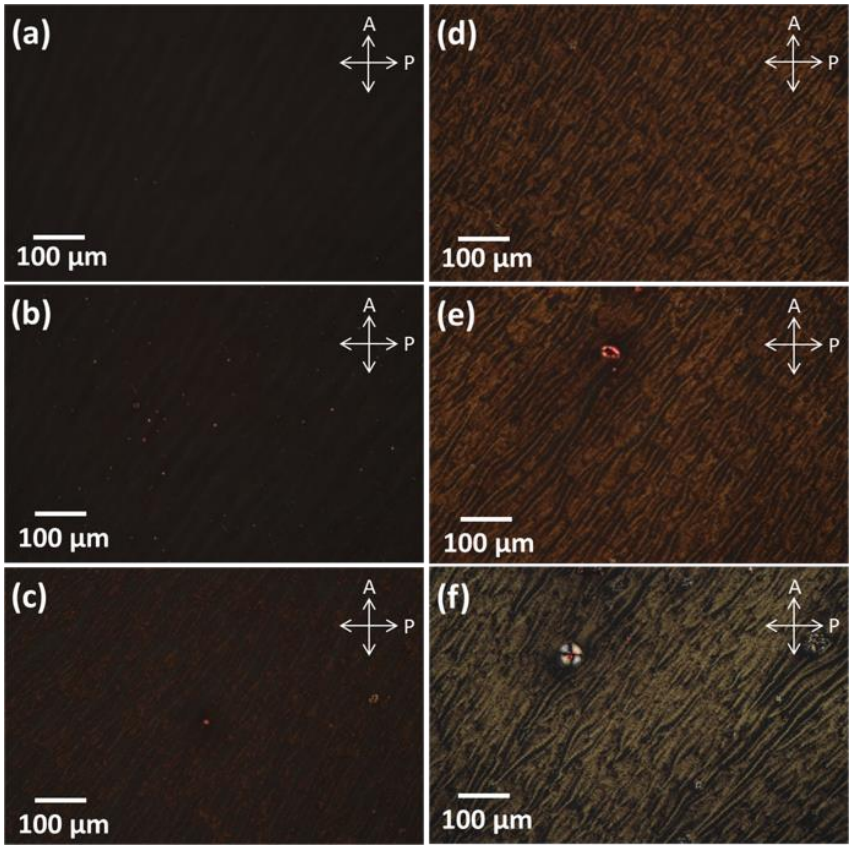

Figure 4.11: Polarized optical microscopic images of P3HT films spin-coated on glass from P3HT/$CHCl_3$ solutions UV irradiated for a) 0, b) 1, c) 2, d) 3, e) 5, and f) 8 min. All images were taken with crossed polarizers.

increasingly bright birefringent textures. The observed birefringence is another indicator for either enhanced conjugated polymer molecular ordering or crystallinity.[46, 47]

Atomic force microscopy (AFM) images of P3HT films obtained from pristine and UV irradiated P3HT solutions are shown in Figure 4.12, demonstrating the clear evolution of anisotropic growth of P3HT aggregates from an initial featureless and amorphous-like structure. In solution, UV irradiation induced polymer backbone planarization would lead to nanofibrillar structured aggregates via favorable π-π stacking of the polymer chains. For instance, UV irradiation of the solutions for a short time (ca. 1 min) leads to the formation

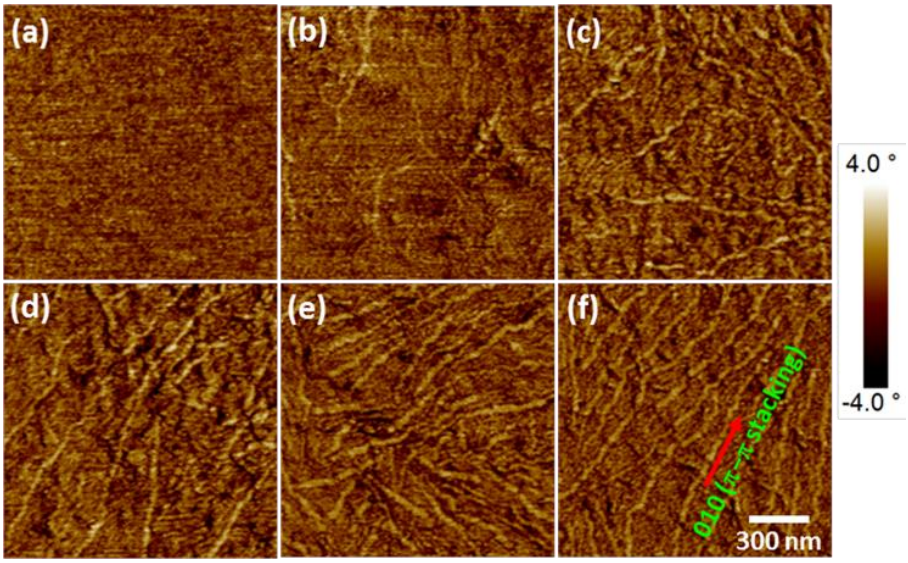

Figure 4.12: Tapping mode AFM phase images of P3HT films obtained by spin-coating from P3HT/$CHCl_3$ solutions UV irradiated for a) 0, b) 1, c) 2, d) 3, e) 5, and f) 8 min.

of distinct nanofibrils that are ca. 30 nm in width and 300–600 nm in length. Increased irradiation time affords not only an increased number of nanofibers, but their length also increases substantially (> 1 μm). The surface roughness of resultant films also changed upon UV exposure. The pristine films show a relatively low root-mean square (RMS), ca. 0.63 nm, while the RMS of films obtained from UV irradiated solutions gradually increases up to ca. 1.97 nm with increased UV irradiation time. The increased roughness is ascribed to the increased size and quantity of nanofibrillar structures within the thin-films.

4.3.6 Impact of Grain Boundaries

The AFM, XRD, and POM results are in good agreement, suggesting that the increase in the degree of polymer thin-film crystallinity is a direct consequence of the increased number and size of microcrystallite-like P3HT nanofibers formed in the precursor solutions during UV irradiation, which are then distributed throughout the solidified films via the spin-coating process. In contrast, the crystalline nanofibers formed

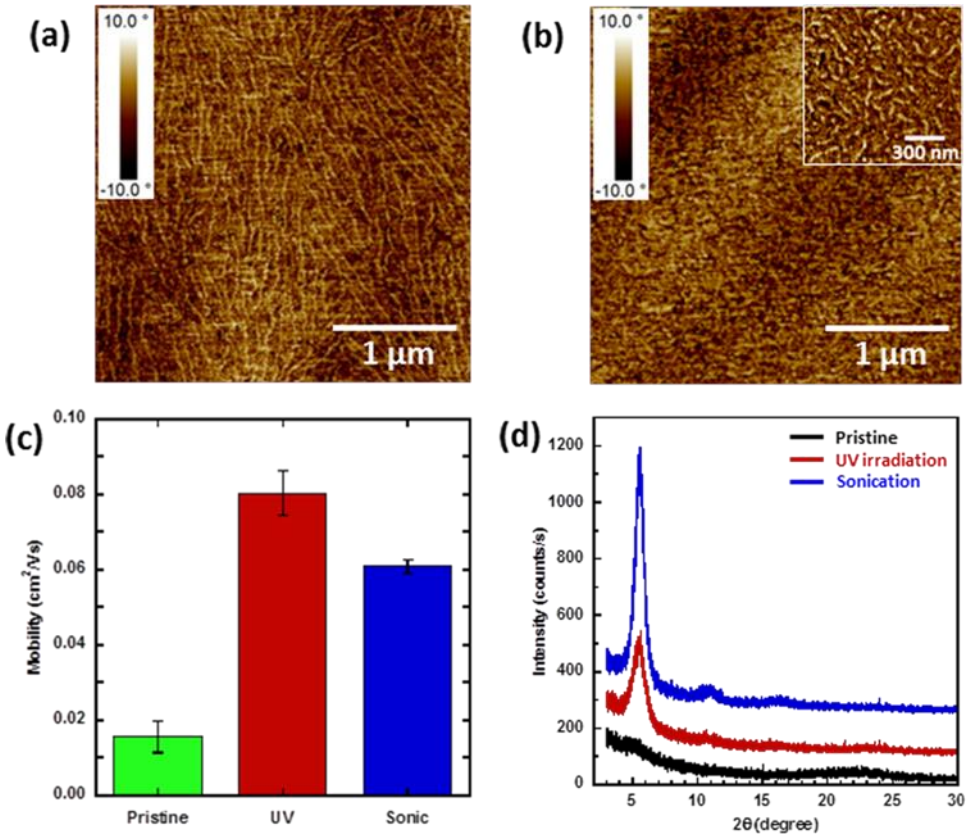

Figure 4.13: Tapping mode AFM phase images of (a) P3HT film obtained from P3HT/$CHCl_3$ solution UV irradiated for 8 min and (b) P3HT film spin coated from P3HT/$CHCl_3$ solution ultrasonicated for 8 min. (c) Field-effect mobilities and (d) grazing incidence X-ray diffraction profiles of pristine and corresponding films obtained from treated solutions. The inset image is a magnification of Figure 4.13b.

within P3HT films obtained from ultrasonicated solutions are shorter (< 300 nm vs. > 1 µm) (Figure 4.13a and b), generating relatively more grain boundaries resistive to efficient charge carrier transport.[9] Thus, the resultant films prepared from ultrasonicated solutions exhibit lower macroscopic mobilities compared to those obtained from UV treatment, even though the former exhibit an enhanced degree of molecular ordering and presumably higher crystallinity (Figure 4.13c and d). These results underscore the significance of grain boundaries, in addition to ordering and/or crystallinity in achieving efficient charge transport within π-conjugated polymer films. To maximize semiconducting polymer thin-

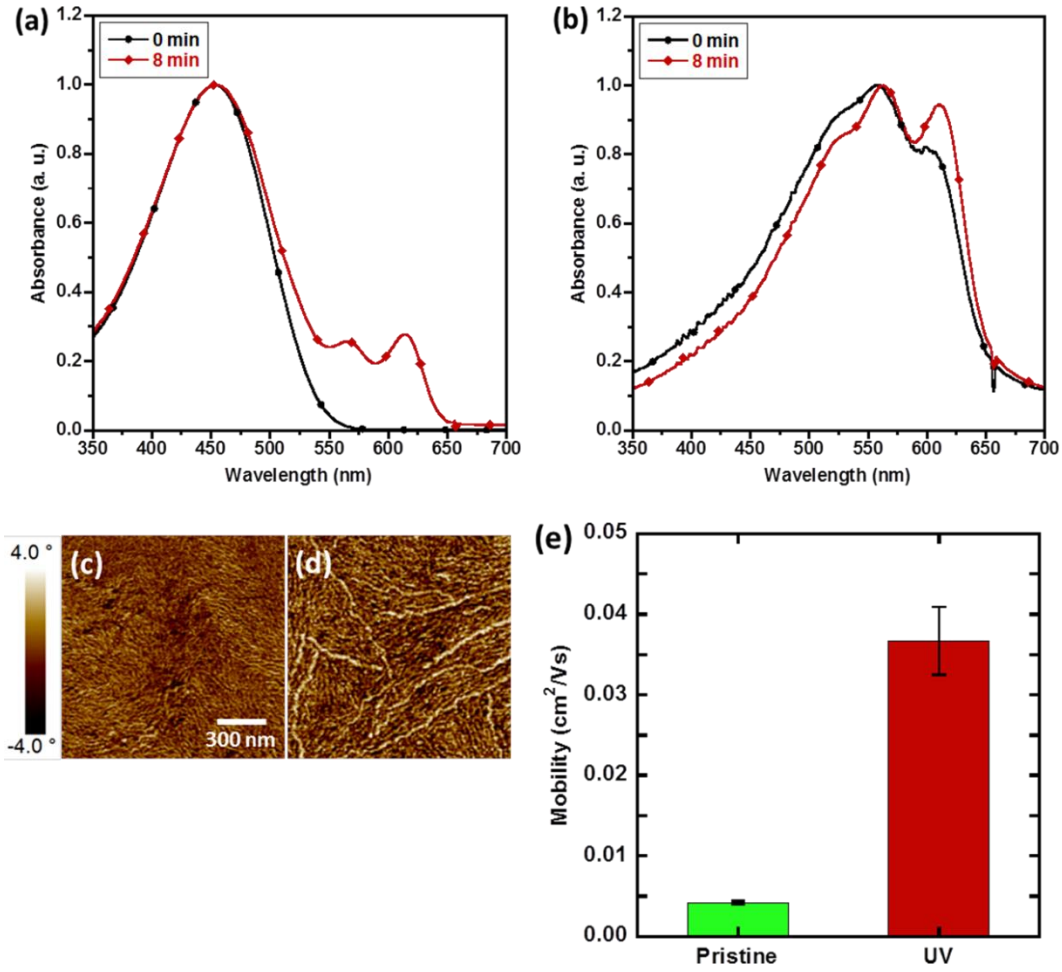

Figure 4.14: Normalized UV-visible absorption spectra of a) P3HT/Toluene solutions before and after 8 min UV irradiation. b) Corresponding P3HT films obtained by spin-coating. Tapping mode AFM phase images of P3HT films obtained by spin-coating from P3HT/Toluene solutions c) before and d) after 8 min UV irradiation. e) Field-effect mobilities of corresponding films.

film charge transport characteristics, the number of grain boundaries within the polymer films should be reduced while the molecular ordering should be enhanced.

4.3.7 Applicability of UV Irradiation Approach

UV irradiation of P3HT solutions prepared in non-chlorinated solvents was also found to facilitate molecular ordering. For instance, irradiation of P3HT/toluene effects dramatic enhancement of charge carrier transport within corresponding films as shown in

Figure 4.14. In toluene solution, the P3HT absorption spectrum exhibits low energy features at ca. 570 and 620 nm, characteristic of well-ordered UV irradiation induced aggregate formation (Figure 4.14a). The solution based nanoaggregates survive a spin-coating process, and provide for enhanced molecular order in the solid thin-films (Figure 4.14b). While thin-films derived from P3HT/chloroform appear amorphous-like (Figure 4.12a), those obtained from P3HT/toluene solution are composed of many small nanofibrillar structures (Figure 4.14c); the lower evaporation rate of toluene vs. chloroform may facilitate polymer chain interactions, alignment and stacking into fibrillar structures during the coating process. In contrast to the pristine sample, the P3HT film obtained from a UV irradiated (8 min) P3HT/toluene solution exhibits noticeably wider and longer fibrils, in addition to the small fibrillar aggregates (Figure 4.14d). As with the chloroform solution, UV irradiation of P3HT/toluene effects an increase in P3HT charge carrier mobility. As shown in Figure 4.14e, mobility increased by a factor of approximately 9, from $0.42 \pm 0.02 \times 10^{-2}$ cm^2 V^{-1} s^{-1} to $3.7 \pm 0.42 \times 10^{-2}$ cm^2 V^{-1} s^{-1}.

4.4 Conclusion

In conclusion, the anisotropic supramolecular assembly of P3HT chains in solution can be achieved simply via short (< 8 min), low-intensity UV irradiation. Polymer degradation was not discernible, and exposure to a low UV dose led to enhanced molecular ordering in solution with resultant dramatic enhancement of corresponding thin-film charge transport characteristics. UV induced enhanced polymer chain intramolecular ordering in solution, thereby effected formation of anisotropic supramolecular assemblies via favorable π-π stacking (intermolecular interaction) of the polymer chains. The nanofibrillar aggregates formed in solution survived the film deposition process and in turn,

evidently enhanced the supramolecular ordering and charge transport characteristics of resultant polymer films. The crystalline-like nanofibrillar aggregates appeared relatively long (> 1 μm) compared to those obtained in films prepared via ultrasonic irradiation, contributing to dramatic improvement of charge carrier mobilities, presumed to arise from a reduction in the number of grain boundaries. Low-dose UV irradiation presents a strategy for enhancing anisotropic molecular ordering of π-conjugated polymers in precursor solution thereby eliminating the need for process steps such as dielectric surface modification or thermal and/or solvent vapor annealing of the polymer thin-films. The approach may prove attractive in the pursuit of robust, low-cost, large-area electronic device fabrication methodologies.

4.5 References

[1] Li, J. H.; Sun, Z. H.; Yan, F. Solution Processable Low-Voltage Organic Thin Film Transistors with High-k Relaxor Ferroelectric Polymer as Gate Insulator. *Adv. Mater.* **2012**, *24*, 88-93.

[2] Yan, H.; Chen, Z. H.; Zheng, Y.; Newman, C.; Quinn, J. R.; Dotz, F.; Kastler, M.; Facchetti, A. A High-Mobility Electron-Transporting Polymer for Printed Transistors. *Nature* **2009**, *457*, 679-686.

[3] Forrest, S. R. The Path to Ubiquitous and Low-Cost Organic Electronic Appliances on Plastic. *Nature* **2004**, *428*, 911-918.

[4] Li, G.; Zhu, R.; Yang, Y. Polymer Solar Cells. *Nat. Photonics* **2012**, *6*, 153-161.

[5] O'Neill, M.; Kelly, S. M. Ordered Materials for Organic Electronics and Photonics. *Adv. Mater.* **2011**, *23*, 566-584.

[6] Kim, B.-G.; Jeong, E. J.; Chung, J. W.; Seo, S.; Koo, B.; Kim, J. A Molecular Design Principle of Lyotropic Liquid-Crystalline Conjugated Polymers with Directed Alignment Capability for Plastic Electronics. *Nat. mater.* **2013,** 12, 659-664.

[7] Coropceanu, V.; Cornil, J.; da Silva, D. A.; Olivier, Y.; Silbey, R.; Bredas, J. L. Charge Transport in Organic Semiconductors. *Chem. Rev.* **2007**, *107*, 926-952.

[8] Goffri, S.; Muller, C.; Stingelin-Stutzmann, N.; Breiby, D. W.; Radano, C. P.; Andreasen, J. W.; Thompson, R.; Janssen, R. A. J.; Nielsen, M. M.; Smith, P.; Sirringhaus, H. Multicomponent Semiconducting Polymer Systems with Low Crystallization-Induced Percolation Threshold. *Nat. Mater.* **2006**, *5*, 950-956.

[9] Chang, M.; Choi, D.; Fu, B.; Reichmanis, E. Solvent Based Hydrogen Bonding: Impact on Poly(3-hexylthiophene) Nanoscale Morphology and Charge Transport Characteristics. *ACS nano* **2013**, *7*, 5402-5413.

[10] Aiyar, A. R.; Hong, J. I.; Reichmanis, E. Regioregularity and Intrachain Ordering: Impact on the Nanostructure and Charge Transport in Two-Dimensional Assemblies of Poly(3-hexylthiophene). *Chem. Mater.* **2012**, *24*, 2845-2853.

[11] Sirringhaus, H.; Brown, P. J.; Friend, R. H.; Nielsen, M. M.; Bechgaard, K.; Langeveld-Voss, B. M. W.; Spiering, A. J. H.; Janssen, R. A. J.; Meijer, E. W.; Herwig, P.; de Leeuw, D. M. Two-Dimensional Charge Transport in Self-Organized, High-Mobility Conjugated Polymers. *Nature* **1999**, *401*, 685-688.

[12] Aiyar, A. R.; Hong, J. I.; Izumi, J.; Choi, D.; Kleinhenz, N.; Reichmanis, E. Ultrasound-Induced Ordering in Poly(3-hexylthiophene): Role of Molecular and Process Parameters on Morphology and Charge Transport. *ACS Appl. Mater. Interfaces* **2013**, *5*, 2368-2377.

[13] Chang, J. F.; Sun, B. Q.; Breiby, D. W.; Nielsen, M. M.; Solling, T. I.; Giles, M.; McCulloch, I.; Sirringhaus, H. Enhanced Mobility of poly(3-hexylthiophene) Transistors by Spin-Coating from High-Boiling-Point Solvents. *Chem. Mater.* **2004**, *16*, 4772-4776.

[14] Kim, D. H.; Jang, Y.; Park, Y. D.; Cho, K. Surface-Induced Conformational Changes in Poly(3-hexylthiophene) Monolayer Films. *Langmuir* **2005**, *21*, 3203-3206.

[15] Fu, Y.; Lin, C.; Tsai, F. Y. High Field-Effect Mobility from Poly(3-hexylthiophene) Thin-Film Transistors by Solvent–Vapor-Induced Reflow. *Org. Electron.* **2009**, *10*, 883-888.

[16] Cho, S.; Lee, K.; Yuen, J.; Wang, G. M.; Moses, D.; Heeger, A. J.; Surin, M.; Lazzaroni, R. Thermal Annealing-Induced Enhancement of the Field-Effect Mobility of Regioregular Poly(3-hexylthiophene) Films. *J. Appl. Phys.* **2006**, *100*, 114503.

[17] Kline, R. J.; McGehee, M. D.; Kadnikova, E. N.; Liu, J. S.; Frechet, J. M. J. Controlling the Field-Effect Mobility of Regioregular Polythiophene by Changing the Molecular Weight. *Adv. Mater.* **2003**, *15*, 1519-1522.

[18] Zhang, R.; Li, B.; Iovu, M. C.; Jeffries-EL, M.; Sauve, G.; Cooper, J.; Jia, S. J.; Tristram-Nagle, S.; Smilgies, D. M.; Lambeth, D. N.; McCullough, R. D.; Kowalewski, T. Nanostructure Dependence of Field-Effect Mobility in Regioregular Poly(3-hexylthiophene) Thin Film Field Effect Transistors. *J. Am. Chem. Soc.* **2006**, *128*, 3480-3481.

[19] Kiriy, N.; Jahne, E.; Adler, H. J.; Schneider, M.; Kiriy, A.; Gorodyska, G.; Minko, S.; Jehnichen, D.; Simon, P.; Fokin, A. A.; Stamm, M. One-Dimensional Aggregation of Regioregular Polyalkylthiophenes. *Nano Lett.* **2003**, *3*, 707-712.

[20] Li, L. G.; Jacobs, D. L.; Che, Y. K.; Huang, H. L.; Bunes, B. R.; Yang, X. M.; Zang, L. Poly(3-hexylthiophene) Nanofiber Networks for Enhancing the Morphology Stability of Polymer Solar Cells. *Org. Electron.* **2013**, *14*, 1383-1390.

[21] Kim, J. S.; Lee, J. H.; Park, J. H.; Shim, C.; Sim, M.; Cho, K. High-Efficiency Organic Solar Cells Based on Preformed Poly(3-hexylthiophene) Nanowires. *Adv. Funct. Mater.* **2011**, *21*, 480-486.

[22] Oh, J. Y.; Shin, M.; Lee, T. I.; Jang, W. S.; Min, Y.; Myoung, J. M.; Baik, H. K.; Jeong, U. Self-Seeded Growth of Poly(3-hexylthiophene) (P3HT) Nanofibrils by a Cycle of Cooling and Heating in Solutions. *Macromolecules* **2012**, *45*, 7504-7513.

[23] Aiyar, A. R.; Hong, J. I.; Nambiar, R.; Collard, D. M.; Reichmanis, E. Tunable Crystallinity in Regioregular Poly (3-Hexylthiophene) Thin Films and Its Impact on Field Effect Mobility. *Adv. Funct. Mater.* **2011**, *21*, 2652-2659.

[24] Kim, B. G.; Kim, M. S.; Kim, J. Ultrasonic-Assisted Nanodimensional Self-Assembly of Poly(3-hexylthiophene) for Organic Photovoltaic Cells. *ACS Nano* **2010**, *4*, 2160-2166.

[25] Jimison, L. H.; Toney, M. F.; McCulloch, I.; Heeney, M.; Salleo, A. Charge-Transport Anisotropy Due to Grain Boundaries in Directionally Crystallized Thin Films of Regioregular Poly (3-hexylthiophene). *Adv. Mater.* **2009**, *21*, 1568-1572.

[26] Horowitz, G.; Hajlaoui, R.; Bouchriha, H.; Bourguiga, R.; Hajlaoui, M. The Concept of "Threshold Voltage" in Organic Field-Effect Transistors. *Adv. Mater.* **1998**, *10*, 923-927.

[27] Chua, L. L.; Zaumseil, J.; Chang, J. F.; Ou, E. C. W.; Ho, P. K. H.; Sirringhaus, H.; Friend, R. H. General Observation of n-Type Field-Effect Behaviour in Organic Semiconductors. *Nature* **2005**, *434*, 194-199.

[28] Wu, P. T.; Xin, H.; Kim, F. S.; Ren, G. Q.; Jenekhe, S. A. Regioregular Poly(3-pentylthiophene): Synthesis, Self-Assembly of Nanowires, High-Mobility Field-Effect Transistors, and Efficient Photovoltaic Cells. *Macromolecules* **2009**, *42*, 8817-8826.

[29] Ruhe, J.; Colaneri, N. F.; Bradley, D. D. C.; Friend, R. H.; Wegner, G. Photoexcited States in Poly(3-alkylthienylenes). *J. Phys.: Condens. Matter* **1990**, *2*, 5465-5477.

[30] Kim, Y. H.; Spiegel, D.; Hotta, S.; Heeger, A. J. Photoexcitation and Doping Studies of Poly(3-hexylthienylene). *Phys. Rev. B* **1988**, *38*, 5490-5495.

[31] Cheng, Y. J.; Yang, S. H.; Hsu, C. S. Synthesis of Conjugated Polymers for Organic Solar Cell Applications. *Chem. Rev.* **2009**, *109*, 5868-5923.

[32] Xu, B.; Holdcroft, S. Molecular Control of Luminescence from Poly(3-hexylthiophenes). *Macromolecules* **1993**, *26*, 4457-4460.

[33] MacDiarmid, A. G. "Synthetic metals": A Novel Role for Organic Polymers (Nobel Lecture). *Angew. Chem. Int. Ed.* **2001**, *40*, 2581-2590.

[34] Bredas, J. L.; Chance, R. R.; Silbey, R. Comparative Theoretical Study of the Doping of Conjugated Polymers: Polarons in Polyacetylene and Polyparaphenylene. *Phys. Rev. B* **1982**, *26*, 5843-5854.

[35] Mike, J. F.; Nalwa, K.; Makowski, A. J.; Putnam, D.; Tomlinson, A. L.; Chaudhary, S.; Jeffries-EL, M. Synthesis, Characterization and Photovoltaic Properties of Poly

(thiophenevinylene-alt-benzobisoxazole)s. *Phys. Chem. Chem. Phys.* **2011**, *13*, 1338-1344.

[36] Son, H. J.; Carsten, B.; Jung, I. H.; Yu, L. P. Overcoming Efficiency Challenges in Organic Solar Cells: Rational Development of Conjugated Polymers. *Energy Environ. Sci.* **2012**, *5*, 8158-8170.

[37] Zhuo, J. M.; Zhao, L. H.; Png, R. Q.; Wong, L. Y.; Chia, P. J.; Tang, J. C.; Sivaramakrishnan, S.; Zhou, M.; Ou, E. C. W.; Chua, S. J.; Sim, W. S.; Chua, L. L.; Ho, P. K. H. Direct Spectroscopic Evidence for a Photodoping Mechanism in Polythiophene and Poly(bithiophene-*alt*-thienothiophene) Organic Semiconductor Thin Films Involving Oxygen and Sorbed Moisture. *Adv. Mater.* **2009**, *21*, 4747-4752.

[38] Hintz, H.; Egelhaaf, H. J.; Luer, L.; Hauch, J.; Peisert, H.; Chasse, T. Reversible and Irreversible Light-Induced p-Doping of P3HT by Oxygen Studied by Photoelectron Spectroscopy (XPS/UPS). *Chem. Mater.* **2011**, *23*, 145-154.

[39] Manceau, M.; Gaume, J.; Rivaton, A.; Gardette, J. L.; Monier, G.; Bideux, L. Further Insights into the Photodegradation of Poly(3-hexylthiophene) by Means of X-Ray Photoelectron Spectroscopy. *Thin Solid Films* **2010**, *518*, 7113-7118.

[40] Hintz, H.; Egelhaaf, H. J.; Peisert, H.; Chasse, T. Photo-Oxidation and Ozonization of Poly(3-hexylthiophene) Thin Films as Studied by UV/VIS and Photoelectron Spectroscopy. *Polym. Degrad. Stab.* **2010**, *95*, 818-825.

[41] Chen, T. A.; Wu, X.; Rieke, R. D. Regiocontrolled Synthesis of Poly(3-alkylthiophenes) Mediated by Rieke Zinc: Their Characterization and Solid-State Properties. *J. Am. Chem.* **1995**, *117*, 233-244.

[42] Woo, C. H.; Thompson, B. C.; Kim, B. J.; Toney, M. F.; Frechet, J. M. J. The Influence of Poly(3-hexylthiophene) Regioregularity on Fullerene-Composite Solar Cell Performance. *J. Am. Chem.* **2008**, *130*, 16324-16329.

[43] Manceau, M.; Rivaton, A.; Gardette, J. L.; Guillerez, S.; Lemitre, N. The Mechanism of Photo-and Thermooxidation of Poly(3-hexylthiophene)(P3HT) Reconsidered. *Polym. Degrad. Stab.* **2009**, 94, 898-907.

[44] Nagarjuna, G.; Baghgar, M.; Labastide, J. A.; Algaier, D. D.; Barnes, M. D.; Venkataraman, D. Tuning Aggregation of Poly(3-hexylthiophene) within Nanoparticles. *ACS Nano* **2012**, *6*, 10750-10758.

[45] Clark, J.; Chang, J. F.; Spano, F. C.; Friend, R. H.; Silva, C. Determining Exciton Bandwidth and Film Microstructure in Polythiophene Films Using Linear Absorption Spectroscopy. *Appl. Phys. Lett.* **2009**, *94*, 163306.

[46] Kinder, L.; Kanicki, J.; Petroff, P. Structural Ordering and Enhanced Carrier Mobility in Organic Polymer Thin Film Transistors. *Synth. Met.* **2004**, *146*, 181-185.

[47] Crossland, E. J. W.; Rahimi, K.; Reiter, G.; Steiner, U.; Ludwigs, S. Systematic Control of Nucleation Density in Poly(3-hexylthiophene) Thin Films. *Adv. Funct. Mater.* **2011**, *21*, 518-524.

CHAPTER 5

ANISOTROPIC ASSEMBLY OF CONJUGATED POLYMER NANOCRYSTALLITES FOR ENHANCED CHARGE TRANSPORT

5.1 Introduction

Conjugated polymer (CP) semiconductors are promising materials for a variety applications including light-emitting diodes,[1-3] optical and amperometric sensors,[4-7] organic solar cells[8-10] and thin-film transistors,[11-14] due to their low-temperature, solution-based processibility, which may provide for low cost, large-area electronic device fabrication.[9, 11, 14-16] However, CP thin-film charge carrier transport is still relatively lower than that observed for their small molecule organic semiconductor counterparts. CPs generally exhibit lower molecular ordering in solidified thin-films;[17, 18] solution processed polymers are semicrystalline, comprised of many small crystalline regions embedded within a largely disordered matrix impeding efficient charge hopping between transport sites.[15, 16, 19]

Regio-regular poly(3-hexylthiophene) (P3HT) is a representative polymer semiconductor investigated for use in a variety of polymer-based organic devices; P3HT self-organizes into a microcrystalline structure,[16, 20] it exhibits acceptable hole transport properties,[21] and exhibits good solubility in selected organic solvents.[15, 22] Self-assembled P3HT aggregates exhibit dramatically improved crystallinity and macroscopic charge transport characteristics compared to comparatively more amorphous films, owing to enhanced intra- and inter molecular ordering of the polymer chains.[12, 16, 23] Polymer chain molecular ordering can be influenced by a range of processing techniques such as

polymer-dielectric interface treatments,[24] film deposition methods (spin-coating, dip-coating, and drop casting),[20, 25] the use of high boiling point solvents,[26] and post-deposition processing (solvent vapor- and thermal annealing),[27, 28] as well as improved molecular design (regioregularity (RR) and molecular weight (MW)).[20, 29, 30] However, such strategies present limitations for large-scale fabrication and high-throughput processing due to associated additional treatments before and/or after polymer film deposition.

In order to eliminate the additional pre- and/or post-deposition steps, several approaches such as tuning solubility,[15, 22] solution aging,[31] and ultrasonic irradiation[16] have been explored to induce formation of well-ordered nanofibillar aggregates in solution, prior to thin-film deposition. In particular, ultrasonic irradiation readily generates crystalline nanofibrillar P3HT aggregates from solutions of the polymer.[16, 25] The aggregates survive a spin-coating process, and in turn impart the corresponding polymer films with a higher degree of intra- and intermolecular ordering, resulting in significant enhancement in charge carrier mobility (e.g., from ≈ 0.016 up to 0.073 $cm^2 V^{-1} s^{-1}$ for 96 % RR P3HT).[23] Alternative approaches requiring steps such as the addition of small quantities of poor solvent to the majority solution, and/or aging the solutions to obtain well-ordered aggregates, also afford a mobility enhancement, but to a lesser extent.[15, 22, 31] However due to strong agitation associated with the method, ultrasonication restricts nanofibrillar structure growth to less than approximately 200 nm in length,[16, 23] and thus grain boundaries between aggregates which will invariably be present in resultant thin films will limit charge transport.

As described in Chapter 4 above, it was demonstrated that low intensity, limited duration ultraviolet (UV) irradiation is an alternative strategy to enhance anisotropic supramolecular ordering of CP chains in solution.[23] Exposure of P3HT solutions to a low UV dose led to highly ordered P3HT aggregates in solution, which was attributed to a conformational change of the polymer chains from 'aromatic-' to 'quinoid-like' upon photoexcitation.[23] The aggregates were nanofibrillar in appearance, where the fibers were longer than > 1 μm in length. The extended structures presumably decreased the number of grain boundaries within the films, resulting in dramatic enhancement of charge carrier mobility up to ≈ 0.082 $cm^2\ V^{-1}\ s^{-1}$ for 96 % RR P3HT.[23]

Ultrasonication of P3HT precursor solutions is an effective way to increase the crystallinity of resultant films, while low-intensity UV irradiation tends to afford films possessing longer-range ordered aggregates.[23] Both molecular ordering of the polymer chains and grain boundaries between the polymer crystallites are key factors impacting CP thin-film charge transport characteristics; enhanced molecular ordering between polymer chains is desirable, while the formation of grain boundaries must be suppressed to maximize transport.

In this chapter, we demonstrate that sequential ultrasonication and UV irradiation of P3HT solutions, compared to treatment via either method alone, very significantly further improves charge transport characteristics of the resultant films. P3HT nanocrystallites formed upon ultrasonication were anisotropically self-assembled into longer nanofibrillar structures by subsequent UV irradiation of the sonicated solutions. Consequently, the hole transport performance, as determined by mobility of the resultant thin-films, was dramatically enhanced up to ≈ 0.120 $cm^2\ V^{-1}\ s^{-1}$ for 96 % RR P3HT

(P3HT1), a value that is higher than any previously reported for P3HT OFETs prepared without additional steps. The approach also effected an order of magnitude improvement in mobility for 92 % RR P3HT (P3HT2) (≈ 0.004 for untreated samples, up to 0.044 $cm^2 V^{-1} s^{-1}$ for solutions undergoing the sequential treatment). The morphology of resultant films was studied by atomic force microscopy (AFM), and quantitative analysis of intra- and intermolecular ordering of polymer chains was performed by means of static absorption spectroscopy and quantitative modeling. Studies on morphology and intra- and intermolecular ordering of P3HT thin-films reveal that the excellent charge carrier transport demonstrated by OFET measurements is attributable to both a reduction in the number of grain boundaries and enhanced molecular ordering of the polymer thin-films.

5.2 Experimental Methods

5.2.1 Materials

P3HT1 was purchased from Rieke Metals Inc. and P3HT2 was purchased from Sigma Aldrich Chemical Co., and were used without further purification. The molecular weight and regioregularity of both samples are summarized in Table 5.1. The molecular weight (MW) was obtained through gel permeation chromatography (GPC) using trichlorobenzene as the eluent and polystyrene as the standard. The head to tail regioregularity (RR) was estimated from the 1H-NMR spectra obtained from deuterated chloroform solution at 293 K using a Bruker DSX 300. Chloroform used in this study was anhydrous grade, purchased from Sigma Aldrich, and used without further purification.

5.2.2 Anisotropic Growth and Assembly of P3HT Aggregates

Table 5.1: Molecular weight and regioregularity of the P3HT samples used.

	Molecular weight (kDa)		
P3HT sample	M_n	M_w	Regioregularity (%)
P3HT1	19.7	43.7	96
P3HT2	34.6	69.0	92

10 mg of polymer was introduced into 2 mL of chloroform in a 20 ml borosilicate glass vial in air. Subsequently, the vial was sealed with a cap and the solution was stirred for at least 30 min at approximately 55 °C to completely dissolve the polymer. The as-prepared solution was cooled to ambient temperature, and in turn the solution was treated by ultrasonication and/or UV irradiation for relevant times:

1) The ultrasonic irradiation of P3HT solutions was performed by following the same procedure as outlined in the literature.[16] A table top ultrasonic cleaner (Bransonic 2510, 40 kHz, ≈ 0.4 W cm^{-2}) was used for ultrasonication of the solution. The sealed glass vials were immersed in the water bath of the ultrasonic cleaner, and then irradiated for relevant times (from 0 to 6 min).

2) To conduct UV irradiation of the solution, the vial containing the solution was placed on a hand-held UV lamp (Entela UVGL-15, 5 mW cm^{-2}, 254 nm) which had been placed on a magnetic stirrer (Corning inc.). Then, the solution was gently stirred and irradiated using the lamp for times ranging from 0 to 6 min. The irradiation was performed through the bottom wall of the borosilicate glass vial which transmits more than 90 % of the incident 254 nm light.

3) For sequentially combined ultrasonication and UV irradiation experiments, ultrasonic irradiation was performed first on the sealed glass vial for times ranging from 0

to 6 min, and then subsequently, exposed to UV irradiation for times also ranging from 0 to 6 min.

5.2.3 OFET Fabrication and Characterization

The OFET devices used for electrical characterization consisted of two contact devices where P3HT films were deposited via spin-coating the relevant polymer solution onto a 300 nm thick SiO_2 gate dielectric. The highly doped substrate wafer served as the gate electrode while Au/Cr was used for the source and drain contacts. The source and drain contacts were fabricated using a standard photolithography based lift-off process, followed by E-beam evaporation (Denton Explorer) of 50 nm Au contacts with 3 nm of Cr as the adhesion layer. Before spin-coating P3HT solutions, all devices were cleaned for 15 min in a UV-ozone cleaner (Novascan PSD-UV) to completely remove any residual photoresist and other organic contaminants. OFET devices were prepared by spin-coating (WS-650MZ-23NPP, Laurell) the solutions onto precleaned substrates at a spin speed of 1500 rpm for 60 s in air, and tested in nitrogen ambient using an Agilent 4155C semiconductor parameter analyzer. The P3HT1 and P3HT2 films obtained by spin-coating were found to have a thickness in the range of 36−48 nm and 33−38 nm, respectively as determined by spectroscopic ellipsometry (M-2000, JA Woollam). The devices were stored in a vacuum oven (1 Torr) overnight at room temperature to remove residual solvent. The field-effect mobility was calculated in the saturation regime of transistor operation (V_{DS} = − 80 V) by plotting the drain current (I_{DS}) versus gate voltage (V_{GS}) and fitting the data to the following equation:

$$I_{DS} = \frac{WC_{OX}}{2L}\mu(V_{GS} - V_T)^2 \tag{5.1}$$

where W (2000 µm) and L (50 µm) are the transistor channel width and length, respectively, V is the threshold voltage and C_{OX} is the capacitance per unit area of the silicon dioxide gate dielectric (1.15×10^{-8} F/cm^2).

5.2.4 UV-vis Spectroscopy

The solution and solid state UV-vis spectra were recorded using an Agilent 8510 UV-vis spectrometer. Films for solid state studies were prepared by spin-coating the requisite solution onto precleaned glass slides following the same procedures used to prepare OFET devices.

5.2.5 Grazing Incidence X-ray Diffraction (GIXD)

Out-of-plane grazing incidence X-ray diffraction data were obtained using a Panalytical X'Pert Pro system equipped with a Cu X-ray source operating at 45 kV and 40 mA. The grazing incidence angle was fixed at 0.2° and the detector was scanned from 3° to 30°.

5.2.6 Atomic Force Microscopy (AFM)

The AFM measurements were performed on films spin-coated onto bottom contact OFET devices using an ICON dimension scanning probe microscope (Bruker) operating in tapping mode with a silicon tip (RTESP, Bruker).

5.3 Results and Discussion

5.3.1 Field-Effect Mobility of P3HT Thin Films

Two P3HT polymers (referred to as P3HT1 and P3HT2) were evaluated as representative CPs (Table 5.1); P3HT1 has 96 % RR and 43.7 kDa MW while P3HT2 has 92 % RR and 69.0 kDa MW. Figure 5.1 represents the field effect mobility for P3HT1 and

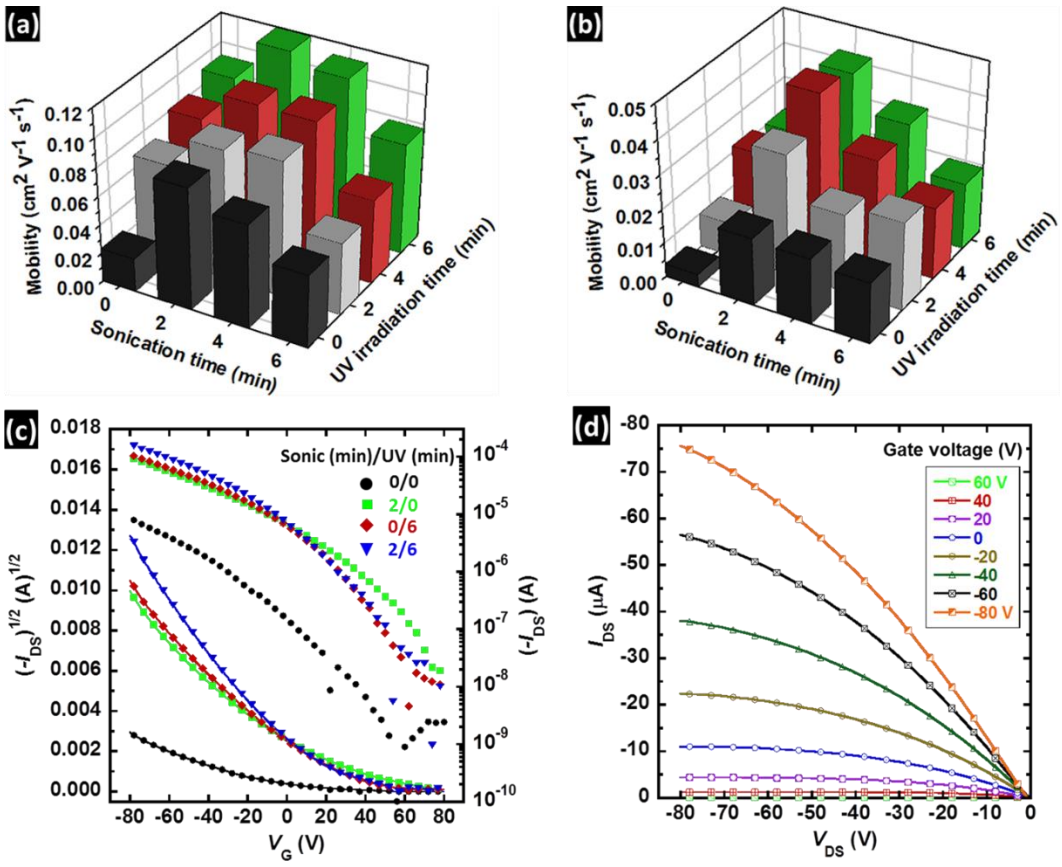

Figure 5.1: Average field-effect mobilities of a) P3HT1 and P3HT2 films spin coated from the polymer solutions treated to ultrasonication and/or UV irradiation for various times. Mobilities were calculated in the saturation regime of operation with $V_{DS} = -80$ V. c) Transfer characteristics of P3HT1 OFET devices fabricated from pristine, 2 min ultrasonicated, 6 min UV irradiated, and sequential 2 min ultrasonicated and 6 min UV irradiated polymer solutions. d) Typical output characteristics obtained from a P3HT1 OFET prepared via spin-coating from the polymer solution irradiated by sequential 2 min ultrasonication and 6 min UV irradiation. All measurements were performed in a nitrogen glovebox.

P3HT2 films spin-coated from solutions treated by sequential ultrasonication and UV irradiation for times ranging from 0 to 6 min, respectively. Consistent with earlier reports, P3HT mobility increased (from 2.34×10^{-2} to 8.50×10^{-2} cm^2 V^{-1} s^{-1} for P3HT1 and from 0.37×10^{-2} to 1.97×10^{-2} cm^2 V^{-1} s^{-1} for P3HT2) after ultrasonication for 2 min, followed by a mobility decrease with further ultrasonication, presumably owing to an increase in

Table 5.2: Average field effect mobilities of P3HT1 and P3HT2 films spin-coated from the solutions treated by ultrasonication and/or UV irradiation for stated times.

Time (min)		Mobility ($cm^2\ V^{-1}\ s^{-1}$)[a)]	
Ultrasonication	UV irradiation	P3HT1	P3HT2
0	0	$2.34 \pm 0.55 \times 10^{-2}$	$0.37 \pm 0.11 \times 10^{-2}$
0	2	$6.86 \pm 0.39 \times 10^{-2}$	$0.98 \pm 0.09 \times 10^{-2}$
0	4	$8.10 \pm 0.73 \times 10^{-2}$	$2.18 \pm 0.90 \times 10^{-2}$
0	6	$9.10 \pm 0.49 \times 10^{-2}$	$2.03 \pm 0.09 \times 10^{-2}$
2	0	$8.50 \pm 0.26 \times 10^{-2}$	$1.97 \pm 0.14 \times 10^{-2}$
2	2	$9.02 \pm 0.78 \times 10^{-2}$	$3.50 \pm 0.07 \times 10^{-2}$
2	4	$10.16 \pm 0.44 \times 10^{-2}$	$4.43 \pm 0.02 \times 10^{-2}$
2	6	$11.95 \pm 0.43 \times 10^{-2}$	$4.22 \pm 0.21 \times 10^{-2}$
4	0	$7.23 \pm 0.55 \times 10^{-2}$	$1.91 \pm 0.06 \times 10^{-2}$
4	2	$9.44 \pm 0.44 \times 10^{-2}$	$2.27 \pm 0.09 \times 10^{-2}$
4	4	$10.12 \pm 0.19 \times 10^{-2}$	$2.98 \pm 0.06 \times 10^{-2}$
4	6	$11.13 \pm 0.44 \times 10^{-2}$	$3.20 \pm 0.17 \times 10^{-2}$
6	0	$5.07 \pm 0.55 \times 10^{-2}$	$1.77 \pm 0.07 \times 10^{-2}$
6	2	$5.03 \pm 0.45 \times 10^{-2}$	$2.56 \pm 0.17 \times 10^{-2}$
6	4	$5.88 \pm 0.74 \times 10^{-2}$	$2.08 \pm 0.11 \times 10^{-2}$
6	6	$7.71 \pm 0.54 \times 10^{-2}$	$1.93 \pm 0.06 \times 10^{-2}$

[a)]Values obtained by testing at least three devices.

the number of grain boundaries (see AFM images, 2 min sonicated P3HT1 in Figure 5.3a and 6 min sonicated P3HT1 in Figure 5.3b). Meanwhile, mobility increased and then gradually saturated (up to 9.10×10^{-2} $cm^2\ V^{-1}\ s^{-1}$ for P3HT1 and 2.03×10^{-2} $cm^2\ V^{-1}\ s^{-1}$ for P3HT2) with increased UV irradiation time. Significantly, UV irradiation of P3HT solutions that had undergone ultrasonication led to further enhancements in mobility. Data for both P3HT1 and P3HT2 is tabulated in Table 5.2. In particular, the mobility of P3HT1 OFET devices reached a maximum value of 11.95×10^{-2} $cm^2\ V^{-1}\ s^{-1}$ when precursor solutions were sequentially treated with 2 min ultrasonication followed by 6 min UV

irradiation (Figure 5.1a). This value is the highest recorded for P3HT devices, fabricated without use of additional steps such as dielectric surface modification and/or thermal or solvent vapor annealing, and is comparable to devices obtained using these methods.[14, 26, 28, 32] P3HT2 device performance was also enhanced up to 4.43×10^{-2} cm^2 V^{-1} s^{-1} through 2 min ultrasonication followed by 4 min UV irradiation of the corresponding P3HT precursor solutions (Figure 5.1b). Figure 5.1c and d depict P3HT1 transfer and characteristic output curves, respectively, which are typical of p-channel OFET operation in the accumulation mode. The high turn-on voltages (V_{ON}) obtained in Figure 5.1c are attributed to the effects of residual doping, acceptor like traps at the P3HT-oxide interface, and/or charge trapping at grain boundaries/interfaces.[23, 25, 31, 33]

5.3.2 Suggested Mechanism of Anisotropic Assembly of P3HT Nanocrystallites

From a mechanistic perspective, P3HT nanoaggregates formed upon ultrasonication grow into relatively longer fibrillar structures via anisotropic assembly of the nanoaggregates; upon UV irradiation, polymer chains present at the ends of the aggregates undergo a photoexcitation induced conformational change from 'aromatic' (random coil conformation) to 'quinoid' (linear or extended coil conformation).[23, 34] The conformation change facilitates anisotropic assembly of the nanoaggregates in a direction perpendicular to the polymer backbone through π–π interactions between the polymer chains existing at the ends of neighboring aggregates. Figure 5.2a presents a mechanistic illustration of the P3HT nanocrystallite assembly process. In a typical experiment, P3HT/$CHCl_3$ solution in a borosilicate glass vial is sealed with a cap, and then ultrasonicated in a table-top ultrasonic cleaner for relevant times as described in the literature, which results in the formation of highly crystalline P3HT nanoaggregates in the

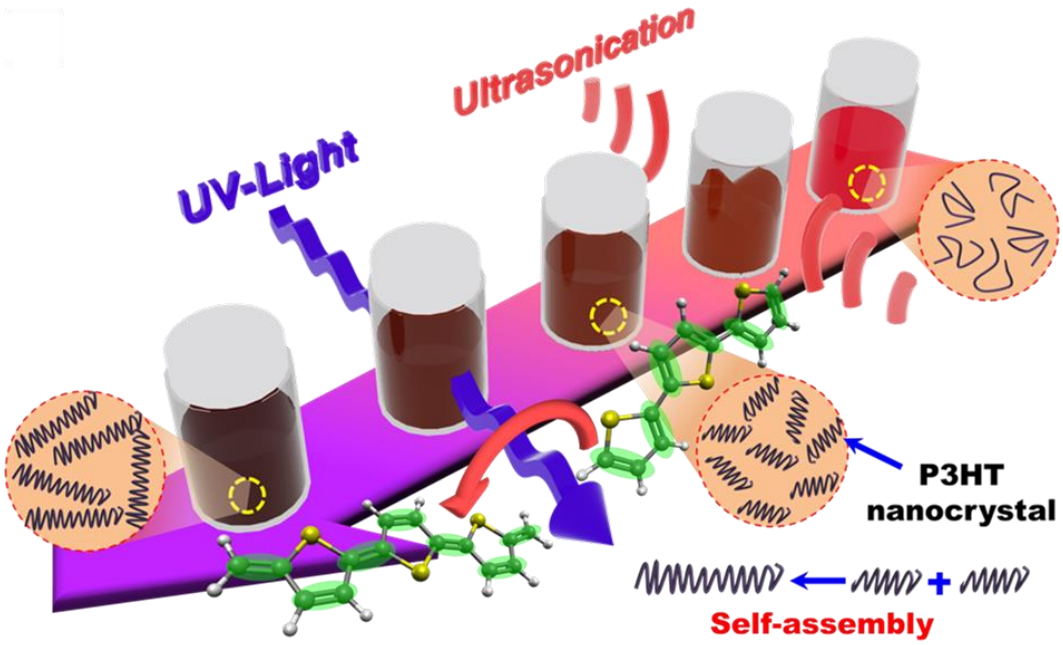

Figure 5.2: The suggested mechanism describing the anisotropic assembly of P3HT nanocrystallites formed by ultrasonication into longer nanofibrillar structures via subsequent UV irradiation of the solution.

solution via a change in the polymer chain conformation (disorder-order transitions).[16] The highly ordered P3HT nanoaggregates appear short (less than 200 nm) in length owing to strong agitation associated with ultrasonication.[16, 23] Subsequently, the ultrasonicated P3HT solution is stirred gently and exposed to UV irradiation for various times, leading to anisotropic assemblies of the crystalline nanoaggregates into longer fibrillar structures.

5.3.3 Morphology Evolution of P3HT Thin Films

Figure 5.3a shows the clear evolution of a nanofibrillar morphology depending on ultrasonication and/or UV irradiation. Both P3HT1 and P3HT2 films appear featureless and amorphous-like in the absence of any irradiation of the corresponding solutions. This observation is ascribed to rapid solvent evaporation, which suppresses the formation of well-ordered structures.[15, 16] Brief (2 min) ultrasonic irradiation of both solutions leads to

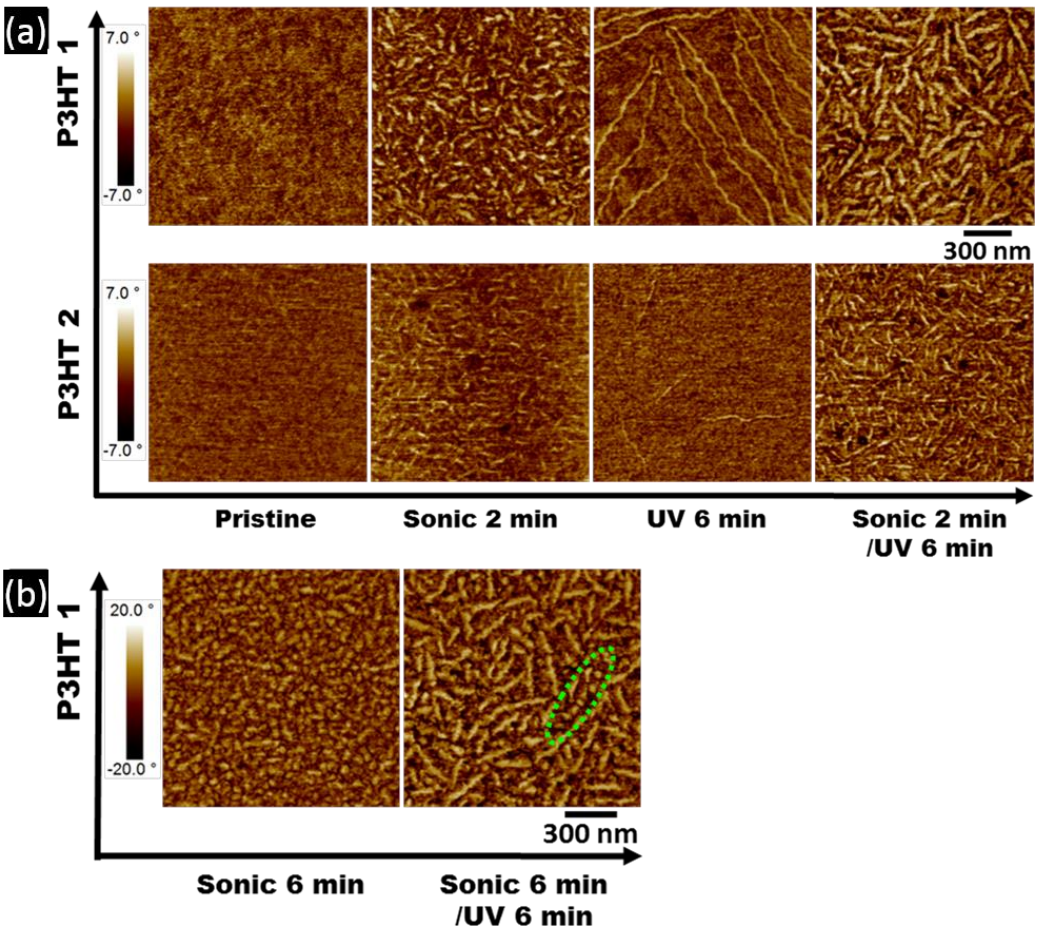

Figure 5.3: a) Tapping mode AFM phase images of P3HT1 and P3HT2 films obtained by spin-coating from the polymer solutions which were treated by ultrasonication and subsequent UV irradiation for 0 min and 0 min, 2 min and 0 min, 0 min and 6 min, and 2 min and 6 min, respectively. b) Tapping mode AFM phase images of P3HT1 films spin-coated from 6 min ultrasonicated, and sequentially 6 min ultrasonicated and 6 min UV irradiated, respectively. The green circle surrounds a small P3HT nanocrystallite undergoing assembly into a fibrillar structure upon subsequent UV irradiation.

the formation of short nanofiber-like structures (i.e., ≈ 30 nm in width and 120 nm in length for P3HT1 and ≈ 15 nm in width and 70 nm in length for P3HT2). It is generally accepted that both higher RR and MW leads to aggregates having wider fibrillar structures owing to a more planarized main chain conformation and longer weight average contour length, respectively.[20, 30] Consistent with previous reports,[20] RR is a more prominent factor than

MW regards to P3HT nanoaggregation; the higher RR but lower MW P3HT1 forms wider aggregates, compared to P3HT2. Moreover, the higher RR materials exhibits longer fibrillar structures, which is attributed to more planarized polymer backbones facilitating favorable π–π interactions between polymer chains.[23, 35, 36]

In contrast to ultrasonic irradiation, UV irradiation (6 min) tends to promote growth of fibrillar features into relatively longer units, however, there appear to be fewer such structures within resultant films.[23] After 2 min sonication and subsequent 6 min UV irradiation, surprisingly, the short nanofibrillar features obtained upon ultrasonication become longer (≈ 300 nm for P3HT1 and ≈ 150 nm for P3HT2), which supports the proposed mechanistic interpretation (Figure 5.2). Examination of Figure 5.3b, which depicts the evolution of P3HT thin-film morphology for samples prepared from solutions sequentially treated with 6 min ultrasonication followed by 6 min UV irradiation provides additional evidence that sonication induced aggregates self-assemble into larger structures. As indicated by the green circle, smaller aggregates formed during ultrasonication for 6 min clearly assemble into longer, anisotropic fibrillar structures via subsequent UV treatment (6 min). Nanofiber length increased upon subsequent UV irradiation, suggesting a reduction in the number of grain boundaries between the initially formed nanofiber aggregates. The surface roughness of resultant films also changed upon ultrasonication and/or UV exposure. The pristine films were relatively smooth with a low root-mean square (RMS), ≈ 0.43 nm for P3HT1 and ≈ 0.39 nm for P3HT2, while that for films obtained from solutions that were sequentially subject to 2 min ultrasonication followed by 6 min UV irradiation gradually increases to ≈ 1.89 nm and ≈ 0.82 nm for P3HT1 and

P3HT2, respectively. The increased roughness is ascribed to the formation of nanofibrillar structures within the thin-films.

5.3.4 Quantitative Analysis of Intra- and Intermolecular Ordering

UV-visible spectral features strongly correlate with the extent of molecular ordering (intra- and intermolecular ordering) in π-conjugated polymer solutions and solid, thin-films.[23, 37] Pristine P3HT solutions exhibit only high energy features (π-π* intraband transition) at ≈ 453 nm and ≈ 450 nm for P3HT1 and P3HT2, respectively. Upon ultrasonication and/or UV irradiation, low energy features appear at ≈ 567 and 623 nm for P3HT1 and at ≈ 558 and 617 nm for P3HT2, suggestive of vibronic bands associated with the (0–1) and (0–0) transitions, respectively[23, 37] (Figure 5.4a and c). The emergence of these features is associated with interchain coupling.[38] For higher RR polymer (P3HT1), the lower energy features remarkably increase in the order UV irradiation (6 min) < ultrasonication (2 min) < sequential ultrasonication (2 min) and UV irradiation (6 min), supporting the premise that polymer chain intermolecular interactions increase in the solution state as a function of the given process. For the less RR material (P3HT2), the lower energy features also increase, but the effect is far less dramatic due to fewer π–π stacking interactions arising from higher steric distortions of polymer chain backbone.

The UV-vis absorption trends observed in the CP solutions is carried through to the corresponding films; the solution based crystalline nanoaggregates survive the spin-coating process, and in turn provide for increased molecular ordering in the solid thin-films as shown in Figures 5.4b and d. Compared to pristine films, the lower energy features are red-shifted in films obtained from solutions subject to sequential 2 min sonication and 6 min UV irradiation (i.e. from ≈ 554 to 566 nm (0–1) and from ≈ 602 to 615 nm (0–0) for

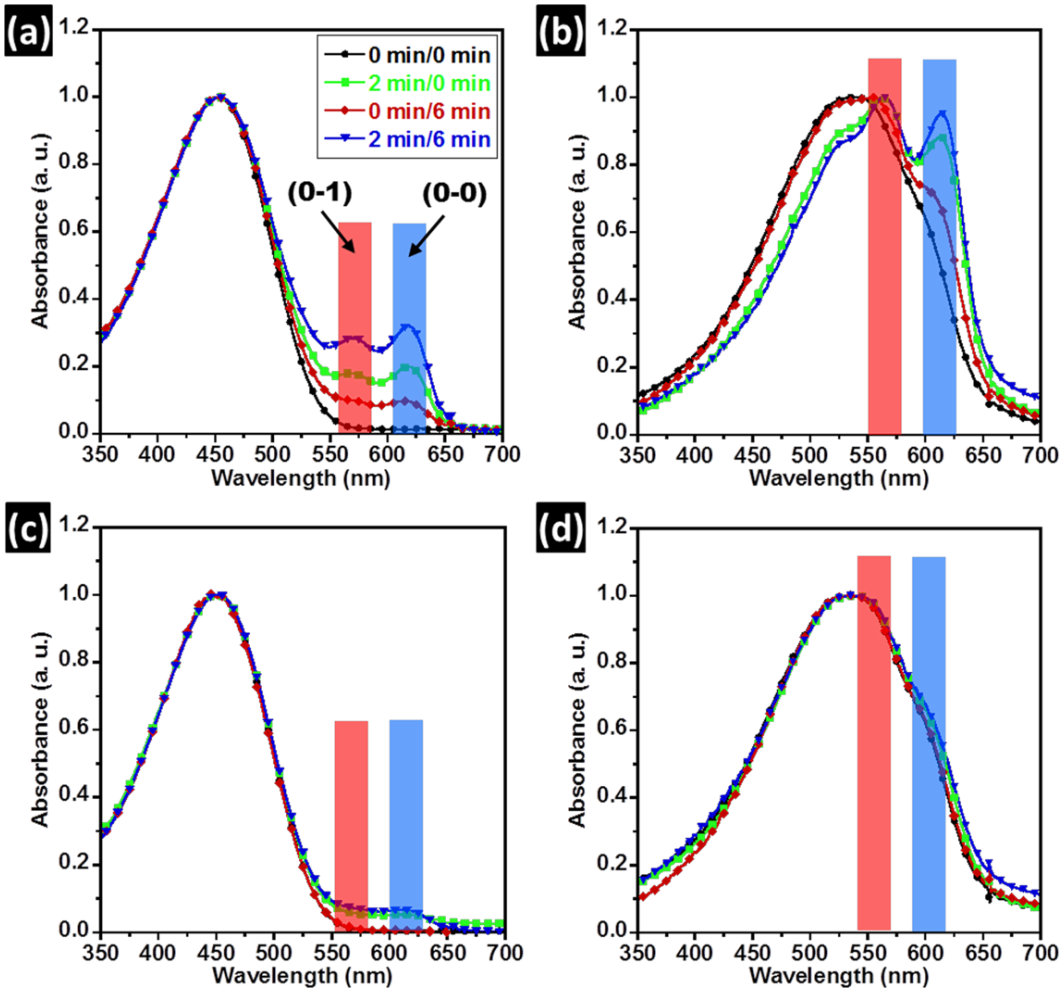

Figure 5.4: Normalized UV-visible absorption spectra of a) P3HT1/$CHCl_3$ solutions under ultrasonication followed by UV irradiation for 0 min and 0 min, 2 min and 0 min, 0 min and 6 min, and 2 min and 6 min, respectively and b) corresponding P3HT1 films obtained by spin-coating. Normalized UV-visible absorption spectra of c) P3HT2/$CHCl_3$ solutions treated by ultrasonication and subsequent UV irradiation for 0 min and 0 min, 2 min and 0 min, 0 min and 6 min, and 2 min and 6 min, respectively and d) corresponding P3HT2 films obtained by spin-coating.

P3HT1 and from ≈ 547 to 550 nm (0–1) and from ≈ 598 to 604 nm (0–0) for P3HT2, owing to more planarized polymer chain backbones compared to those from pristine films.[16, 23] In addition, the intensity of the (0–0) transition increases, relative to the (0–1) transition. The intensity differences indicate that sequential sonication and UV irradiation of the

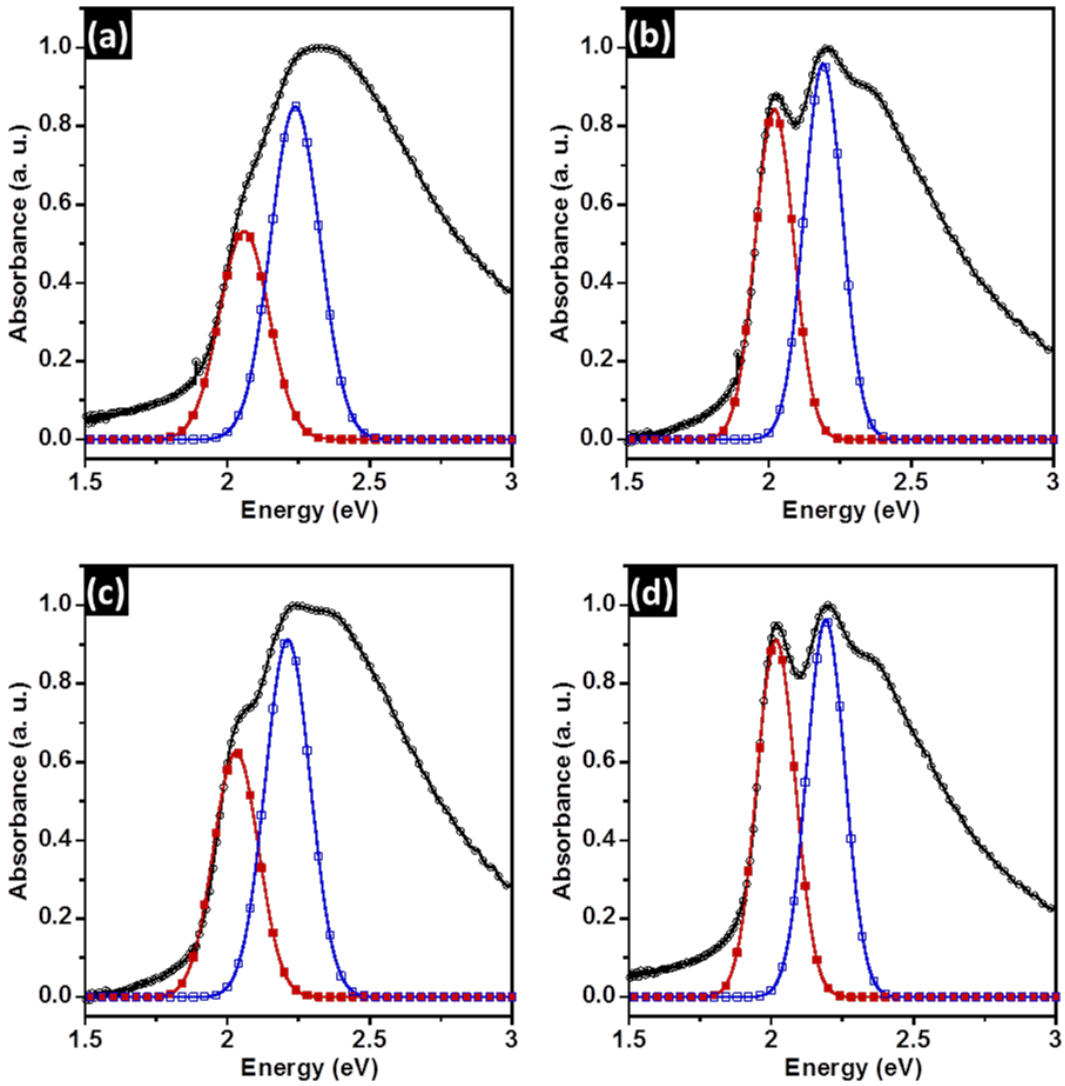

Figure 5.5: Absorption spectra of P3HT1 films spin-coated from P3HT1/$CHCl_3$ solutions treated by a) 0 min ultrasonication and 0 min UV irradiation, b) 2 min ultrasonication and 0 min UV irradiation, c) 0 min ultrasonication and 6 min UV irradiation, and d) 2 min ultrasonication and 6 min UV irradiation. The lines with filled red and open blue squares indicate the Gaussians corresponding to the (0−0) and (0−1) bands respectively. The lines with black open circles depict the experimental absorption spectra.

polymer solutions leads to enhanced intramolecular ordering within polymer chains in corresponding solidified films.[23, 37, 38]

Quantitative analysis of intra- and intermolecular ordering of polymer chains can be performed by means of static absorption spectroscopy and quantitative modeling.[37, 38]

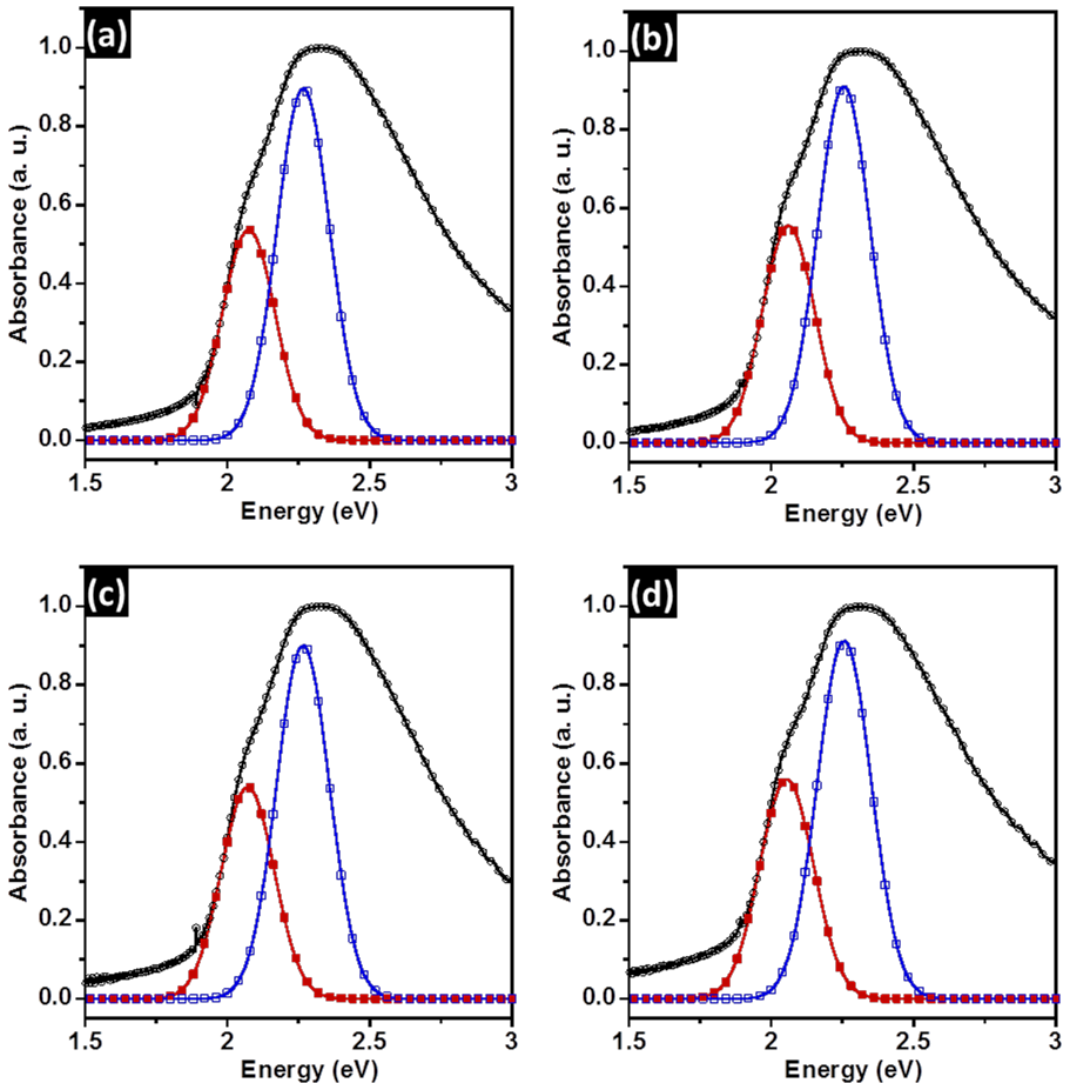

Figure 5.6: Absorption spectra of P3HT2 films spin-coated from P3HT2/$CHCl_3$ solutions treated by a) 0 min ultrasonication and 0 min UV irradiation, b) 2 min ultrasonication and 0 min UV irradiation, c) 0 min ultrasonication and 6 min UV irradiation, and d) 2 min ultrasonication and 6 min UV irradiation. The lines with filled red and open blue squares indicate the Gaussians corresponding to the (0−0) and (0−1) bands respectively. The lines with black open circles depict the experimental absorption spectra.

The P3HT absorption spectrum is composed of two phases, a crystalline region due to ordered chains and an amorphous region due to disordered chains.[38] According to Spano's model, interchain coupling leads to vibronic bands in the absorption spectrum.[38] Further, the vibronic bands can be related to the free exciton bandwidth (*W*) which correlates with

intrachain ordering of an individual polymer chain within the aggregates.[23, 37, 38] An increase in intramolecular order leads to a decrease in W.[23, 37, 38] Equation 1 is used to calculate the W values, using the intensities of the (0–0) and (0–1) transitions obtained from fits to the experimental spectra (Figure 5.5 and 5.6).

$$\frac{I_{0-0}}{I_{0-1}} \approx \left(\frac{1 - 0.24W / E_p}{1 + 0.073W / E_p} \right)^2 \tag{5.2}$$

I_{0-0} and I_{0-1} represent the intensities of the (0–0) and (0–1) transitions, respectively and E_P is the vibrational energy of the symmetric vinyl stretch (taken as 0.18 eV).[38] As shown in Figure 5.7a, while W of P3HT1 films obtained from pristine solution appears at 135.6 meV, the value significantly decreases to 99.1, 36.6, and 15.4 meV after 6 min UV irradiation, 2 min ultrasonication, and sequential ultrasonication (2 min) followed by 6 min UV irradiation, indicative of enhanced intramolecular ordering of P3HT chains. In contrast, the W value decreases only slightly from 137.8 to 137.2, 133.3, and 131.9 meV for P3HT2 films obtained through the same treatments to the precursor solutions (Figure 5.7a).

The number of aggregates in the resultant films was also affected by ultrasonication and/or UV irradiation of the precursor solutions. The absorption contributions of the photophysical aggregates and amorphous P3HT regions can be separated using Equation 2 which accounts for the effect of aggregates on the relative vibronic intensities, based on weakly interacting H-aggregates in polythiophenes.[37, 38]

$$A \propto \sum_{m=0} \left(\frac{e^{-S} S^m}{m!} \right) \times \left(1 - \frac{We^{-S}}{2E_P} G_m \right)^2 \times \exp\left(- \frac{(E - E_{0-0} - mE_P - 1/2WS^m e^{-S})^2}{2\sigma^2} \right) \tag{5.3}$$

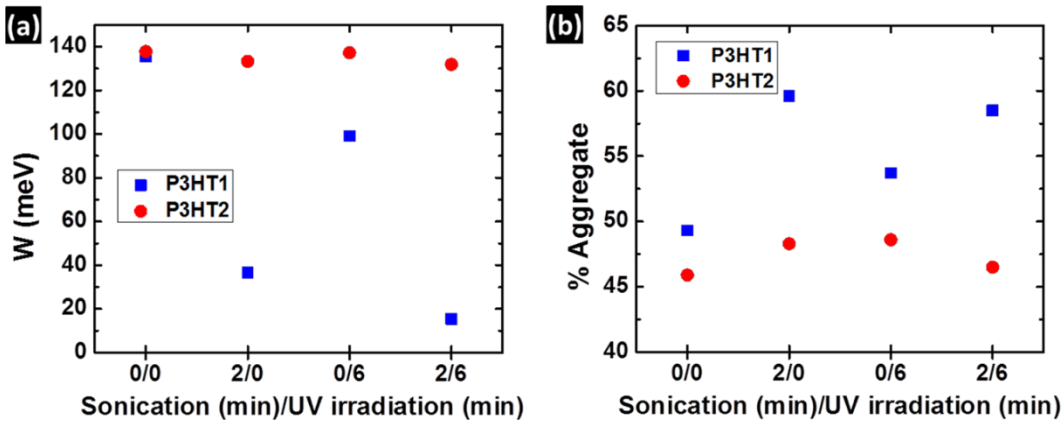

Figure 5.7: The evolution of a) exciton bandwidth *W* and b) percentage of ordered aggregates in the P3HT1 and P3HT2 films spin-coated from pristine, 2 min ultrasonicated, 6 min UV irradiated, and sequentially 2 min ultrasonicated and 6 min UV irradiated polymer solutions.

where A is the absorbance as a function of the photon energy (E), S is the Huang-Rhys factor (taken as 1.0),[38] G_m is a constant that depends on the vibrational level, m (for e.g., m=0 for the (0–0) transition) as given by the equation, $G_m = \sum_{n(\neq m)} S^n/n!(n-m)$, where n is the vibrational quantum number, $E_{0\text{-}0}$ is the 0-0 transition energy, and σ is the Gaussian linewidth. As shown in Figure 5.7b, the extent of aggregation was found to be ≈ 49.3 % for pristine P3HT1 thin-films, and significantly increased to 53.7, 59.6, and 58.5 %, respectively for films obtained from 6 min UV irradiated, 2 min ultrasonicated, and sequential 2 min ultrasonicated and 6 min UV irradiated solutions, suggesting increased P3HT chain intermolecular ordering. In contrast, the number of aggregates from P3HT2 films also increased, but to a lesser extent, changing from ≈ 45.9 to 48.6, 48.3, and 46.5 %, which supports experimental results showing that lower RR P3HT is less sensitive to ultrasonication and/or UV irradiation induced changes associated with intermolecular ordering (Figure 5.7b).

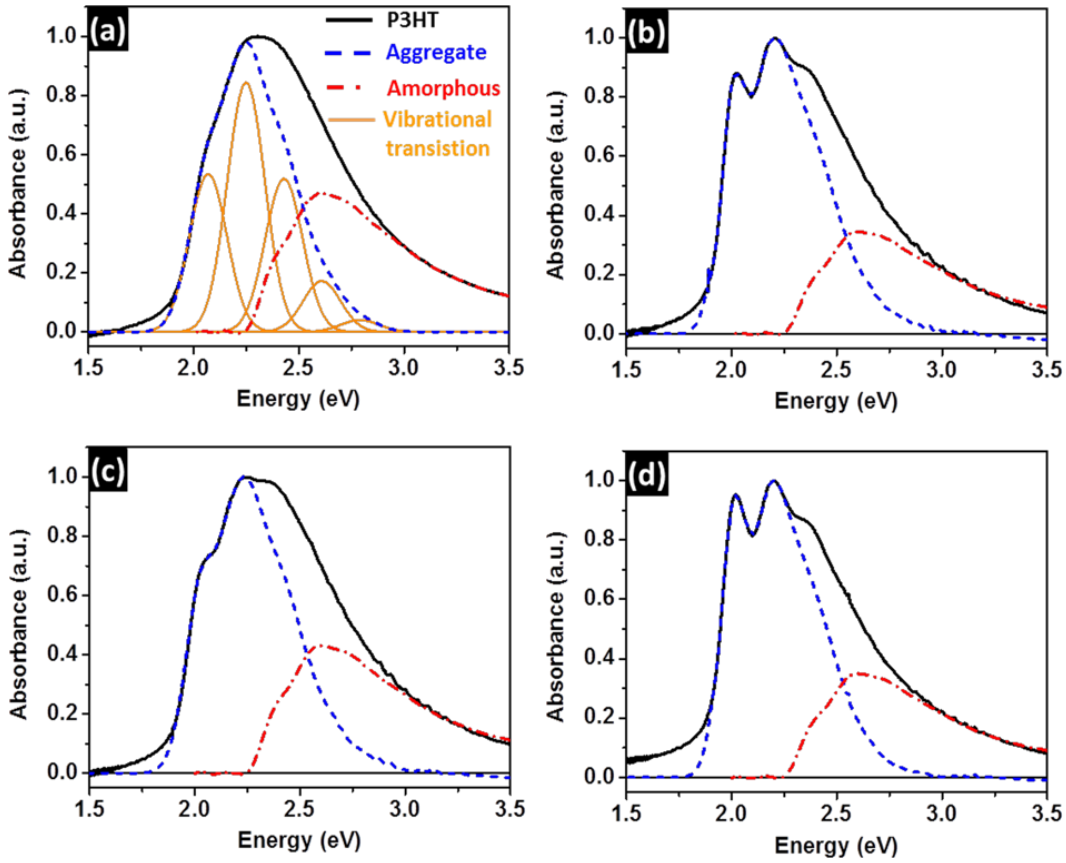

Figure 5.8: Absorption spectra of P3HT1 films spin-coated from P3HT1/$CHCl_3$ solutions treated by a) 0 min ultrasonication and 0 min UV irradiation, b) 2 min ultrasonication and 0 min UV irradiation, c) 0 min ultrasonication and 6 min UV irradiation, and d) 2 min ultrasonication and 6 min UV irradiation. The dashed blue lines indicate the spectra of aggregates and the dash-dotted red lines indicate the absorption spectra associated with amorphous P3HT chains in the respective films. The black lines depict the experimental absorption spectra.

To calculate the relative proportions of aggregated vs amorphous regions for each pristine P3HT1 and P3HT2 sample, as shown in Figure 5.8 and 5.9, the theoretical spectra of P3HT aggregates were fit to the experimental spectra of pristine P3HT films in the spectral range from 1.95 to 2.20 eV, given that amorphous P3HT chains should not contribute to absorption energies below ~2.30 eV.[37, 38] Energy transitions up to the 0-4 vibrational level were considered in this manuscript. Both amorphous P3HT1 and P3HT2 spectra were obtained by subtraction of the theoretical spectrum from each experimental

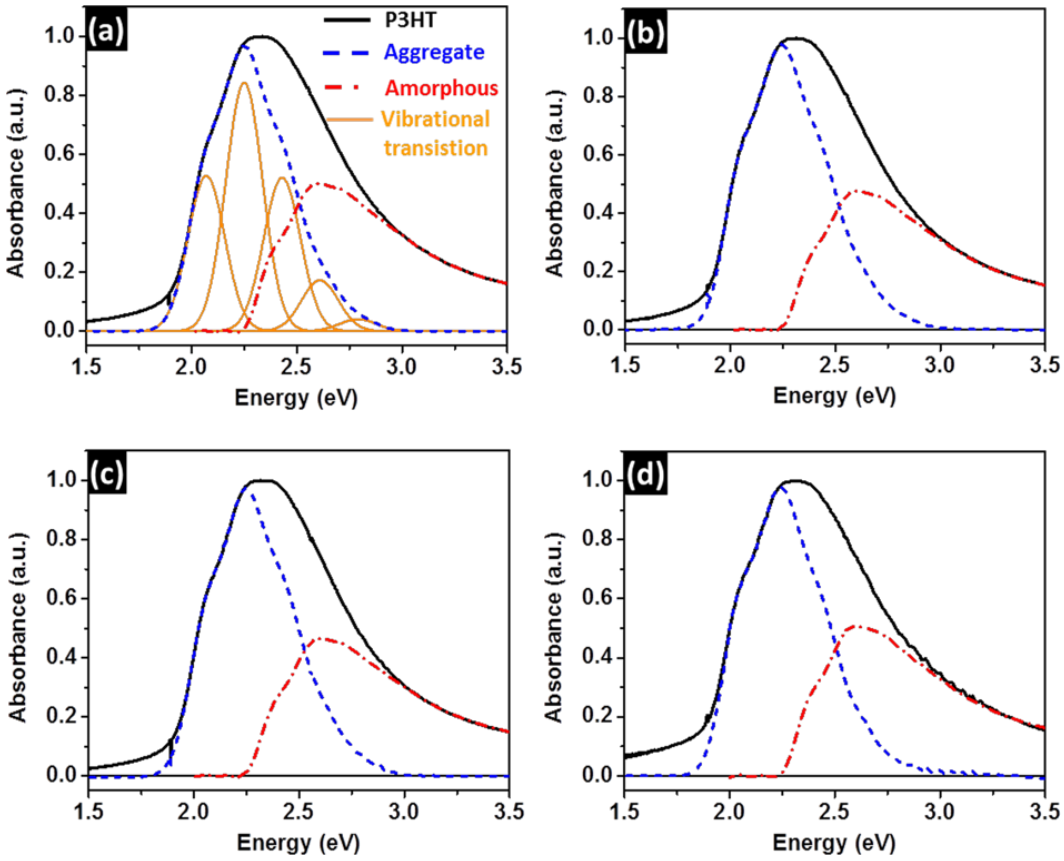

Figure 5.9: Absorption spectra of P3HT2 films spin-coated from P3HT2/$CHCl_3$ solutions treated by a) 0 min ultrasonication and 0 min UV irradiation, b) 2 min ultrasonication and 0 min UV irradiation, c) 0 min ultrasonication and 6 min UV irradiation, and d) 2 min ultrasonication and 6 min UV irradiation. The dashed blue lines indicate the spectra of aggregates and the dash-dotted red lines indicate the absorption spectra of amorphous P3HT chains in the films. The black lines depict the experimental absorption spectra.

spectrum. The relative oscillator strength of the aggregates to amorphous chains was taken as approximately 1.4, a value that Clark et al. obtained for commercial P3HT.[38] In general, P3HT films prepared from spin-coating well dissolved polymer solutions are composed of weakly interacting H-aggregate states and amorphous chains. However, other aggregate states such as H-, J-, and HJ aggregates, which exhibit different intra- and/or intermolecular interactions, can be formed depending on the processing conditions used for polymer film deposition.[37, 39, 40] Both ultrasonication and UV irradiation lead to well-ordered aggregates

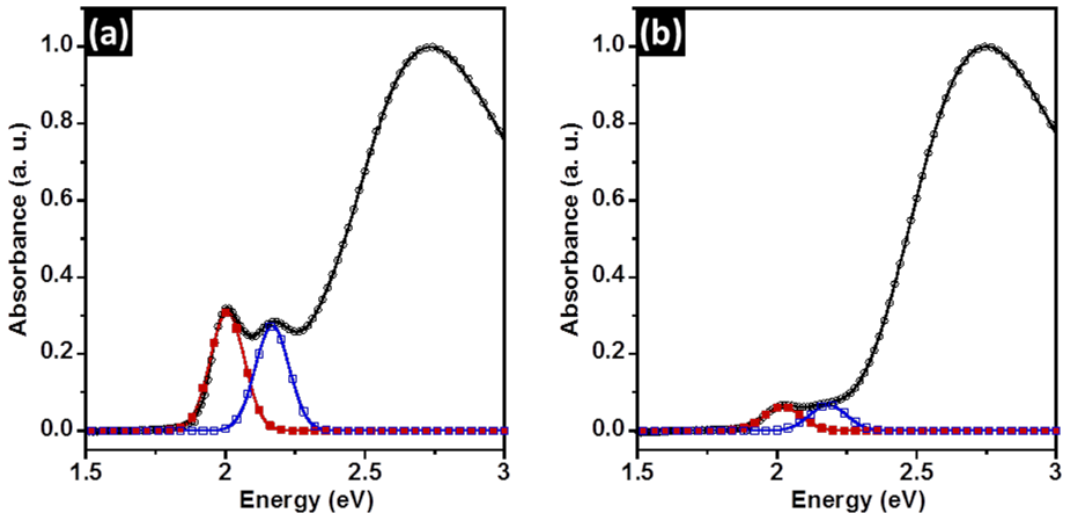

Figure 5.10: Absorption spectra of a) P3HT1/$CHCl_3$ and b) P3HT2/$CHCl_3$ solutions under sequential 2 min ultrasonication and 6 min UV irradiation. The lines with filled red and open blue squares indicate the Gaussians corresponding to the (0−0) and (0−1) bands respectively. The lines with black open circles depict the experimental absorption spectra.

having enhanced intramolecular ordering. Figure 5.10 depicts the (0−0) and (0−1) bands obtained by fitting the experimental absorption spectra of P3HT1 and P3HT2 films spin-coated from solutions which underwent 2 min ultrasonication and subsequent 6 min UV irradiation of the corresponding precursor solutions. While the aggregates formed in P3HT1 and P3HT2 pristine films show higher values, 135.6 and 137.8 meV, respectively (Figure 5.7a), the aggregates formed in the P3HT1 and P3HT2 solutions exhibit remarkably lower W values, -35.42 and 17.93 meV, respectively, indicative of enhanced intramolecular interactions between P3HT chains. The aggregates survived a spin-coating process, and appear as nanofibrillar structures in resultant thin-films. Therefore, in the present case, at least two different phases of aggregates are believed to exist in films obtained from ultrasonicated and/or UV irradiated solutions: 1) weakly interacting H-aggregate states prepared from well-dissolved polymer chains and 2) aggregate states arising from the well-ordered aggregates formed upon ultrasonication and/or UV

irradiation of the solutions. In order to separate the aggregated portion to calculate the extent of aggregates formed in P3HT films obtained from the treated solutions, amorphous P3HT spectra obtained from pristine films were fit to the experimental spectra of the resultant films in the spectral range from 3.0 to 3.5 eV; the aggregates are not expected to contribute to the absorption in this range as seen from Figure 5.8a and 5.9a.[37, 38]

The increased sensitivity to changes in intra- and intermolecular ordering of the higher RR P3HT polymer chains upon ultrasonication and/or UV irradiation, can also be understood in light of solubility effects. The more planar and rigid chain conformation associated with the higher RR material, afforded by fewer steric distortions imposed by the hexyl side chains, is expected to lead to lower solubility in solvents.[23, 25] Thus, polymer-polymer interactions become more favorable than polymer-solvent interactions. Consistently, the aforementioned treatments to the higher RR P3HT dissolved in chlorobenzene and trichlorobenzene, both of which have better solubility relative to P3HT than $CHCl_3$, did not afford the spectroscopic changes observed for either $CHCl_3$ or toluene solutions.

5.3.5 Crystallinity and Microstructure of P3HT Thin Films

The enhanced intra- and intermolecular interactions of P3HT chains are expected to lead to higher thin-film crystallinity.[15, 23] Figures 5.11a and b depict X-ray diffractograms obtained from grazing incidence (GIXD) measurements of P3HT1 and P3HT2 films spin-coated from the polymer solutions irradiated by sonication and/or UV for different times. The crystallinity of resultant films increases in order of UV irradiation (6 min), ultrasonication (2 min), and sequential ultrasonication (2 min) and UV irradiation (6 min), which is consistent with observed UV-visible spectral changes. Clearly, the XRD

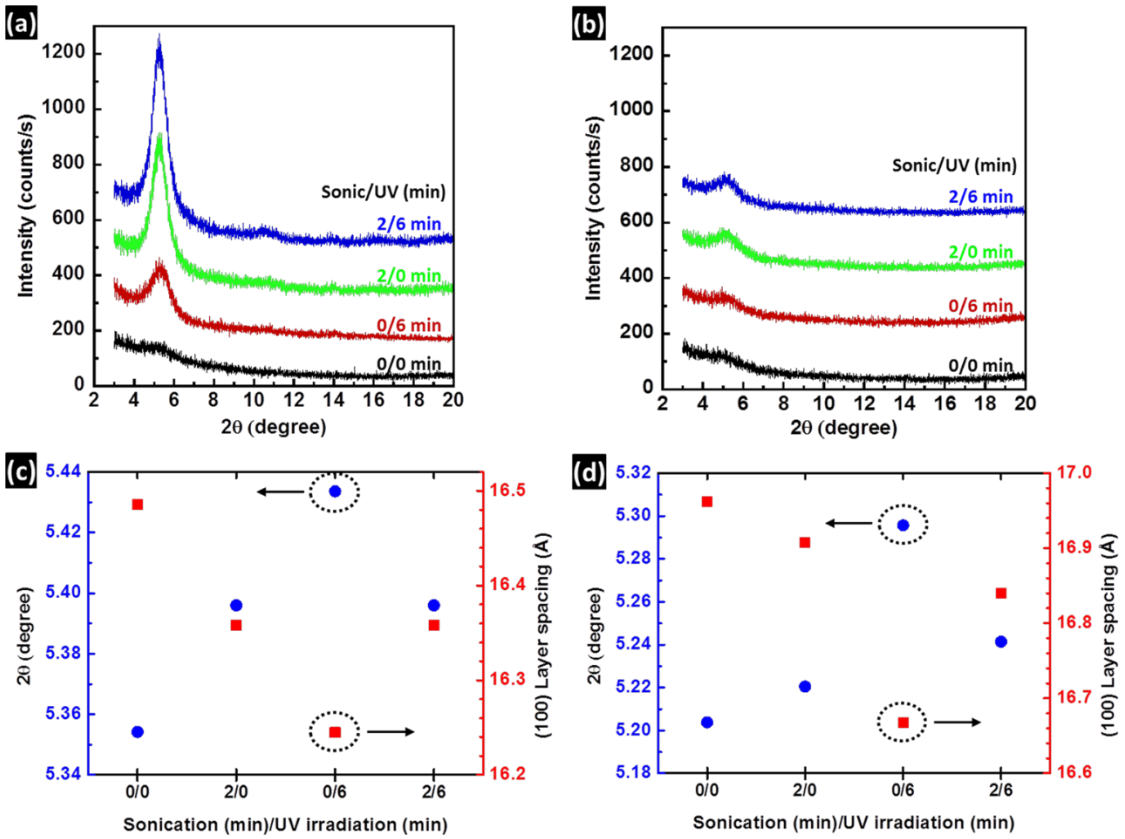

Figure 5.11: Grazing incidence X-ray diffraction profiles of a) P3HT1 and b) P3HT2 films obtained from pristine, 2 min ultrasonicated, 6 min UV irradiated, and sequentially 2 min ultrasonicated and 6 min UV irradiated polymer solutions. 2θ angle (left axis) of the (100) peak and corresponding layer spacing (right axis) of corresponding c) P3HT1 and d) P3HT2 films.

profiles reflect the enhanced polymer chain intra- and intermolecular ordering. The sequential treatment of P3HT precursor solutions to 2min sonication and 6 min UV irradiation affords the highest intensity enhancement of the (100) peak which is associated with polymer chain lamellar packing along the crystallographic direction perpendicular to the backbone.[16, 23] This increase could be attributed to either an increase in the size of individual crystallites, the number of crystallites, or both.[16, 23] In addition, the (100) peak of P3HT1 shifts to higher angle, from 5.35 to 5.40° (from a d-spacing of 16.49 to 16.36 Å) (Figure 5.11c), while the P3HT2 (100) peak shifts from 5.20 to 5.24° (from 16.96 to 16.84

Å) after the same treatment (Figure 5.11d), which suggests either increased interdigitation between P3HT alkyl side chains or a change in side chain tilt.[15, 22]

5.4 Conclusion

In conclusion, this work demonstrates that sequential ultrasonication and UV irradiation of P3HT precursor solutions is an effective strategy to achieve a remarkable increase in mobility of corresponding films, without additional process steps such as dielectric surface modification and/or thermal or solvent vapor annealing. Small P3HT nanocrystallites formed via ultrasonication were anisotropically self-assembled into longer nanofibrillar structures by subsequent UV irradiation of the sonicated solutions. Consequently, enhanced intra- and intermolecular ordering with a concomitant reduction in grain boundaries within P3HT films was achieved via sequential ultrasonication and UV irradiation of the precursor solution, and contributes to the devices exhibiting excellent charge carrier transport properties ($\mu \approx 0.120$ cm^2 V^{-1} s^{-1} for 96 % RR P3HT). The hole mobility of the lower RR P3HT also underwent a significant enhancement. Higher RR P3HT appears more sensitive to ultrasonication and/or UV irradiation induced changes in intra- and intermolecular ordering and the polymer chain nano- and microstructure. The approach described here is expected to be applicable to alternative π-conjugated polymer semiconductors and suitable for the fabrication of high performance, large-area, flexible electronic devices for a wide range of commercial applications.

5.5 References

[1] Burroughes, J. H.; Bradley, D. D. C.; Brown, A. R.; Marks, R. N.; Mackay, K.; Friend, R. H.; Burns, P. L.; Holmes, A. B. Light-Emitting Diodes Based on Conjugated Polymers. *Nature* **1990**, *347*, 539-541.

[2] Friend, R. H.; Gymer, R. W.; Holmes, A. B.; Burroughes, J. H.; Marks, R. N.; Taliani, C.; Bradley, D. D. C.; Dos Santos, D. A.; Bredas, J. L.; Logdlund, M.; Salaneck, W. R. Electroluminescence in Conjugated Polymers. *Nature* **1999**, *397*, 121-128.

[3] Han, T. H.; Lee, Y.; Choi, M. R.; Woo, S. H.; Bae, S. H.; Hong, B. H.; Ahn, J. H.; Lee, T. W. Extremely Efficient Flexible Organic Light-Emitting Diodes with Modified Graphene Anode. *Nat. Photonics* **2012**, *6*, 105-110.

[4] Thomas, S. W.; Joly, G. D.; Swager, T. M. Chemical Sensors Based on Amplifying Fluorescent Conjugated Polymers. *Chem. Rev.* **2007**, *107*, 1339-1386.

[5] Huang, H. M.; Wang, K.; Tan, W. H.; An, D.; Yang, X. H.; Huang, S. S.; Zhai, Q.; Zhou, L.; Jin, Y. Design of a Modular-Based Fluorescent Conjugated Polymer for Selective Sensing. *Angew. Chem. Int. Ed.* **2004**, *43*, 5635-5638.

[6] Janata, J.; Josowicz, M. Conducting Polymers in Electronic Chemical Sensors. *Nat. Mater.* **2003**, *2*, 19-24.

[7] You, C. C.; Miranda, O. R.; Gider, B.; Ghosh, P. S.; Kim, I. B.; Erdogan, B.; Krovi, S. A.; Bunz, U. H. F.; Rotello, V. M. Detection and Identification of Proteins Using Nanoparticle–Fluorescent Polymer 'Chemical Nose' Sensors. *Nat. Nanotechnol.* **2007**, *2*, 318-323.

[8] Park, S. H.; Roy, A.; Beaupre, S.; Cho, S.; Coates, N.; Moon, J. S.; Moses, D.; Leclerc, M.; Lee, K.; Heeger, A. J. Bulk Heterojunction Solar Cells with Internal Quantum Efficiency Approaching 100 %. *Nat. Photonics* **2009**, *3*, 297-302.

[9] Li, G.; Zhu, R.; Yang, Y. Polymer Solar Cells. *Nat. Photonics* **2012**, *6*, 153-161.

[10] Lipomi, D. J.; Tee, B. C. K.; Vosgueritchian, M.; Bao, Z. N. Stretchable Organic Solar Cells. *Adv. Mater.* **2011**, *23*, 1771-1775.

[11] Kim, B. G.; Jeong, E. J.; Chung, J. W.; Seo, S.; Koo, B.; Kim, J. S. A Molecular Design Principle of Lyotropic Liquid-Crystalline Conjugated Polymers with Directed Alignment Capability for Plastic Electronics. *Nat. Mater.* **2013**, *12*, 659-664.

[12] Qiu, L. Z.; Lee, W. H.; Wang, X. H.; Kim, J. S.; Lim, J. A.; Kwak, D.; Lee, S.; Cho, K. Organic Thin-film Transistors Based on Polythiophene Nanowires Embedded in Insulating Polymer. *Adv. Mater.* **2009**, *21*, 1349-1353.

[13] Sirringhaus, H. Device Physics of Solution-Processed Organic Field-Effect Transistors. *Adv. Mater.* **2005**, *17*, 2411-2425.

[14] Ikawa, M.; Yamada, T.; Matsui, H.; Minemawari, H.; Tsutsumi, J.; Horii, Y.; Chikamatsu, M.; Azumi, R.; Kumai, R.; Hasegawa, T. Simple Push Coating of Polymer Thin-Film Transistors. *Nat. Commun.* **2012**, *3*,1176.

[15] Chang, M.; Choi, D.; Fu, B.; Reichmanis, E. Solvent Based Hydrogen Bonding: Impact on Poly(3-hexylthiophene) Nanoscale Morphology and Charge Transport Characteristics. *ACS Nano* **2013**, *7*, 5402-5413.

[16] Aiyar, A. R.; Hong, J. I.; Nambiar, R.; Collard, D. M.; Reichmanis, E. Tunable Crystallinity in Regioregular Poly (3-Hexylthiophene) Thin Films and Its Impact on Field Effect Mobility. *Adv. Funct. Mater.* **2011**, *21*, 2652-2659.

[17] Hamilton, R.; Smith, J.; Ogier, S.; Heeney, M.; Anthony, J. E.; McCulloch, I.; Veres, J.; Bradley, D. D. C.; Anthopoulos, T. D. High-Performance Polymer-Small Molecule Blend Organic Transistors. *Adv. Mater.* **2009**, *21*, 1166-1171.

[18] Allard, S.; Forster, M.; Souharce, B.; Thiem, H.; Scherf, U. Organic Semiconductors for Solution-Processable Field-Effect Transistors (OFETs). *Angew. Chem. Int. Ed.* **2008**, *47*, 4070-4098.

[19] Goffri, S.; Muller, C.; Stingelin-Stutzmann, N.; Breiby, D. W.; Radano, C. P.; Andreasen, J. W.; Thompson, R.; Janssen, R. A. J.; Nielsen, M. M.; Smith, P.; Sirringhaus, H. Multicomponent Semiconducting Polymer Systems with Low Crystallization-Induced Percolation Threshold. *Nat. Mater.* **2006**, *5*, 950-956.

[20] Aiyar, A. R.; Hong, J. I.; Reichmanis, E. Regioregularity and Intrachain Ordering: Impact on the Nanostructure and Charge Transport in Two-Dimensional Assemblies of Poly(3-hexylthiophene). *Chem. Mater.* **2012**, *24*, 2845-2853.

[21] Sirringhaus, H.; Brown, P. J.; Friend, R. H.; Nielsen, M. M.; Bechgaard, K.; Langeveld-Voss, B. M. W.; Spiering, A. J. H.; Janssen, R. A. J.; Meijer, E. W.; Herwig, P.; de Leeuw, D. M. Two-Dimensional Charge Transport in Self-Organized, High-Mobility Conjugated Polymers. *Nature* **1999**, *401*, 685-688.

[22] Park, Y. D.; Lee, H. S.; Choi, Y. J.; Kwak, D.; Cho, J. H.; Lee, S.; Cho, K. Solubility-Induced Ordered Polythiophene Precursors for High-Performance Organic Thin-Film Transistors. *Adv. Funct. Mater.* **2009**, *19*, 1200-1206.

[23] Chang, M., Lee, J., Kleinhenz, N., Fu, B. and Reichmanis, E. Photoinduced Anisotropic Supramolecular Assembly and Enhanced Charge Transport of Poly(3-hexylthiophene) Thin Films. *Adv. Funct. Mater.* **2014**, *24*, 4457-4465.

[24] Kim, D. H.; Jang, Y.; Park, Y. D.; Cho, K. Surface-Induced Conformational Changes in Poly(3-hexylthiophene) Monolayer Films. *Langmuir* **2005**, *21*, 3203-3206.

[25] Aiyar, A. R.; Hong, J. I.; Izumi, J.; Choi, D.; Kleinhenz, N.; Reichmanis, E. Ultrasound-Induced Ordering in Poly(3-hexylthiophene): Role of Molecular and Process Parameters on Morphology and Charge Transport. *ACS Appl. Mater. Interfaces* **2013**, *5*, 2368-2377.

[26] Chang, J. F.; Sun, B. Q.; Breiby, D. W.; Nielsen, M. M.; Solling, T. I.; Giles, M.; McCulloch, I.; Sirringhaus, H. Enhanced Mobility of Poly(3-hexylthiophene) Transistors by Spin-Coating from High-Boiling-Point Solvents. *Chem. Mater.* **2004**, *16*, 4772-4776.

[27] Fu, Y.; Lin, C.; Tsai, F. Y. High Field-Effect Mobility from Poly(3-hexylthiophene) Thin-Film Transistors by Solvent–Vapor-Induced Reflow. *Org. Electron.* **2009**, *10*, 883-888.

[28] Cho, S.; Lee, K.; Yuen, J.; Wang, G. M.; Moses, D.; Heeger, A. J.; Surin, M.; Lazzaroni, R. Thermal Annealing-Induced Enhancement of the Field-Effect Mobility of Regioregular Poly(3-hexylthiophene) Films. *J. Appl. Phys.* **2006**, *100*, 114503.

[29] Kline, R. J.; McGehee, M. D.; Kadnikova, E. N.; Liu, J. S.; Frechet, J. M. J. Controlling the Field-Effect Mobility of Regioregular Polythiophene by Changing the Molecular Weight. *Adv. Mater.* **2003**, *15*, 1519-1522.

[30] Zhang, R.; Li, B.; Iovu, M. C.; Jeffries-EL, M.; Sauve, G.; Cooper, J.; Jia, S. J.; Tristram-Nagle, S.; Smilgies, D. M.; Lambeth, D. N.; McCullough, R. D.; Kowalewski, T. Nanostructure Dependence of Field-Effect Mobility in Regioregular Poly(3-hexylthiophene) Thin Film Field Effect Transistors. *J. Am. Chem. Soc.* **2006**, *128*, 3480-3481.

[31] Chua, L. L.; Zaumseil, J.; Chang, J. F.; Ou, E. C. W.; Ho, P. K. H.; Sirringhaus, H.; Friend, R. H. General Observation of n-Type Field-Effect Behaviour in Organic Semiconductors. *Nature* **2005**, *434*, 194-199.

[32] Crossland, E. J. W.; Tremel, K.; Fischer, F.; Rahimi, K.; Reiter, G.; Steiner, U.; Ludwigs, S. Anisotropic Charge Transport in Spherulitic Poly (3-hexylthiophene) Films. *Adv. Mater*. **2012**, *24*, 839-844.

[33] Wu, P. T.; Xin, H.; Kim, F. S.; Ren, G. Q.; Jenekhe, S. A. Regioregular Poly(3-pentylthiophene): Synthesis, Self-Assembly of Nanowires, High-Mobility Field-Effect Transistors, and Efficient Photovoltaic Cells. *Macromolecules* **2009**, *42*, 8817-8826.

[34] Kim, Y. H.; Spiegel, D.; Hotta, S.; Heeger, A. J. Photoexcitation and Doping Studies of Poly(3-hexylthienylene). *Phys. Rev. B* **1988**, *38*, 5490-5495.

[35] Cheng, Y. J.; Yang, S. H.; Hsu, C. S. Synthesis of Conjugated Polymers for Organic Solar Cell Applications. *Chem. Rev.* **2009**, *109*, 5868-5923.

[36] Son, H. J.; Carsten, B.; Jung, I. H.; Yu, L. P. Overcoming Efficiency Challenges in Organic Solar Cells: Rational Development of Conjugated Polymers. *Energy Environ. Sci.* **2012**, *5*, 8158-8170.

[37] Zhao, K.; Khan, H. U.; Li, R. P.; Su, Y. S.; Amassian, A. Entanglement of Conjugated Polymer Chains Influences Molecular Self-Assembly and Carrier Transport. *Adv. Funct. Mater.* **2013**, *23*, 6024-6035.

[38] Clark, J.; Chang, J. F.; Spano, F. C.; Friend, R. H.; Silva, C. Determining Exciton Bandwidth and Film Microstructure in Polythiophene Films Using Linear Absorption Spectroscopy. *Appl. Phys. Lett.* **2009**, *94*, 163306.

[39] Niles, E. T.; Roehling, J. D.; Yamagata, H.; Wise, A. J.; Spano, F. C.; Moule, A. J.; Grey, J. K. J-Aggregate Behavior in Poly(3-hexylthiophene) Nanofibers. *Phys. Chem. Lett.* **2012**, *3*, 259-263.

[40] Spano, F. C.; Silva, C. H- and J-Aggregate Behavior in Polymeric Semiconductors. *Annu. Rev. Phys. Chem.* **2014**, *65*, 477-500.

CHAPTER 6

CONCLUSIONS AND RECOMMENDATIONS

6.1 Conclusions

The objectives in this thesis were 1) to identify alternative processing parameters which can contribute to enhancement of molecular ordering and charge transport characteristics of P3HT thin films, eliminating the need for additional pre- and/or post-processing steps such as film deposition method (spin vs. drop cast),[1] solvent boiling point (low vs. high boiling point),[2] polymer-dielectric interface treatment,[3] and post-deposition processing (solvent vapor or thermal annealing)[4, 5] and 2) to understand the relationship between processing parameters, intra- and intermolecular interactions of the polymer chains, micro- through macroscopic morphologies, and the charge transport characteristics of the resultant thin-films.

In Chapter 3, we identified an alternative processing parameter (i.e., dipole-dipole interaction between a relatively good and poor solvent of P3HT), which effects molecular ordering of the polymer chains, and thereby charge transport characteristics of the resultant films. Supramolecular assembly and subsequent enhancement of charge transport characteristics of conjugated polymers were facilitated simply by adding small amounts of a more volatile poor solvent, which can interact with the majority solvent via dipole-dipole interaction. Two-dimensional molecular ordering of the polymer film was controlled by varying the quantity of poor solvent added to the precursor solution, and the correlation between field-effect mobility and molecular ordering was investigated. Addition of up to 2 vol % acetone to a precursor solution of P3HT in chloroform led to approximately a 4-

fold increase in P3HT field-effect mobility along with improvement in molecular ordering of the polymer chains in the corresponding film. However, the mobility began to decrease, even though crystallinity of resultant films continued to increase over 2 vol % acetone, which was ascribed to other factors such as grain boundaries that negatively impact charge transport that began to predominate. We demonstrated that the improvement of molecular ordering of the polymer chains is associated with dipole-dipole interactions between acetone and chloroform. As the film evolves, solvent molecules not involved in dipole-dipole interaction evaporate faster than their counterparts, resulting in gradual increase of the volume ratio of acetone to chloroform. P3HT is less soluble in the chloroform/acetone solvent complexes than in the more readily vaporized chloroform component, and this characteristic enables the supramolecular assembly of P3HT chains at the nanoscale. Hansen solubility parameters were used to systematically understand how the solvent mixture enhances the alignment and assembly of polymer chains and influences subsequent thin film properties. The value of the relative energy difference (RED) of the solvent with respect to P3HT increased from less than 1 to more than 1 during film formation, which indicates that the solvent mixture gradually changes from a good solvent into a poor solvent. Consequently, molecular ordering of the polymer chains improves due to a gradual transition from favorable to unfavorable solvent-solute interactions.

Chapter 4 highlights that the processing parameter, UV irradiation of P3HT precursor solutions, can profoundly enhance the molecular ordering of P3HT chains and thus charge carrier transport characteristics of the corresponding films. The low UV dose to the precursor solutions resulted in no discernable degradation of the polymer chains, while it provided for enhanced intramolecular ordering of solubilized polymer chains, and

thereby effects formation of anisotropic supramolecular polymer assemblies via favorable π-π stacking (intermolecular interaction). The nanofibrillar aggregates formed in solution survived the film deposition process and in turn, evidently improved the supramolecular ordering and charge transport characteristics of resultant polymer films. The UV irradiation afforded crystalline-like nanofibrillar aggregates which are relatively longer (> 1 μm) than those (< 300 nm) obtained in films prepared via ultrasonic irradiation, suggesting that a reduction in the number of grain boundaries in the resultant films will be observed. As a result, the films obtained from the UV irradiated solutions exhibited relatively higher charge carrier mobilities than those obtained from the ultrasonicated solutions.

Chapter 5 extends the work in Chapter 4 to study whether the charge carrier mobility of P3HT thin films can be maximized through a synergetic effect of sequentially combining two different solution treatment methods (i.e., ultrasonication and UV irradiation). This chapter showed that enhanced intra- and intermolecular ordering with a concomitant reduction in grain boundaries within P3HT films can be achieved via sequential ultrasonication and UV irradiation of the precursor solution. Consequently, the method which sequentially combines the two methods very significantly further improved charge transport characteristics of the resultant films, compared to treatment via either method alone.

In summary, using P3HT as a model polymer of OSCs, we identified alternative processing parameters, which can contribute to enhancement of molecular ordering and charge transport characteristics of OSC thin films, eliminating the additional pre- and/or post-steps aforementioned. Further, we investigated the relationship between the processing parameters, intra- and intermolecular interactions of the polymer chains, micro-

through macroscopic morphologies, and thus charge transport characteristics of the thin-films. Finally, we showed that the charge carrier mobility of resultant films can be maximized via a sequential combination of two different parameters along with an optimization of processing conditions. The approaches using the processing parameters or their combinations do not require additional process steps such as dielectric surface modification or thermal and/or solvent vapor annealing of polymer thin-films, while they do provide for outstanding charge carrier mobilities of polymer thin-films. Therefore, such approaches would be applicable to alternative π-conjugated polymer semiconductors and suitable for the fabrication of high performance, large-area, flexible electronic devices for a wide range of commercial applications. In addition, understanding the relationship between processing parameters identified in this thesis, intra- and intermolecular interactions of polymer chains, micro- through macroscale morphologies, and charge transport characteristics of the resultant films would be expected to greatly contribute to developing new π-conjugated polymer semiconductors, their thin-film processing, and device structures.

6.2 Recommendations for Future Work

6.2.1 Extraction of Intrinsic Field-Effect Mobility of Organic Semiconductors

In this thesis, we investigated the relationship of charge transport characteristics of resultant films with processing parameters identified here and morphologies of the films, provided that the charge transport properties of the polymer films are identical to those of the OFETs. It is typically assumed that the contact resistance between an electrode and organic layer is a negligible factor affecting charge transport characteristics in an ideal OFET, because the contact resistance is much lower than the channel resistance of active

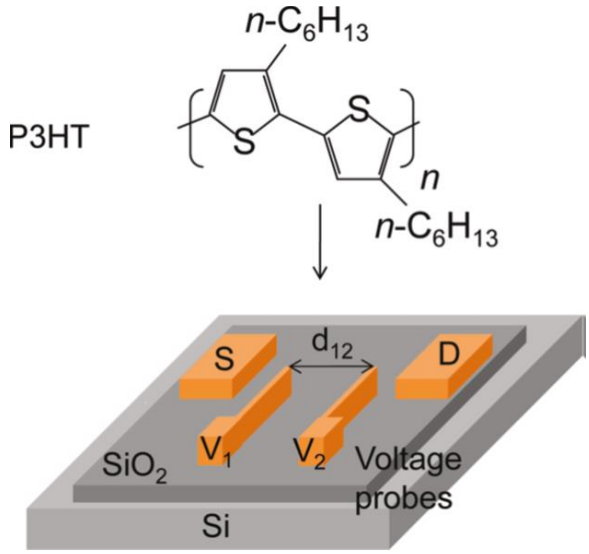

Figure 6.1: Schematic illustration of a bottom-contact OFET geometry with two voltage probes between the source and drain electrode. Figure taken from[8].

organic layers.[6] However, as the intrinsic mobility of organic semiconductors improves, the contact resistance becomes a dominant factor governing charge transport characteristics of OFETs.[6, 7] The morphology of organic semiconductor layers is one of the key parameters which significantly influence the contact resistance, and is significantly affected by processing parameters identified here as presented in this thesis. In general, the contact resistance increases with increased roughness of the films which are contacting the electrodes.[6, 7] Therefore, further experiments must be conducted to explore a more reliable relationship between the processing parameters, morphologies, and charge transport characteristics of resultant films.

A bottom contact FET configuration with two voltage probes between the source and drain electrode (Figure 6.1) is very useful to extract the intrinsic charge transport characteristics of organic semiconductor layers from the transport characteristics of the OFET devices; the four contact geometry device allows measurement of the intrinsic

polymer channel mobilities independent of the contact properties between electrodes and organic semiconductor layer.[6-8] In the measurement, the potential along the conducting channel under an applied drain and gate voltage above the threshold voltage is monitored using two voltage probes between the source and drain electrode. The sheet conductance, σ_{sq} is calculated using Equation 6.1:

$$\sigma_{sq} = \frac{d_{12}}{W} \cdot \frac{I_D}{V_{12}} \tag{6.1}$$

where W is the channel width, I_D is the drain current, and d_{12} and V_{12} are the distance and potential difference between two voltage probes (V_1 and V_2), respectively. The values of the intrinsic mobility of polymer semiconductor layers are extracted from the plot of sheet conductance as a function of gate voltage, as described in Equation 6.2:

$$\mu = \frac{1}{C_{ox}} \cdot \frac{d\sigma_{sq}}{dV_G} \tag{6.2}$$

where C_{ox} is the capacitance of the gate dielectric per unit area. The relation in Equation 6.2 is valid in the linear regime of transistor operation.

6.2.2 Encapsulation of Organic Semiconductors with Insulating Polymers

As well as low charge carrier transport characteristics, polymer semiconductor-based devices have often suffered from poor environmental stability, which is generally attributed to chemical impurities, chemical structure, ionization potential, and oxygen, water, and light exposure.[9-11] Typically, high off-currents, large and unstable onset voltages, and large subthreshold slopes result from the exposure of OFETs to the environment.[9-11] In this respect, it is inevitable that some encapsulation process will be required to protect the polymer semiconductors from environmental exposure.

Polymer semiconductor/insulating polymer blends deposited through solution-based processing have been explored to achieve insulating polymer encapsulation of organic semiconductors, because they can provide for reduced cost, enhanced mechanical properties, and improved environmental stability, together with the electrical properties of polymer semiconductors.[9-11] In such approaches, phase separation between a polymer semiconductor and a polymer insulator is a crucial factor which affects the connectivity and encapsulation of the organic semiconductor layer within the insulating polymer matrix.[9-11] For example, Arias et al. demonstrated that a vertical phase separation between poly[5,5´-bis(3-dodecyl-2,2´-bithiophene)] and poly(methyl methacrylate) (PMMA) can be realized by controlling the surface energy of a substrate using octyltrichlorosilane.[12] As a result, the OFETs exhibited high mobility (~ 0.1 cm^2 $V^{-1}s^{-1}$) owing to good connectivity of the semiconductor layer, and also good environmental stability owing to the PMMA layer protecting the semiconductor from environmental exposure.[12] Kippelen et al. showed that a vertical phase separation between 6,13-bis(triisopropylsilylethynyl) pentacene (TIPS-pentacene) between amorphous polymer matrix (poly(α-methyl styrene) or poly(triarylamine)) can be achieved by using an appropriate solvent; tetralin was used as a solvent, which provided enough time for TIPS-pentacene migration through, and then phase separation/crystallization within, a relatively fluid (solvent-rich, low viscosity) film.[13] Consequently, the OFETs showed high mobility values up to 2.82 cm^2 $V^{-1}s^{-1}$ owing to excellent crystallinity and connectivity of TIPS-pentacene layers.[13]

In a bottom-gate/bottom-contact OFET, vertical phase separation with an insulating polymer top and polymer semiconductor bottom is desirable to achieve successful formation of the organic semiconductor channel in contact with a dielectric and to protect

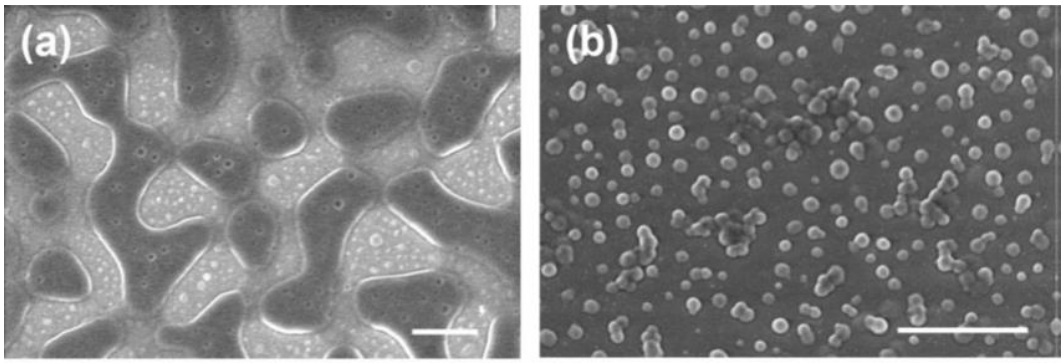

Figure 6.2: SEM images of P3HT/PS blends with different P3HT contents, prepared by means of spin-casting from solutions of $CHCl_3$ after selectively dissolving PS with cyclohexane: (a) 60 wt % and (b) 10 wt %. The scale bar is 1 μm. The figures taken from[9].

the polymer semiconductor layer from environmental exposure as well. Therefore, in order to realize this configuration within OFET devices, understanding of how the processing parameters effect phase separation between two polymer components must be conducted.

To effectively understand phase separation between two polymer components, morphologies of the composite films could be investigated using a microscopic technique such as a SEM (scanning electron microscopy) or TEM (transmission electron microscopy).[9, 10]

First, morphologies of the blend films can be observed by a SEM (scanning electron microscopy) after one of two polymer components is selectively removed by a solvent which selectively dissolve one polymer component.[9] The morphologies of entire films could be effectively investigated using a SEM, because the thickness of the films used in OFETs is typically less than 100 nm. Figure 6.3 shows SEM images of the P3HT phase in samples spin-cast from a $CHCl_3$ solution at different P3HT contents.[9] Qui et al. selectively dissolved polystyrene (PS) regions from the blend films using cyclohexanone to investigate the morphologies of the blend films. A bicontinuous network of P3HT and PS is observed

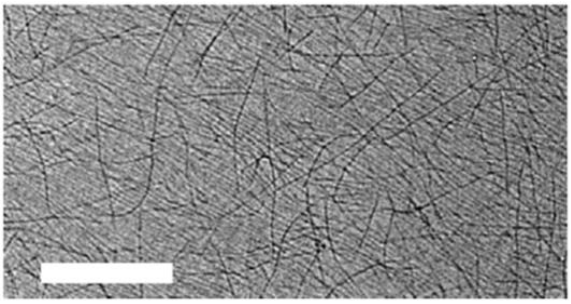

Figure 6.3: TEM image of the P3BT/PS (5 wt % P3BT) blend film spin-coated from solution of *o*-dichlorobenzene (8 mg/ml). The scale bar is 1 μm. The image taken from[10].

in the blend film containing 60 wt% P3HT, while isolated spherical P3HT domains with a diameter of about 100-150 nm are observed in the films containing 10 wt% P3HT.[9]

Second, a TEM (transmission electron microscopy) would be useful to examine the thin film morphologies because it probes the entire films rather than just the surfaces[10]. Although ultrathin films (less than 100 nm thick) are generally cut by a ultramicrotomy using a diamond knife for better visualization of the films, the blend films prepared for active layers in OFETs would be not necessary to be cut down by a ultramicrotomy because those are typically less than 100 nm in thickness. Figure 6.3 shows a TEM image of the poly(3-butylthiophene) (P3BT)/PS (5 wt% P3BT) blend film spin-coated from the solution of *o*-dichlorobenzene, which was observed by Lu et al.[10] The film for TEM measurement was peeled up directly from the transistor device through exposure of the device to hydrofluoric acid vapor for ca. 1s, and then floated onto deionized water. The polymer film was then picked up using copper grid without any supporting film. P3BT is aggregated into nanofibers in the solution of *o*-dichlorobenzene with decrease of the solution temperature from 100 ºC to room temperature (~22 ºC), because the solvent acts as a poor solvent to P3BT at room temperature. Therefore, the blend film consists of a network of interconnected P3BT fibers as shown in Figure 6.3.[10] As depicted above, such SEM and

TEM characterizations would be suitable to study morphologies of the resultant composite films, formed through the phase separation between two polymer components.

6.3 References

[1] Aiyar, A. R.; Hong, J. I.; Izumi, J.; Choi, D.; Kleinhenz, N.; Reichmanis, E. Ultrasound-Induced Ordering in Poly(3-hexylthiophene): Role of Molecular and Process Parameters on Morphology and Charge Transport. *ACS Appl. Mater. Interfaces* **2013**, *5*, 2368-2377.

[2] Chang, J. F.; Sun, B.; Breiby, D. W.; Nielsen, M. M.; Solling, T. I.; Giles, M.; McCulloch, I.; Sirringhaus, H. Enhanced Mobility of Poly(3-hexylthiophene) Transistors by Spin-Coating from High-Boiling-Point Solvents. *Chem. Mater*. **2004**, 16, 4772-4776.

[3] Kim, D. H.; Jang, Y.; Park, Y. D.; Cho, K. Surface-Induced Conformational Changes in Poly(3-hexylthiophene) Monolayer Films. *Langmuir* **2005**, *21*, 3203-3206.

[4] Cho, S.; Lee, K.; Yuen, J.; Wang, G. M.; Moses, D.; Heeger, A. J.; Surin, M.; Lazzaroni, R. Thermal Annealing-Induced Enhancement of the Field-Effect Mobility of Regioregular Poly(3-hexylthiophene) Films. *J. Appl. Phys*. **2006**, 100, 114503.

[5] Fu, Y.; Lin, C.; Tsai, F. Y. High Field-Effect Mobility from Poly(3-hexylthiophene) Thin-Film Transistors by Solvent–Vapor-Induced Reflow. *Org. Electron.* **2009**, 10, 883-888.

[6] Horowitz, G. Organic Thin Film Transistors: From Theory to Real Devices. *J. Mater. Res*. **2004**, 19, 1946-1962.

[7] Di, C. A.; Liu, Y.; Zhu, D. Interface Engineering: An Effective Approach toward High-Performance Organic Field-Effect Transistors. *Acc. Chem. Res.* **2009**, 42, 1573-1583.

[8] Park, B.; Aiyar, A.; Park, M. S.; Srinivasarao, M.; Reichmanis, E. Conducting Channel Formation in Poly(3-hexylthiophene) Field Effect Transistors: Bulk to Interface. *J. Phys. Chem. C* **2011**, 115, 11719-11726.

[9] Qiu, L.; Lee, W. H.; Wang, X.; Kim, J. S.; Lim, J. A.; Kwak, D.; Lee, S.; Cho, K. Organic Thin-film Transistors Based on Polythiophene Nanowires Embedded in Insulating Polymer. *Adv. Mater*. **2009**, 21, 1349-1353.

[10] Lu, G.; Blakesley, J.; Himmelberger, S.; Pingel, P.; Frisch, J.; Lieberwirth, I.; Salzmann, I.; Oehzelt, M.; Pietro, R. D.; Salleo, A.; Koch, N.; Neher, D. Moderate Doping Leads to High Performance of Semiconductor/Insulator Polymer Blend Transistors. *Nat. Commun*. **2013**, 4, 1-8.

[11] Lee, W. H.; Park, Y. D. Organic Semiconductor/Insulator Polymer Blends for High-Performance Organic Transistors. *Polymer*s **2014**, 6, 1057-1073.

[12] Arias, A. C.; Endicott, F.; Street, R. A. Surface-Induced Self-Encapsulation of Polymer Thin-Film Transistors. *Adv. Mater.* **2006**, *18*, 2900-2904.

[13] Hwang, D. K.; Fuentes-Hernandez, C.; Berrigan, J. D.; Fang, Y.; Kim, J.; Potscavage, W. J.; Cheun, H.; Sandhage, K. H.; Kippelen, B. Solvent and Polymer Matrix Effects on TIPS-Pentacene/Polymer Blend Organic Field-Effect Transistors. *J. Mater. Chem.* **2012**, *22*, 5531-5537.

VITA

Mincheol Chang

Mincheol Chang was born and raised in Haenam in South Jeolla Province of the Korean Peninsula. He graduated with a B.S. in Chemical Engineering from Chonnam National University in 2004 and a M.S. degree in Chemical Engineering from Seoul National University in 2006. He worked for LG Chem. Ltd. and Korea Research Institute of Chemical Technology before he joined the Reichmanis group to pursue his Ph.D. in the School of Chemical & Biomolecular Engineering at Georgia Tech in 2009. When he is not working on his research, Mincheol enjoys playing tennis.